To the Graduate Council,

I am submitting herewith a thesis written by Gyanendra Dutt entitled "Characterization and Structure-Property Relationships in Syndiotactic Polystyrene – Polyphenylene Oxide Blends". I have examined the final copy of this thesis for form and content and recommend that it be accepted in partial fulfillment of the requirements for the degree of Master of Science, with a major in Polymer Engineering.

Kevin M. Kit, Major Professor

We have read this thesis
and recommend its acceptance:

Accepted for the Council:

Associate Vice Chancellor and
Dean of The Graduate School

CHARACTERIZATION AND STRUCTURE-PROPERTY RELATIONSHIPS IN SYNDIOTACTIC POLYSTYRENE AND POLYPHENYLENE OXIDE BLENDS

A Thesis
Presented for the
Master of Science Degree
The University of Tennessee, Knoxville

Gyanendra Dutt
December, 1999

Acknowledgements

I would like to express my gratitude to my advisor and friend, Dr. K. M. Kit, for his ideas, guidance and support during the course of this work. He has taught me most of the things I know about polymers. Sincere thanks are also due to my thesis committee members Dr. J. E. Spruiell and Dr. R. S. Benson for their critical appreciation of this work. Their help in troubleshooting of several problems through different stages of the work is also gratefully acknowledged.

I wish to thank Dr. Mark Dadmun for his help with the molding of bulk samples. I am also indebted to Dr. Molly Dever for her encouragement and help with the mechanical testing. I appreciate the help of Greg Jones, Dr. D. C. Joy and Dr. C. R. Brooks with different aspects of the microscopy work. I would also like to thank Doug Fielden and Mechanical Systems Workshop for fabrication of several gadgets used in this project. Thanks are also due to Frank Holiway and Randy for their help in obtaining supplies.

I thank all my colleagues and friends for their friendship and support. Special thanks are due to Ketan Panse, Pitt Supaphol, Gary Holt, Darnell Worley and Bhushan Deshpande for useful discussions related to this work.

TABLE OF CONTENTS

LIST OF FIGURES

LIST OF TABLES

Abstract

Miscible rigid-rigid polymer blend systems, although not always tough, tend to show better modulus and yield strength than the rubber-toughened systems. The understanding of the relationships between structure and energy absorption mechanisms in these blends is still lacking. The objective of this work is to characterize melt miscible syndiotactic polystyrene (sPS) and poly(phenylene oxide) (PPO) blends which form a rigid-rigid system. Specifically, the effect of the spherulitic texture and the scale of segregation of PPO on mechanical properties and fracture are discussed.

The sPS/PPO blends, prepared by melt blending, were found to be miscible in melt phase at all compositions studied. These miscible blends were crystallized from melt as well as quenched state at different temperatures. Dynamic mechanical analysis was then used to study the change in composition of the amorphous phases formed after crystallization. In melt crystallized blends, the scale of segregation of PPO increased with slow crystallization at high temperatures. In cold crystallized blends, the extent of segregation of the PPO was much lower. Tensile testing of the bulk samples showed that for melt-crystallized blends, tensile properties are a strong function of the crystallization temperature. The samples crystallized the slowest showed the highest tensile strength, strain at break and tensile toughness. The tensile properties of the cold crystallized blends varied weakly with the crystallization temperature. The

observation of the spherulitic morphology in the scanning electron microscope revealed that bundle thickness, bundle spacing and size of amorphous domains increase with increasing crystallization temperatures in melt crystallized blends. The cold crystallized blends did not show substantial change in morphology at different crystallization temperatures. The SEM micrographs of the fractured surfaces of melt crystallized blends suggest that while intraspherulitic fracture occurs at low crystallization temperatures, interspherulitic fracture takes place at high crystallization temperatures. Wide Angle X-ray diffraction studies and density measurements suggest complex polymorphic behavior of the sPS after blending with PPO.

The correlation of the morphology and mechanical properties suggests that redistribution of the amorphous PPO strongly influences the ultimate tensile properties of the sPS/PPO blends. Blends melt crystallized slowly formed larger interfibrillar amorphous phase domains and showed better tensile properties. It is interesting to note that slow crystallization of the neat sPS resulted in poorer mechanical properties than fast crystallization. The fracture surface of these tougher blends suggest that some stress concentration effect led to drawing of the large amorphous domains between the bundles.

Chapter 1

INTRODUCTION

Several important engineering polymers tend to fail by crazing and are brittle in nature. The percent strain at fracture, under tensile loads, for these polymers are very small. Typical examples of such polymers are polystyrene and poly(methyl methacrylate) [1-2]. Increasing the toughness of such polymers by promoting energy absorbing mechanisms such as stretching-tearing, crazing, yielding or some combination of these, has been a focus of extensive research [2-6]. The most common method used is the *rubber toughening*. It involves addition and control of an immiscible, discontinuous elastomeric phase. The elastomeric phase acts as stress concentrator and facilitates multiple local crazing and yielding processes, which absorb the applied energy. This multiple deformation mechanism leads to a large degree of plastic deformation and increase in volume before failure. This large plastic deformation usually leads to simultaneous decrease in modulus, yield strength and creep resistance.

Recently, another approach involving incorporation of rigid, thermoplastic particles to a rigid matrix has been developed. Immiscible polymer blends, phase separated on the microscale, have been used to achieve better mechanical properties, especially better toughness. Miscible blends, homogeneous on the segmental level, have generally shown negative deviation from the linear rule of mixtures of toughness.

They, however, usually show better modulus and yield strength. It has been attributed to the specific molecular interactions that reduce the mobility of the chains. The understanding of mechanisms of deformation and energy absorption in these rigid-rigid systems is still lacking.

Semicrystalline polymers, under certain conditions, develop textures consisting of bundles. Amorphous regions of the same scale separate these bundles. The amorphous material, having different composition and modulus, might also be trapped in other asymmetric regions formed by branching and splaying of the lamellae. In case of the melt-miscible blends, the interfacial strength between these regions can be expected to be very high because of entanglement of the chains in the amorphous phase with loops and tie chains, and incorporation of the chain ends in the lamellar crystals. At certain crystallization condition and blend composition, it is possible to achieve an amorphous phase composition that might result in these amorphous phases acting as stress concentrators. In that event, it can be reasonably hoped that some kind of energy absorbing deformation process may occur.

Objectives

The main objective of the present work is to understand the effect of spherulitic texture of miscible, rigid-rigid semicrystalline blends on their mechanical properties. Blend samples of different textures will be produced by varying the composition and crystallization conditions. It is hoped that different processing conditions will result in

different levels of segregation of the amorphous phase during crystallization, which may result in different properties. The resulting texture and morphology will be correlated to the tensile properties of the bulk samples. The completely miscible sPS/PPO system has been chosen for this study.

The miscible aPS/PPO blend has been around for a long time [13]. Since both the components have T_gs above the room temperature (around 100°C for aPS and 210°C for PPO), it forms a rigid-rigid system and has been processed easily to get very high toughness without any decreased stiffness or strength. The PS chain (in amorphous state) has low entanglement density (0.056 mmole/cc) and high characteristic ratio of 10.8 [62]. Both these parameters favor crazing. PPO, on the other hand, has higher entanglement density (0.295 mmole/cc) and lower characteristic ratio (3.2); both favoring yielding. This mis-match in the structure initiates energy absorbing crazing/yielding processes. The stereoregular syndiotactic form of polystyrene (sPS) with high crystallinity may give better adhesion through tie chain molecules. The strong adhesion and the spherulitic morphology of sPS/PPO system might result in some different mode of energy absorbing processes and failure. Finally, the system may be of some commercial interest because of the huge popularity of the atactic polystyrene blend with the PPO.

Chapter 2

BACKGROUND AND LITERATURE REVIEW

2.1 Polymer Blends

A polymer blend may be defined as a single, continuous polymer mixture that results from intimate mixing of two or more polymers [7]. This mixing of polymers offers a powerful way of tailoring performance and economic relationships using existing materials. Blending offers an opportunity to develop materials that might be more easy to process, dimensionally stable and resistant to high temperatures and solvents. If one of the components is a commodity polymer, its use can reduce the cost for the more expensive blended product. For example, the miscible blend of polystyrene (PS) and poly(2,6-dimethyl-1,4-phenylene oxide)(PPO) can be processed at much lower temperatures and cost than the pure PPO. The addition of polystyrene can be used for adjusting the rheological processing "window" which lies between the glass transition and the chemical degradation temperatures.

2.1.1 Miscibility

Blends of two or more different polymers may exist in completely homogeneous state where their segments are mixed at the most intimate level or they may segregate into distinct phases. Phase separation may occur because of crystallization of one or more components or due to their thermodynamic incompatibility.

The miscibility of polymer blends has been investigated by studying the optical, morphological, glass transition and crystalline melting behavior and has been described by many authors [8-11]. In recent years, scattering techniques such as neutron scattering have led to increased emphasis on conformations of individual polymer chains in the mixture [12].

The observation of a single phase, in itself, is a relative rather than absolute concept and can depend on the method used for the study. The glass transition temperature, T_g, which marks the characteristic transition of the amorphous region of a polymer or blend from a glassy state to a rubbery state, is the most convenient way of studying miscibility [12]. Assuming that a single glass transition can be equated with segment level mixing, a *miscible* blend may be characterized as the one, which shows a single, monotonic, composition-dependent glass transition temperature. Example of miscible blends are PS / PPO [13] and poly(methyl methacrylate) (PMMA) / poly (vinylidene fluoride) (PVDF) [14]. A blend having more than one phase (each containing both the components) shows transition temperatures corresponding to each of the phases and may be termed as *partially miscible.* Poly(ethylene oxide) – polyethersulphone and Phenoxy resin – polyethersulphone [15] are examples of partially miscible blends. Finally, a blend that exhibits the individual glass transition temperatures of the neat components may be termed as *immiscible*. Most polymer blends are immiscible, and fall in the third category. Important examples are polyethylene – polypropylene and polyethylene-polystyrene [16].

2.1.2 The Glass Transition (T_g) Criteria

A very large variety of physical measurements can be made to determine the glass transition temperatures for studying blend miscibility. The most widely used are:

(a) Calorimertic determination of heat capacities as a function of temperature.

(b) Dynamical mechanical (low strain) measurements of complex modulus as a function of temperature.

Sometimes, a term 'compatible' is also used to describe the stability and homogeneity of polymer blends. It usually refers to the mechanically processible blends that resist phase separation and/or give desirable properties. A compatible blend may consist of two or more phases with their corresponding glass transitions. The term miscibility is used more in thermodynamic sense.

2.1.3 Composition dependence of T_g in Miscible Blends

In general, the T_g of miscible blends increases monotonically as a function of composition, with more or less pronounced negative deviation from linearity. Several theoretical and semi-empirical models have been proposed to approximate this composition dependence of the T_g. The earliest theoretical expression is the *Kelly-Beueche equation* [17] derived from the isofree volume model of glass transition. If α_i is thermal coefficient of expansion of the melt, and ϕ_i is the volume fraction of the

constituent polymer *i*, where $\Sigma\phi_i = 1$, the Kelly-Bueche expression for glass transition temperature (T_g) of a miscible blend of polymers 1 and 2 is given by

$$T_g = \frac{\alpha_1\phi_1 T_{g1} + \alpha_2\phi_2 T_{g2}}{\alpha_1\phi_1 + \alpha_2\phi_2}$$

One of the most general relations, given by *Couchman and Karasz* [18], is based upon the classical thermodynamic treatment in which the glass-transition temperature is the temperature at which the entropies of the glass and the liquid phases becomes equal. If w_1 and w_2 are the weight fractions of the constituent polymers, and ΔC_{p1} and ΔC_{p2} are the corresponding change in their specific heats at the T_g, the equation for a binary system is given by

$$\ln\left(\frac{T_g}{T_{g1}}\right) = \frac{w_2\Delta C_{p2}\ln(T_{g2}/T_{g1})}{w_1\Delta C_{p1} + w_2\Delta C_{p2}}$$

Assuming that $T_g\Delta C_p$ is constant for all polymers, the above equation reduces to

$$\ln\left(\frac{T_g}{T_{g1}}\right) = \frac{w_2\ln(T_{g2}/T_{g1})}{w_1(T_{g2}/T_{g1}) + w_2}$$

If only the first term of the expansion of the logarithm in the Couchman-Karasz equation [18] is considered, and if T_{g2}/T_{g1} is close to unity, the equation reduces to

$$T_g = \frac{w_1 T_{g1} + k w_1 T_{g1}}{w_1 + k w_2}$$

This is the Gordon-Taylor equation if k is defined by $\Delta\beta_2/\Delta\beta_1$ where $\Delta\beta_i$ is the cubic volume expansion coefficient of polymer i.

Finally, if the glass transition temperatures of the polymers are not too different, a truncated Taylor series expansion of the log terms and rearrangements gives the most commonly used *Fox equation* [20]. It is given by

$$\frac{1}{T_g} = \frac{w_1}{T_{g1}} + \frac{w_2}{T_{g2}}$$

2.2 Semicrystalline Polymer Blends

The majority of polymer blends used in engineering applications contain some level of crystallinity. The reinforcing action of the crystallites and the tie molecules sometimes improves the mechanical and chemical properties of the blend. In case of an immiscible blend, crystalline melting point remains unaffected by addition of an amorphous polymer. In case of a miscible blend, the addition of an amorphous polymer to a semicrystalline polymer affects its crystallization behavior. The addition of diluent results in depression of melting point, which acts to increase in lamellar thickness at same crystallization temperature. The fold surface and lateral surface energies are also affected. Depression in melting point for the miscible PVDF /

PMMA [14] and poly(ethylene oxide) – polyethersulphone [21] blends has also been reported.

2.2.1 Spherulitic Morphology of Polymer Blends

The most common morphology of semicrystalline polymers is that of the spherulite growth in a radially symmetric polycrystalline aggregate consisting of thousands of lamellar crystals radiating from the center. Due to the nature of the high polymer molecules and possible presence of non-crystalline species (melt-miscible with the crystalline species), the common order of crystallinity in a spherulite is of the order of 30% to 90%. An idealized spherulite would consist of an array of lamellar crystals of same thickness separated by amorphous regions of similar dimensions. The thickness of the lamellar crystals and the amorphous regions is of the order of 10 nm. These crystals, typically, have dimensions which are much larger (by two to three orders of magnitude) in the directions normal to the thickness direction.

Under certain conditions, structures called bundles can be responsible for an additional texture on the scale of 100 nm. These bundles consist of lamellar crystals stacked on one another in the thickness direction, and separated by amorphous regions, which are also of the order of 100 nm. This texturing was described by Keith and Padden [22] in terms of spherulite *coarseness* and *compactness*. Coarseness refers to the absolute size of the bundles. A coarse texture is due to large cross section of the bundles, and fine texture is due to small cross-section bundles. Compactness

may be defined as the proportion of the material contained within the spherulite boundary, which has already crystallized. It is a measure of the ratio of bundle thickness to bundle spacing and is sometimes referred to as *bundle fraction.* A compact texture refers to high bundle fraction (close to unity), and an open texture refers to a low bundle fraction.

Keith and Padden, in a series of papers [22,23,24], developed a theory of spherulitic crystallization and the formation of the fibrous structures called bundles. They predicted that the diameters of these bundles should be on the order of a parameter known as *diffusion length* δ. The diffusion length is an approximate measure of the extent of a diffusive boundary layer, which precedes a growing crystal and is equal to the ratio of the diffusion coefficient of the rejected non-crystallizable species to the crystalline growth rate.

$$\delta = \frac{D}{G}$$

Here D is the diffusion coefficient of the rejected species and G is the crystal growth rate. The diffusion coefficient, D, depends upon the glass transition temperature of the rejected species (and hence, on the composition of the amorphous melt) and the absolute temperature at the growth front. Interaction between the blend components (the interaction parameter χ), blend composition, and temperature affect the crystallization rate.

2.2.2 Amorphous phase behavior

It is possible to control the redistribution of the amorphous component of the melt miscible blend by varying the crystallization conditions (most importantly the crystallization rate and the mobility of the polymer chains which are both affected by temperature, molecular weight, and local composition). The mobility of the amorphous diluent, the crystal growth rate and the segmental interactions between the components determine the length scale of segregation [25]. Depending upon these factors, the amorphous diluent may be located at three levels. It may be segregated completely ahead of the growing front between the spherulites (*interspherulitic segregation.*). Alternatively, it may be trapped in the pockets between lamellar bundles (*interfibrillar segregation*). Finally, it may also be rejected between the individual lamellae (*inter-lamellar segregation*). These three scales of rejection are shown schematically in Figure 2.1 [25]. Recent experimental studies have shown that similar to the interphase region in the semicrystalline homopolymers, there exists an additional *interphase region* between the crystallite surface and the amorphous region in some of the blends [26,27] from which the diluent is rejected. The existence of the crystal-amorphous interphase is necessitated by the difficulty in dissipating order at the crystal surface owing to chain connectivity.

The study of texture of spherulites, under different crystallization conditions, compositions and molecular weight, can be used to determine the scale of rejection at those conditions. Usually the coarseness of a spherulite is a strong function of the

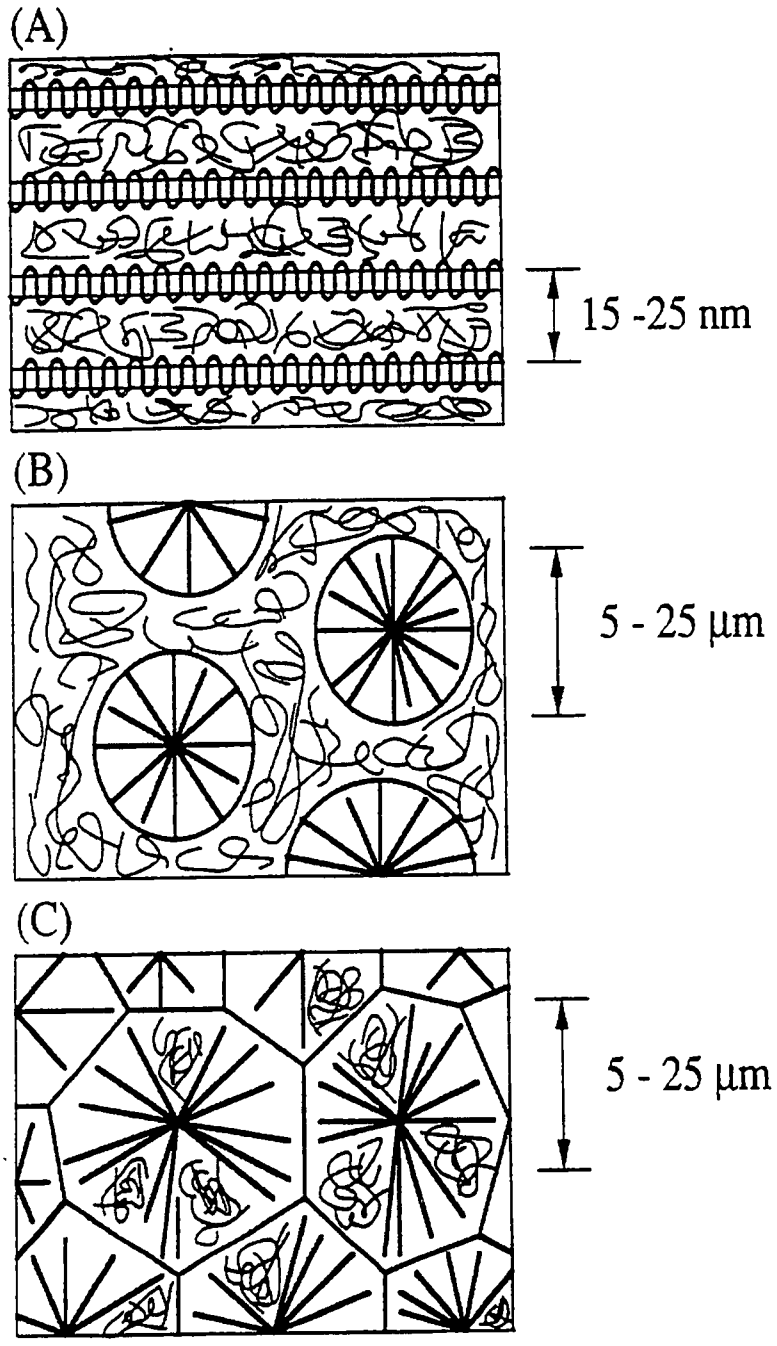

Figure 2.1. **Schematic diagram of three different scales of segregation of non-crystallizable species in a blend: (A) interlamellar, (B) interspherulitic and (C) interfibrillar [19].**

crystallization temperature and changes little with the composition of the non-crystallizable species and the degree of crystallinity [28]. The bundle fraction, however, decreases with the increase in the diluent species. Hudson et *al* [29] have shown in morphological studies that in poly(aryl ether ether ketone) (PEEK) / poly(ether imide) (PEI) system slow crystalllization at high temperatures (320°C and above) results in exclusion of PEI to the spherulite boundaries. At 300°C, while the interspherulitic segregation is still observed, most of the PEI is trapped between the bundles. At 270°C the interspherulitic rejection is not seen at all and all PEI is trapped in the interfibrillar region.

Several studies have been made using the mechanical or dielectric spectroscopy techniques combined with the small-angle x-ray scattering (SAXS) to determine the actual location of the noncrystallizable species [26,27,31]. The miscible PVDF/PMMA [27] and poly(ethylene oxide) (PEO) / PMMA [26] systems show a major relaxation corresponding to a mixed amorphous phase. In SAXS studies on both the blends, a systematic increase in interlamellar thickness with the increasing PMMA content across the entire composition range is observed. This evidence strongly suggests interlamellar trapping of the PMMA. The SAXS studies on the poly(butylene terepthalate) (PBT) / polyarylate (PAr) system [30] show that while the long period and amorphous layer thickness increase linearly with the PAr content, the crystal thickness remains relatively constant. Again it leads to the conclusion that PAr resides in the interlamellar zones. Using an appropriate Tg-composition relation

and the relaxation temperatures observed from the dynamic mechanical spectra, the composition of the corresponding amorphous phases has also been calculated. The change in composition of these phases with the change in bulk blend composition has also been used to predict the location of the non-crystallizable polymer. Dynamic relaxation studies on miscible PEEK / PEI blend have revealed two relaxations originating from interlamellar amorphous populations in the PEEK-rich and PAr-rich phases [31]. Absence of any transition for the neat PEI indicates that there is no large-scale exclusion of the PEI to interfibrillar and interspherulitic regions.

2.3 Toughness of Polymer Materials

The tensile toughness or the total deformational energy absorbed per unit volume, for a polymeric material is defined as the area under the stress-strain curve. It is therefore, directly related to the energy absorbing processes such as stretching and tearing, crazing, yielding or some combination of these. To increase the toughness, it is required to increase the volume of the material in which plastic deformation proceeds. Large, homogeneous plastic deformation zone formation, however, leads to poor mechanical properties such as strength and modulus. Hence the deformation processes have to be local and multiple so as to achieve an optimum balance between toughness and other important properties.

2.3.1 Rubber Toughening

Rubber Toughening consists of incorporation of a second rubbery phase in the matrix of a brittle polymer. The elastomeric phase facilitates multiple local crazing and yielding processes, which absorb the impact energy. Polymers modified in this manner include polystyrene (PS) [3], styrene-acrylonitrile copolymers (SAN) [4], polyamide 6 (nylon 6) [2], and epoxies [5].

The factors that influence the toughness of these blends include the rubber volume fraction, the size and shape of the rubber particles and matrix, and the degree of adhesion between the particles and the matrix. Based on these requirements, several energy absorbing deformation mechanisms have been proposed.

2.3.1.1 Multiple Crazing

In this mechanism, the absorption of energy occurs mainly by the generation and growth of the crazes in large volumes of the brittle matrix. The matrices toughened by this method are generally brittle. It has been used to explain the toughening of PS by grafting of polybutadiene rubber particles to yield high-impact polystyrene (HIPS) [3]. Other examples include toughening of SAN [4] and PMMA [6].

The main point of this mechanism is that when the toughened polymer is subjected to an applied load, the small rubber particles act as stress concentrators. It leads to the formation of highest triaxial stress concentrations (*plane strain condition*) at the

equators of the rubber particles. When the stress concentrations at these points reach a critical value for craze formation, massive tiny crazes are initiated. These crazes grow in the direction perpendicular to the direction of the applied stress until they are terminated by the fall in the stress by another rubber particle or end in the matrix. Since craze formation absorbs a significant amount of energy, the toughness of the polymer is increased.

Michler has shown that there is an optimum rubber-particle diameter range, which facilitates most efficient crazing [4]. Smaller particles are unable to initiate crazes, while the larger particles show a reduced ability. After a certain volume fraction of rubber is attained, a stress-field superposition among the particles occurs and further enhances the toughness.

2.3.1.2 Multiple Shearing

The matrices toughened by this mechanism are called the pseudo-ductile matrices. It has been used to explain the energy absorption processes in the toughened nylon 6 [2] and poly(vinyl chloride) (PVC) [6]. In this method the energy absorption occurs by the shearing of the matrix between the rubber particles.

The underlying mechanism is that when rubber particle are sufficiently close to each other, plastic constraint on the material between them is removed, and *plane stress*

condition between the thin matrix ligaments are developed. As a result shear yielding of the matrix between this overlapped stress field is activated.

Wu [2] has shown that there exists a critical surface-to-surface interparticle distance, τ_c, below which the matrix will undergo shear yielding. τ is a function of rubber particle size (d_f) and rubber volume fraction (V_f) and has been expressed as

$$\tau = d_f \left[\left(\frac{\pi}{6V_f} \right)^{\frac{1}{3}} - 1 \right]$$

The critical value, τ_c, has been suggested to be a characteristic property of the matrix at a given temperature and rate and is independent of the particle size and rubber volume fraction.

2.3.1.3 Rubber Stretching and Tearing

It has been used to explain the energy absorption in some rubber toughened epoxies [32]. The rubber particles between the crack surfaces are stretched as the crack surface opens up and finally fractures. This deformation mechanism accounts for very small fraction of the total energy absorbed and occurs with the multiple shearing and multiple crazing mechanisms.

It has been proposed that cavitation and shear yielding occur simultaneously and contribute to the energy absorption [33]. Rubber particles act not only as stress

concentrators but also relieve the triaxial stress field and enable the matrix to undergo shear yielding.

2.3.2 Rigid Particle Toughening

In case of rigid-rigid blend systems the difference in the modulus of the matrix and toughening polymer is typically small. Hence the most likely modes of failure are the breakdown or debonding at their interface and generation of massive crazes. Although the exact deformation mechanisms that absorb energy in these blends are yet to be understood, many quantitative models have been proposed to explain the toughening effect achieved.

In case of rigid paricle toughened epoxies, debonding or microcracking effectively lowers the modulus in the frontal process zone around the crack tip and hence reduces the stress intensity there. A quantitative model [34] has been developed to predict toughness for rigid blends that have poor interfacial strength. For this mechanism, smaller particles provide better toughness.

Particle bridging by the rigid particles has also been used to explain the toughening of rigid-rigid blends [35]. The rigid particle applies compressive traction against the crack and provides crack shielding. In this case, larger particles result in higher toughness.

2.3.3 Percolation Theory

Percolation theory has been used for pseudo-ductile matrices to describe the energy absorbing yielding processes in terms of percolation (or connectivity) of thin ligaments [36]. According to this theory the tough behavior occurs only when the thin matrix ligaments ($\tau<\tau_c$) are interconnected, allowing the yielding process to propagate and pervade over the entire matrix in the deformation zone. It predicts that uniform-sized rubber particles are more effective than the polydisperse-sized ones and asymmetrical (high-aspect ratio) particles such as ribbons, networks and fibrils are more effective than the spheroidal ones. Flocculation to form interconnected rubber particle network is also beneficial.

2.3.4 Spherulitic morphology as toughening base.

The crystallization of melt miscible blends leads to segregation of the homogeneous melt into two or more amorphous phase of different compositions. As mentioned before, the scale of segregation depends upon interaction parameter between the polymers, mobility of the diluent and the crystalline growth rate, the latter being a strong function of processing temperature. The resultant spherulitic morphology consists of asymmetric interlamellar and interfibrillar amorphous regions of very fine spacings (50 - 1000 nm). As per the percolation theory, these asymmetric, less rigid amorphous regions may act as better toughening phases than spherical particles. The crystallization conditions can be varied to control the fineness of the bundles and bundle spacings, thereby changing the repeat distance (similar to inter-particle

distance) between the less rigid structures. The two distinct but miscible polymers should also interact entropically and enthalpically to cause negative volume of mixing, which leads to high rigidity and good adhesion. In the spherulitic morphology, entanglement of the chains in the amorphous phase with the loops and tie chains and partial incorporation of the chain ends in the lamellar crystals may also lead to formation of very strong interface between the phases.

It has been reported that the elongation at break of semicrystalline polyoxymethylene is greatly increased upon addition of a low molecular weight, low modulus novolak [37]. Interestingly, this high elongation at break occurs only when novolak is distributed completely within the spherulites. Therefore, there must exist some novolak rich amorphous regions in the spherulite acting as a toughening phase. Another blend system which behaves similarly is poly(aryl ether ether ketone) (PEEK) and amorphous poly(ether imide) (PEI) . This blend shows a maximum in fracture toughness at an intermediate PEI phase content [38], and this could be due to the formation of a toughening base by the amorphous PEI.

2.4 Syndiotactic Polystyrene (sPS)

Syndiotactic polystyrene (sPS) is a stereoregular form of polystyrene in which the phenyl rings alternate regularly from side to side with respect to the polymer chain backbone. The different tacticity results in a number of properties that are different from conventional styrenics and makes the sPS superior for many practical

applications [39]. It has highest melting point (above 270°C) of any single-monomer polymerization product, high crystallization rate (compared to isotactic polystyrene), high crystallinity (as high as 70%), and good chemical stability, and is easy to process using standard thermoplastic fabrication technologies. Products made from this semicrystalline polymer have excellent dimensional stability and low-moisture absorption. It competes with polyesters, nylons, and other resins in high temperature applications. However, it is inherently very brittle, the tensile strength and percent strain at fracture being lower than most of the comparable polymers.

2.4.1 Structure

sPS shows very complex polymorphic behavior and its structure has been studied by diffraction and spectroscopic techniques [40,41]. It is known to form at least four different polymorphs, termed as α, β, γ, and δ. α and β phases consist of planar zigzag backbones and exhibit hexagonal and orthorhombic symmetries respectively [42] with the repeat period of 5.06Å. The β form is more stable [43] and is the form stable in the presence of several solvents (e.g., methylene chloride and chloroform). It has been established that the formation of α and β forms is affected by melt temperature, cooling rate, starting material, and external pressure. The two other crystalline forms, described as γ and δ, are characterized by chains in a helix conformation with repeat period of 7.5Å and arise from solvent crystallization.

The study of structure is made still more complicated by the fact that both α and β forms can exist in different modifications characterized by limiting various degrees of structural order (between limiting disordered α' and β'' and limiting ordered α'' and β'') [41-43].

2.4.2 Crystallization, Melting Behavior and Morphology

sPS crystallizes much faster than the isotactic polystyrene, but slower than polyethylene. Crystallization study has been done using the non-isothermal DSC analysis [44] and a non-integral Avrami index of 2 and 3 has been reported. The crystallization rate is a function of molecular weight; lower molecular weight sPS crystallizes fastest at lower temperatures, while the higher molecular weight sPS crystallizes faster at higher temperatures.

Melting behavior of sPS is quite complex and is further complicated by its polymorphism. Multiple melting peaks are observed in the DSC thermograms, depending upon the crystallization conditions and the starting material. For the β form, two melting peaks are observed while the α form gives a single peak [45]. The equilibrium melting point, measured according to the Hoffman-Weeks treatment and the melting depression has been found to be between 270°C and 285°C [45,46].

When crystallized from melt, sPS shows spherulitic morphology [47]. Both sheaf-like and rounded spherulites are observed. They all show positive birefringence and have the same isothermal radial growth rate.

2.4.3 sPS blends

sPS is inherently brittle and its properties are adversely affected by its fast crystallization. Its potential applications may require blending to balance its service and processing properties. It has been found melt miscible with poly(2,6-dimethyl-1,4-phenylene oxide)(PPO) [48] and atactic polystyrene (aPS) [49]. Its partial miscibility with poly(vinyl methyl ether) (PVME) has also been reported [50].

Blending causes substantial changes in the polymorphic forms and crystallization of the sPS and its blends have been studied by Guerra et *al* [50] and Cimmino et *al* [52]. Blending with PPO depressed the overall crystallization rate and favored the formation of the β form. For the sPS/PVME blends, instead, the addition of PVME caused an increase in spherulitic growth rate. For both blends the morphology was spherulitic.

2.5 Polyphenylene Oxide (PPO)

Polyphenylene oxide is a trade name used to refer to polyphenylene ether with two methyl groups substituted on the phenylene ring. It is an important engineering thermoplastic with very high glass transition temperature (around 210°C) and melting

temperature (around 265°C). The narrow range of these temperatures results in very small crystallinity and the polymer is considered essentially amorphous. Its density in amorphous state is very low (around 1.06 g/cm^3) and changes little with crystallization.

Unlike syndiotactic polystyrene, PPO is ductile, even below its glass transition temperature [53]. The phenylene ring imparts inherent stiffness to it. It also has very high entanglement density, which favors yielding and results in very high tensile strength and toughness. The water absorption is lowest among the thermoplastics and resistance to acid and bases is excellent. The dielectric properties are good with low and constant dielectric constant and dissipation factor.

PPO has very high melt viscosity, which renders it unsuitable for extrusion and molding. It also degrades rapidly, in the presence of oxygen above 250°C. Almost all of the PPO is used in blend with other polymers like polystyrene and nylon.

2.6 Atactic Polystyrene (aPS) and PPO Blends

The blend of aPS and poly(2,6-dimethyl-1,4-phenylene ether) (PPO) in optimum ratios was marketed under the trade name Noryl® by General Electric Co [13]. Dilatometry [13], calorimetry and dynamic mechanical analysis [54], neutron scattering [55] and small-angle x-ray diffraction methods [56] have shown that the blend is completely miscible over the entire composition range. It has also been shown that this miscibility is due to the favorable exothermic interaction, which

occurs because of the presence of methyl groups on the aromatic ring of the PPO [57]. Both the aromatic ring and the methyl groups undergo an electronic rearrangement to produce a repeat unit, which interacts favorably with the aPS.

Mechanical properties of the aPS/PPO blends have been extensively studied. The synergistic effect of the tensile strength and flexural modulus was first reported by Cizek [53]. Yee and Maxwell [58] found that both compressive modulus and the yield stress are much higher than the linear rule of mixtures, while the fracture energy was much lower. They attributed the decrease in the fracture energy to the increase in the craze localization in the vicinity of the crack. Serrano et al [59] found a very rapid increase in critical stress-intensity factor (K_{Ic}) in the vicinity of 75% PPO. SEM fractography, uniaxial tensile stress-strain data and fatigue data, all indicated a similar transition from brittle-to-ductile behavior in this composition range. Finally, Chun [60] has also reported increased stress at break and modulus with decrease in the strain at break.

The enhanced mechanical properties achieved have been explained on the basis of the molecular structure achieved in the blend [61]. Specific interactions and intermolecular attractions tend to align the chain segments, decrease the free volume and stiffen the chains; this process results in increased modulus and yield stress, but a decrease in ductility. This observation is similar to the anti-plasticization phenomena.

The most common polymer blended with the PPO is the High-Impact-Polystyrene (HIPS) produced by a mass-suspension process with high *cis*-polybutadiene. The rubber particles in the HIPS significantly affect the impact, tensile, and modulus properties of these blends. Bucknall and co-workers [61] have done an extensive study of the HIPS/PPO blends. It was shown that in the blends containing less than 50% PPO, crazing is the dominant failure mechanism, whereas in the blends containing more than 50% PPO, shear yielding was dominant. When both components are present in equal proportions, a combination of massive crazing and shear band formation results in greatly enhanced toughness. Particle size and phase volume of the polybutadiene has a strong effect on the properties.

Chapter 3

EXPERIMENTAL PROCEDURES

3.1 Materials

The syndiotactic polystyrene (sPS) used for this study was kindly provided by Dow Chemical Company (Questra LA 320). The polyphenylene oxide (PPO) was purchased from Scientific Polymer Products Inc. (CAT#126). The relevant properties of the neat polymers are given in Table 3.1.

3.2 Melt Blending

sPS and PPO were melt blended in a twin blade Brabender mixer-measuring head at 290-295°C temperature. 0.3% Irganox® 1076B by mass was used as an antioxidant. The polymers and the antioxidant were physically mixed and the mixture was poured slowly in the pre-heated mixer with the driving blade rotating at 15rpm. Once all the mixture was put in the mixer, the mixer ram was closed tightly and the blade rpm was increased to 70. The blending was done for approximately 12 minutes, after which, the homogeneous mixture formed was scraped out and broken down in small pellets in a kitchen blender. Three sPS/PPO compositions (83/17, 67/33, 50/50 by weight) were melt blended in two batches each. The three different composition blends obtained were designated as sPS83PPO, sPS67PPO and sPS50PPO, the middle digits being the weight percentage of the sPS in the blend.

Table 3.1 Relevant physical properties of the as received sPS and PPO.

Polymer	$\bar{M}_w$	Glass-Transition Temperature (°C) (DSC)	Melting Point (°C) (DSC)	Density (g/cm^3)
sPS	320,000	97.1	272.2	1.04
PPO	50,000	219.5	268.0	1.06

3.3 Bulk Samples Molding

Dog-bone shaped bulk samples of sPS50PPO and sPS67PPO blends, were molded in Atlas Mixing Molder for mechanical testing. The mold conformed to the ASTM 1708-B standard. The mixing cup temperature was kept at 304°C, and the mold was heated to approximately 240°C. After the injection, the mold was taken out of the clamp and quenched in water. For mechanical testing of the pure sPS, neat sPS was compression molded into 1mm thick sheets in a rectangular 5×6 inch aluminum frame.

3.4 Crystallization

The bulk samples were crystallized from the melt as well as the quenched state. The Wabash hot-press used for crystallization was calibrated in atactic polystyrene (aPS) melt using an external thermocouple.

The as-molded samples were put in an aluminum frame, designed for holding the dog-bone samples, and melted in a furnace. The samples to be cold crystallized were immediately quenched in an ice bath and then transferred to the preheated hot-press. The cold crystallization temperatures were 180°C, 190°C and 220°C. For melt crystallization, the samples from the furnace were transferred directly to the hot-press preheated to the crystallization temperature. Melt crystallization was done at 220°C, 245°C and 255°C.

Injection molded samples of neat sPS could not be crystallized in the dog-bone shaped aluminum frame because of their brittleness. Therefore, the neat sPS sheets, compression molded in the rectangular frame, were subjected to the same crystallization treatment. Finally dog-bone samples conforming to ASTM D-638 (type M-II) standard were machined from these rectangular sheets.

The crystallization times were determined from spherulite impingement times observed under the polarized optical microscope. Melt crystallized samples were crystallized for 50% time longer than the time taken for spherulite impingement. In case of the quenched blends it was observed that during crystallization of the quenched blends, a fast primary stage is followed by a slow secondary stage. It resulted in a second exotherm in the blend samples isothermally crystallized in the DSC. Therefore, the quenched samples were put for twice the time required for the completion of the second DSC enxotherm. The times required for the spherulite impingement and the DSC exotherms for crystallized sPS50PPO blend are shown in Figure 3.1.

Film samples for Dynamic Mechanical Analysis (DMA) and Scanning Electron Microscopy (SEM) were crystallized by the exact same procedure used for the bulk samples. Instead of using the dog-bone shaped mold, approximately 0.3 mm thick films were made in mold made from layered aluminum foil.

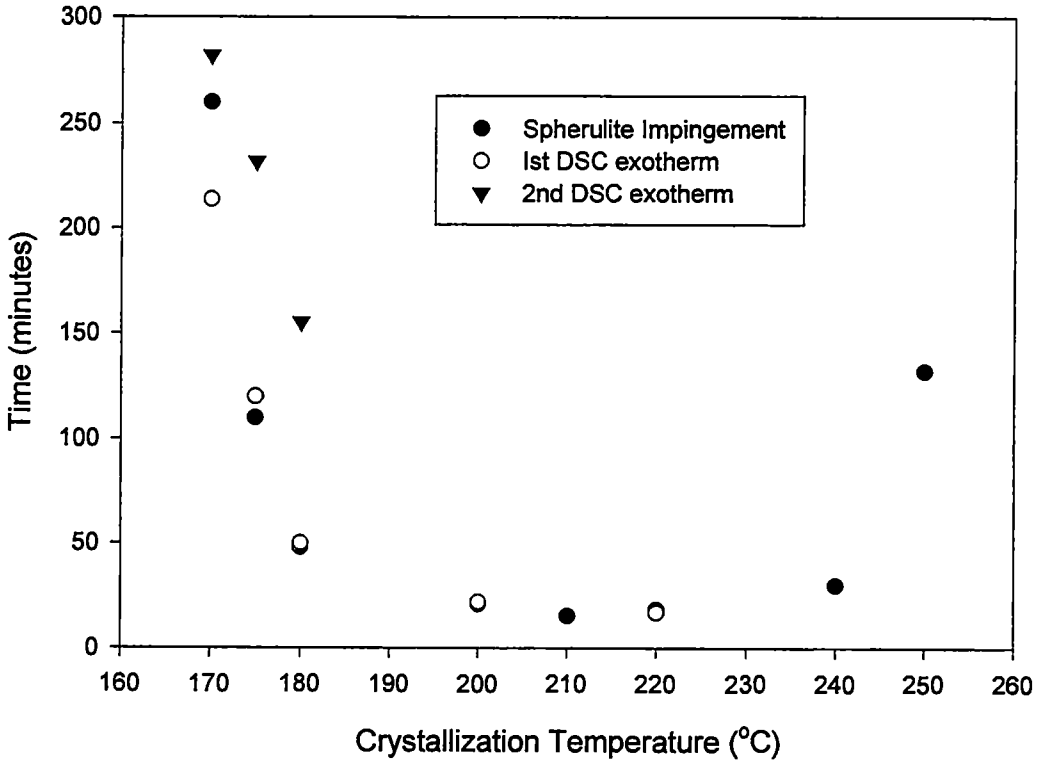

Figure 3.1 **Crystallization times for sPS50PPO blend by microscopy and DSC.**

3.5 Differential Scanning Calorimetry (DSC)

Thermal analysis of the quenched blends was carried out in a Perkin-Elmer DSC 7 in a purging nitrogen atmosphere. After the baseline run without any sample pans, the instrument was calibrated for melting onset and heat of fusion of pure iridium. 6 to 8 mg of the blend sample was heated to 305°C, at the rate of 20 °C minute^{-1}, and kept at that temperature for 8 minutes to ensure complete melting. The sample pan was then taken out of the sample chamber and quickly quenched in liquid nitrogen. It was then heated from 25°C to 300°C at the rate of 10°C minute^{-1}. The glass transition temperature was taken to be the temperature at the center of the transition.

3.6 Wide Angle X-Ray Diffraction (WAXD)

WAXD studies were performed on the quenched, cold and melt crystallized blend samples to calculate the crystallinity index and study the phase changes in the sPS after blending. Rigaku Diffractometer, in reflection mode, was used with CuKα (λ=1.542 Å) radiation. A silicon standard (2θ = 28.465°) was used to calibrate the instrument. The operating voltage and current of the tube were kept at 35kV and 30mA respectively. The 2θ scan-range was 5°- 40° and the scan step-size was 0.03°.

The Peak Fit ® program was used to fit Gaussian peaks for reflections from crystalline and amorphous regions by using the second derivative method. In the first step, diffraction pattern of the quenched (essentially amorphous) sample of the same

composition blend was fit with the Gaussian peaks. It served as a template to identify the position of the amorphous phase peaks in that blend composition. Efforts were made to limit the number of amorphous peaks to a manageable number (usually 5-6). In the second step, the diffraction pattern of the crystallized blends was subjected to the same treatment. Then the program was used to locate the amorphous peaks in the crystallized samples. If the program did not select a particular amorphous peak, it was added manually. Finally the heights and FWHM (full width half maximum) widths of all the peaks were scaled such that the total intensity at any 2θ angle was the sum of the intensities of all the peaks at that angle. During the scaling it was tried to ensure, as far as possible, that the changes in heights and FWHM remained in the same original proportion before scaling.

The relative crystallinity (or Crystallinity Index) was calculated from the ratio of the areas of the crystalline peaks to the total area under the scattering curve.

3.7 Density Gradient Column (DGC)

A sodium bromide - water density gradient column was made for the density range of 1.02-1.08 g/cm^3, according to the ASTM D1505-85 standard method. After allowing 24 hours for equilibrium to establish, reference beads of known densities were placed in the column. The column was calibrated with these standard beads and a linear gradient (correlation coefficient = 0.99) was obtained. Pure sPS, PPO and blend samples, crystallized at different temperatures, were then placed in the column. The

position of these samples was measured after 24 hours. The density of the samples was then calculated by linear interpolation.

3.8 Dynamic Mechanical Analysis (DMA)

Dynamic Mechanical relaxation Measurements were made on a Rheovibron Visco-elastometer (Toyo Instruments), working in the tensile mode. The storage modulus E' and loss tangent tanδ were obtained at fixed frequencies of 1.1 Hz, 11 Hz and 110Hz, but only 1.1 Hz data was used for the analysis. A temperature sweep from 70°C (or 75°C) to 250°C was performed at a heating rate of 1°C. The specimens used were rectangular strips, approximately 3 mm wide, 0.3 mm thick and 25 mm long. A variable tension of 16-21 grams was applied to all the samples. Quenched samples were predominantly amorphous and required smaller tension (16 or 17 grams) to prevent the elongation of the sample from exceeding the maximum allowed length in the DMA sample chamber. The crystallized samples were subjected to 20-21 grams of tension.

3.9 Scanning Electron Microscopy (SEM)

3.9.1 Sample Preparation

The films of crystallized samples and tensile fracture surface specimens were etched in 66% and 33% solutions of 1,2-dichlorobenzene in amyl acetate, at room temperature, in an ultrasonic bath for 35 s each. These were then rinsed in amyl

acetate to avoid the precipitation of sPS. Finally the films were washed in methanol, rinsed in water and dried.

This etching process dissolved the amorphous material in the crystallized blend samples and provided the contrast for the observation of the crystalline bundles. The removed amorphous regions appeared as voids in the SEM micrographs.

All samples were mounted on a stub and sputtered with gold in Technics Hummer I sputter before observation.

3.9.2 Observation

The specimens were observed in a Cambridge electron microscope (Oxford Instruments) and a Hitachi S-3000N (Hitachi) electron microscope. In both the microscopes an accelerating voltage of 15 kV was used.

The Scion Image® program was used for making the bundle thickness and spacing measurements from the SEM micrographs. At least 50 measurements of a particular feature were made from a micrograph and the average values were reported.

3.10 Tensile Testing

All tensile testing was done on a Thwing-Albert EJA-2000 tensile tester. All tests were done in a thermally conditioned room at 23 ± 2°C temperature and

approximately 60% relative humidity. Dog bone shaped samples of the crystallized blends (ASTM –1708-95) were tested at cross head speed of 1mm/min. Crystallized neat sPS samples (ASTM D-638 (M-II)) were tested at crosshead speed of 5.0 mm/min. In all the tests the strain rate was 6.67×10^{-4} s^{-1}. At least five samples of each composition were tested.

Chapter 4

RESULTS

4.1 Differential Scanning Calorimetry

The DSC scans of melt-quenched blends of different compositions and neat homopolymers are shown in Figure 4.1. A well defined, composition-dependent glass transition is observed at all the compositions. Crystallization temperature (T_c), (as observed from the temperature of the crystallization exotherm), and the temperature of the melting endotherm also vary with the composition. Increase in PPO content leads to an increase in the T_c, and a depression in the melting point. The areas under both the crystallization exotherm and the melting endotherm also decrease. For the sPS50PPO blend and neat PPO, no crystallization and melting peaks are seen.

4.2 Dynamic Mechanical Analysis

4.2.1 Quenched Blends

The mechanical loss tangent (tanδ) of the quenched sPS/PPO blends obtained from the DMA measurements at 1.1 Hz is shown in the Figure 4.2. A single, composition-dependent relaxation peak is seen in all the scans. Neat sPS, and all the blends show a long horizontal shoulder to the relaxation peak. This shoulder may be due to cold crystallization during heating or relaxation of a second amorphous phase present in the segregated blend.

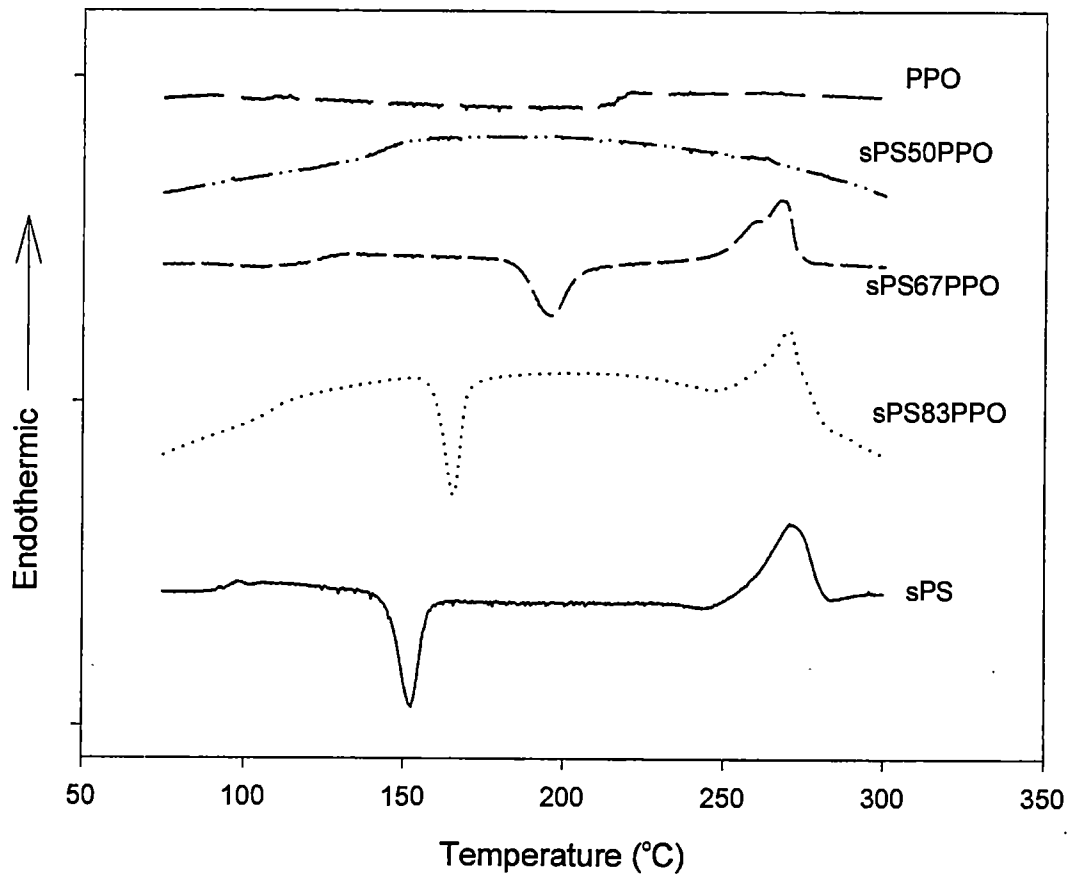

Figure 4.1. DSC curves for quenched sPS/PPO blends.
Heating Rate = 10°C/minute.

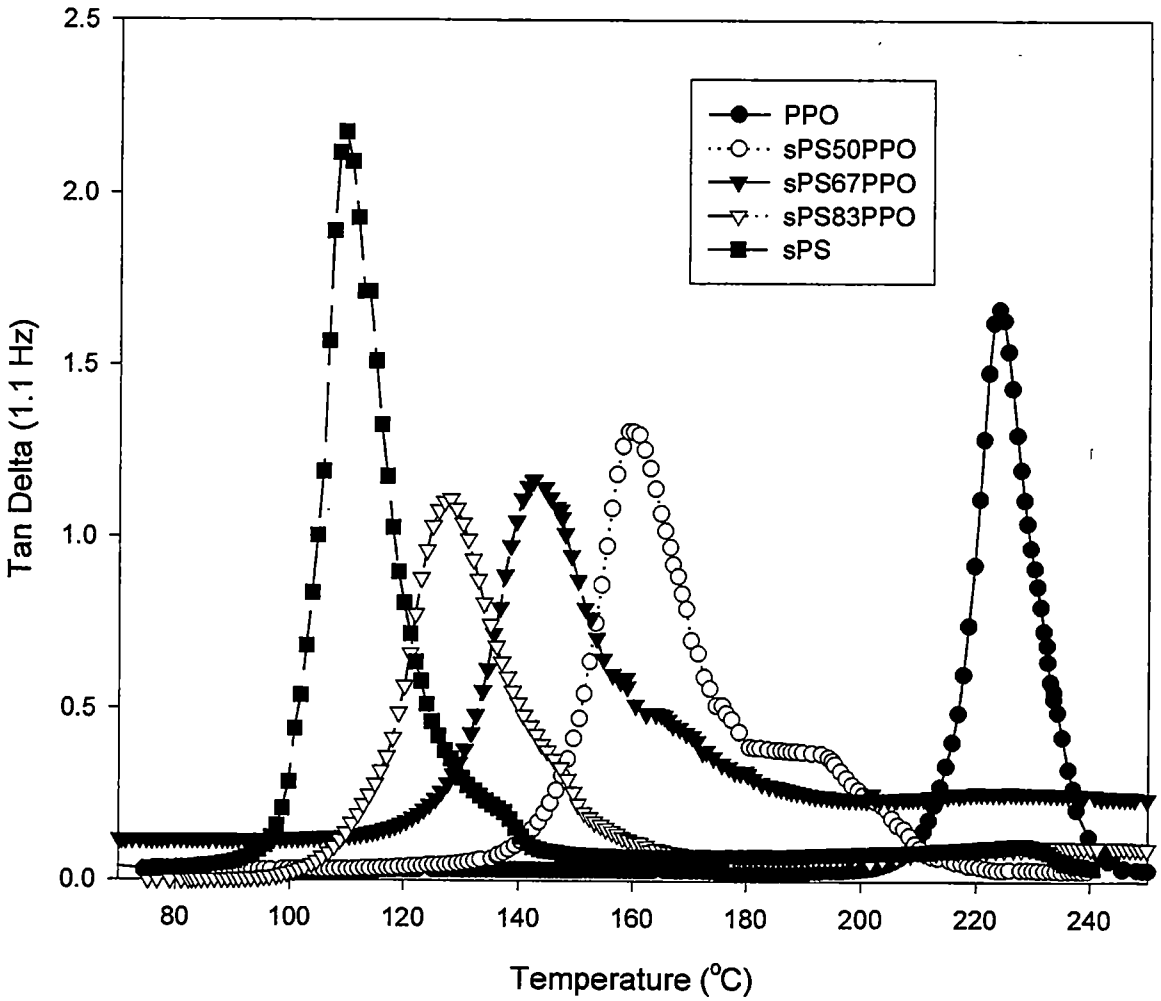

Figure 4.2. DMA loss tangent (tanδ) of Quenched sPS/PPO blends at 1.1 Hz.

4.2.2 Cold Crystallized Blends

The loss tangent peaks for the different composition sPS/PPO blends cold crystallized at 180°C, 190°C and 220°C are shown in figures 4.3 through 4.5 respectively. The effect of the crystallization temperature on the relaxation of cold crystallized sPS50PPO blends is shown in Figure 4.6.

In all the DMA scans of the crystallized blends shown in the Figures 4.3 through 4.6, the horizontal crystallization and modulus recovery shoulders, observed in the scans of the quenched blends, are absent. Instead, the DMA scans of all the sPS50PPO and sPS67PPO blends, crystallized at different temperatures, show a distinct shoulder to the major relaxation peak observed in the quenched amorphous blends. Interestingly, this shoulder is very small and difficult to observe in the DMA scans of crystallized sPS83PPO blends.

For the sPS50PPO and sPS67PPO compositions, the blends crystallized at 220°C (highest crystallization rate) show a relaxation peak with the smallest shoulder (Figure 4.5). The blends crystallized at lower temperatures (180°C and 190°C) show much broader primary relaxation peaks with more distinct shoulders (Figures 4.3 and 4.4). Again both the position (temperature) and width of relaxations is composition dependent. Higher PPO content increases the relaxation temperature and narrows the transition. Figure 4.6 clearly shows that blends crystallized slowly (at lower temperatures) show transitions at higher temperatures with more prominent shoulders.

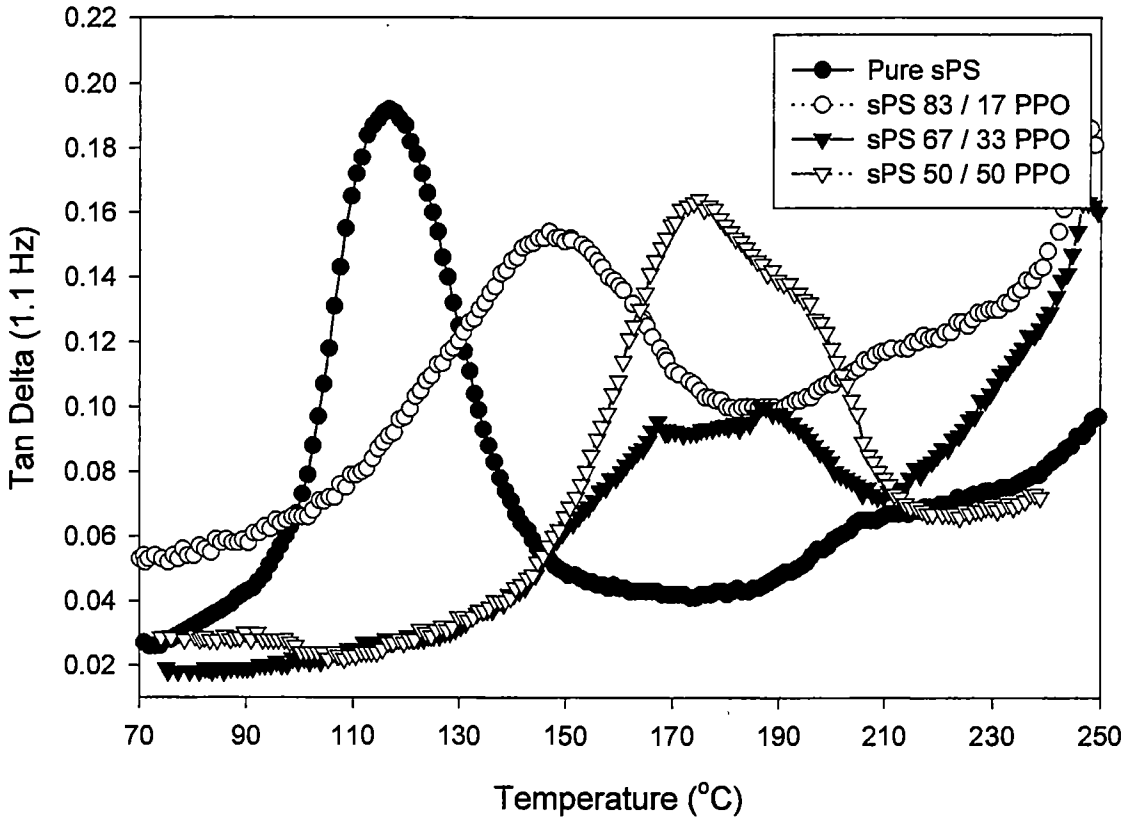

Figure 4.3. DMA loss tangent (tanδ) for sPS/PPO blends crystallized at 180°C.

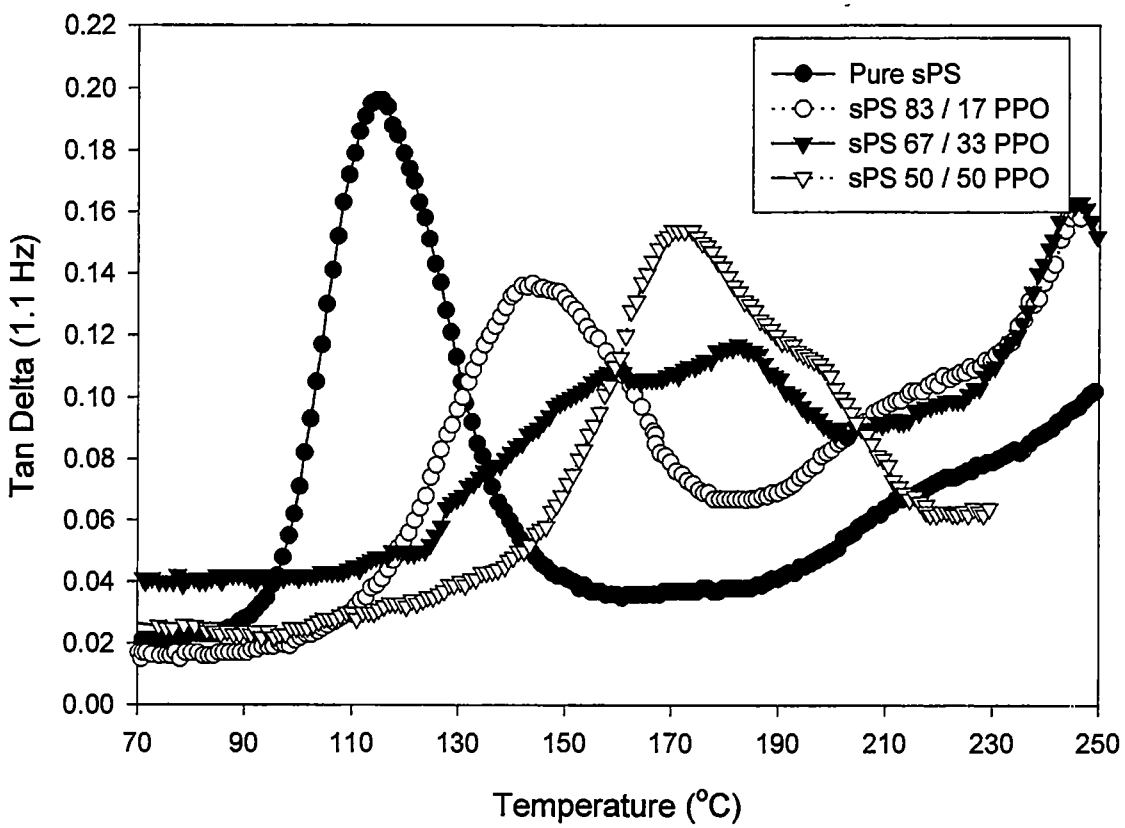

Figure 4.4. DMA loss tangent (tanδ) for sPS/PPO blends cold crystallized at 190°C.

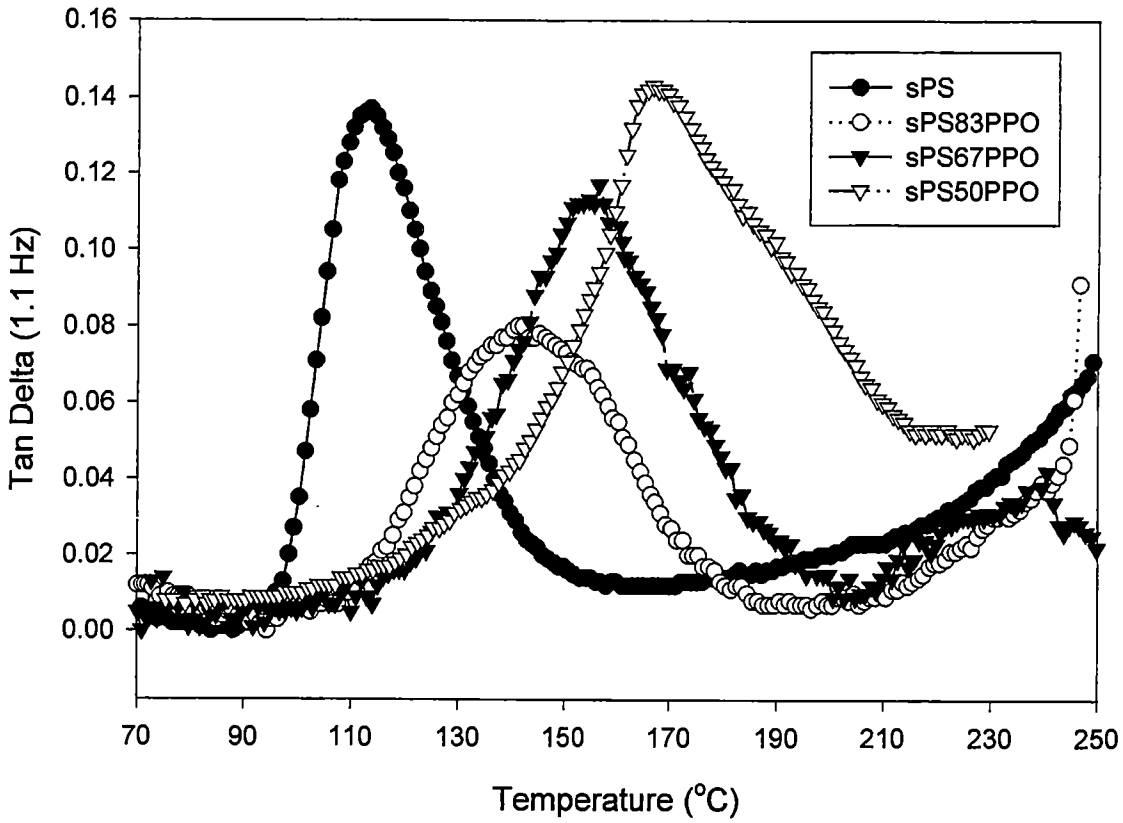

Figure 4.5. **DMA loss tangent (tanδ) for sPS/PPO blends cold crystallized at 220°C.**

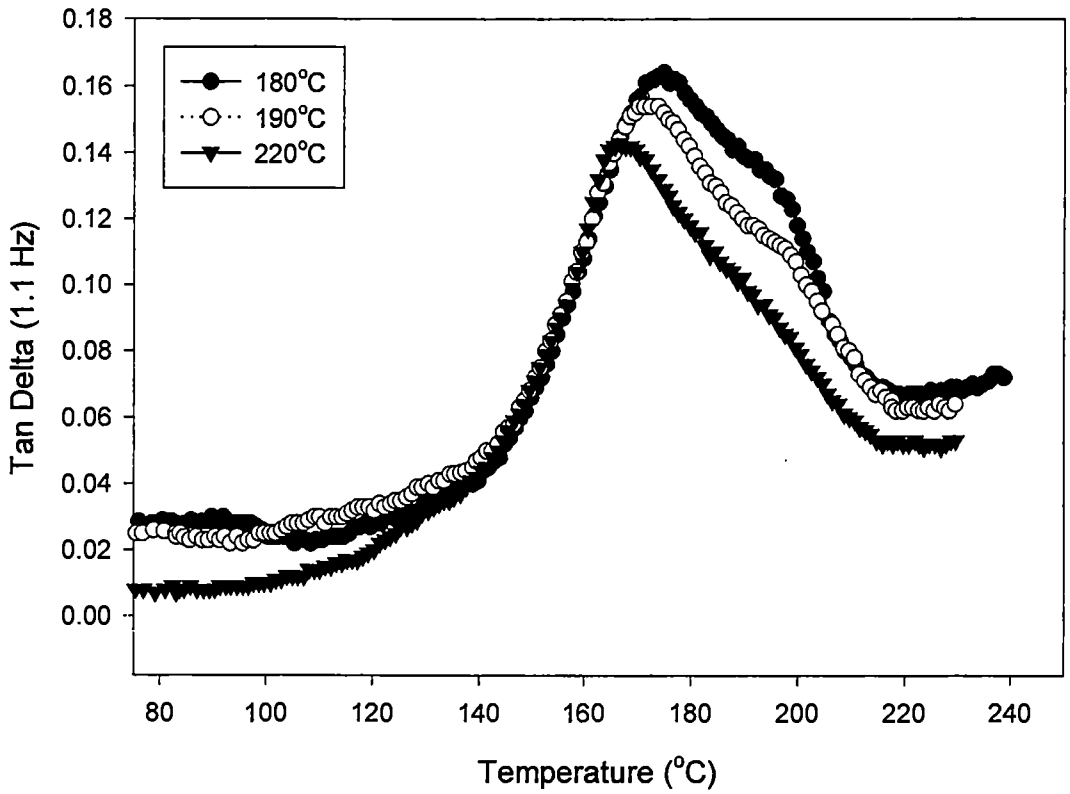

Figure 4.6. DMA loss tangent (tanδ) of cold crystallized sPS50PPO blends.

4.2.3 Melt Crystallized Blends

The mechanical loss tangent (tanδ) scans for different composition sPS/PPO blends melt crystallized at 220°C, 245°C and 255°C are shown in Figures 4.7 through 4.9. The variation in the tanδ for sPS50PPO blends crystallized at different temperatures is shown in Figure 4.10.

All scans show a primary composition-dependent relaxation peak. Again, sPS50PPO and sPS67PPO blends also show distinct shoulders to the primary relaxation peak. These shoulders are more prominent in the blends crystallized at higher temperatures, which correspond to lower supercoolings and lower crystallization rate. The increase in PPO content increases the transition temperatures and narrows their width. For a single composition blend (Figure 4.10), slower crystallization decreases the transition temperatures of the primary relaxation and increases the temperatures of the secondary relaxation. In general, for both cold and melt crystallized blends, slower crystallization leads to more pronounced shoulder.

4.3 Wide Angle X-Ray Diffraction

4.3.1 Polymorphic changes in sPS

As stated before, sPS exhibits a very complex polymorphic behavior. It exists in at least four different polymorphic forms, termed as α, β, γ, and δ. Moreover, different structural modifications of phases α and β may exist. WAXD studies of the sPS and

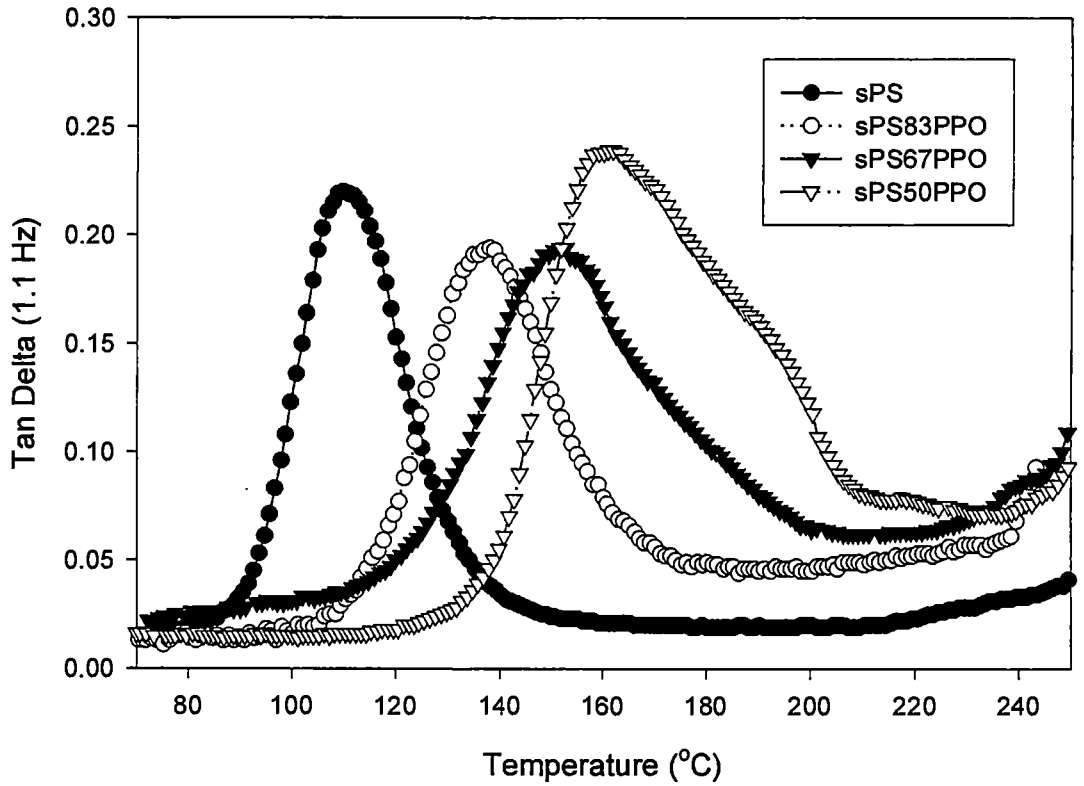

Figure 4.7. **DMA loss tangent (tanδ) of sPS/PPO blends melt crystallized at 220°C.**

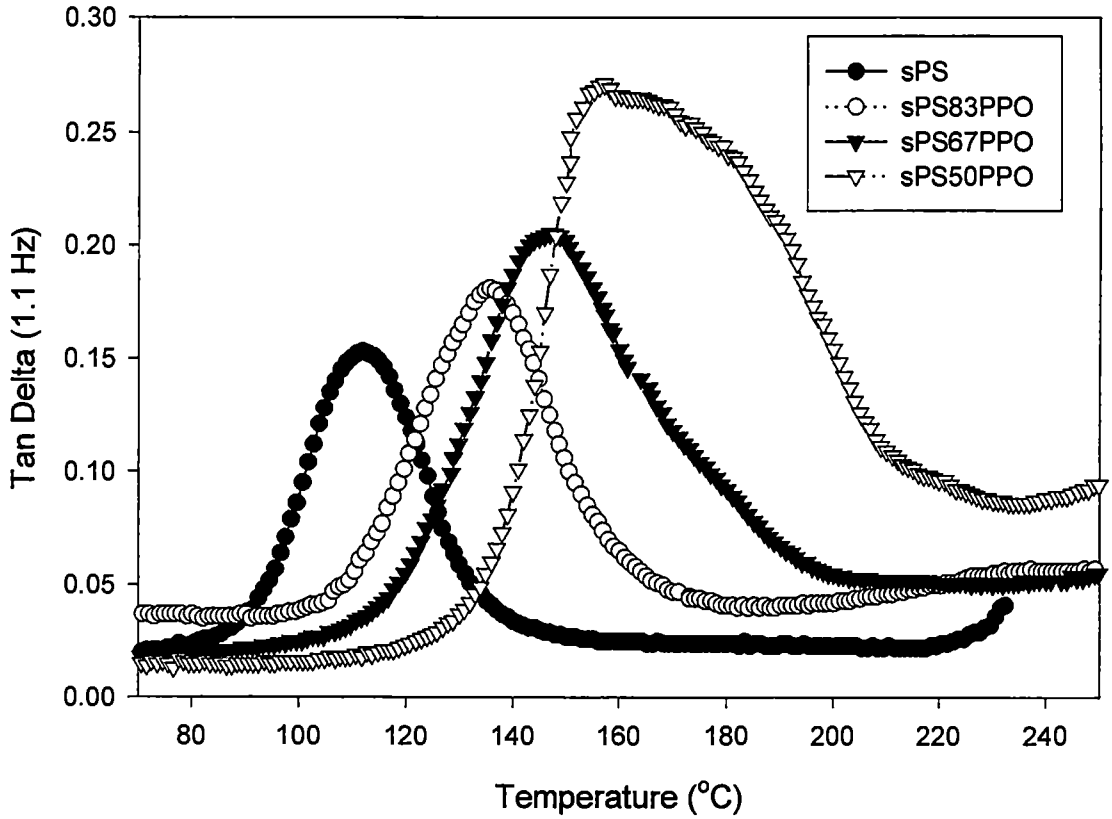

Figure 4.8. **DMA loss tangent of sPS/PPO blends melt crystallized at 245°C.**

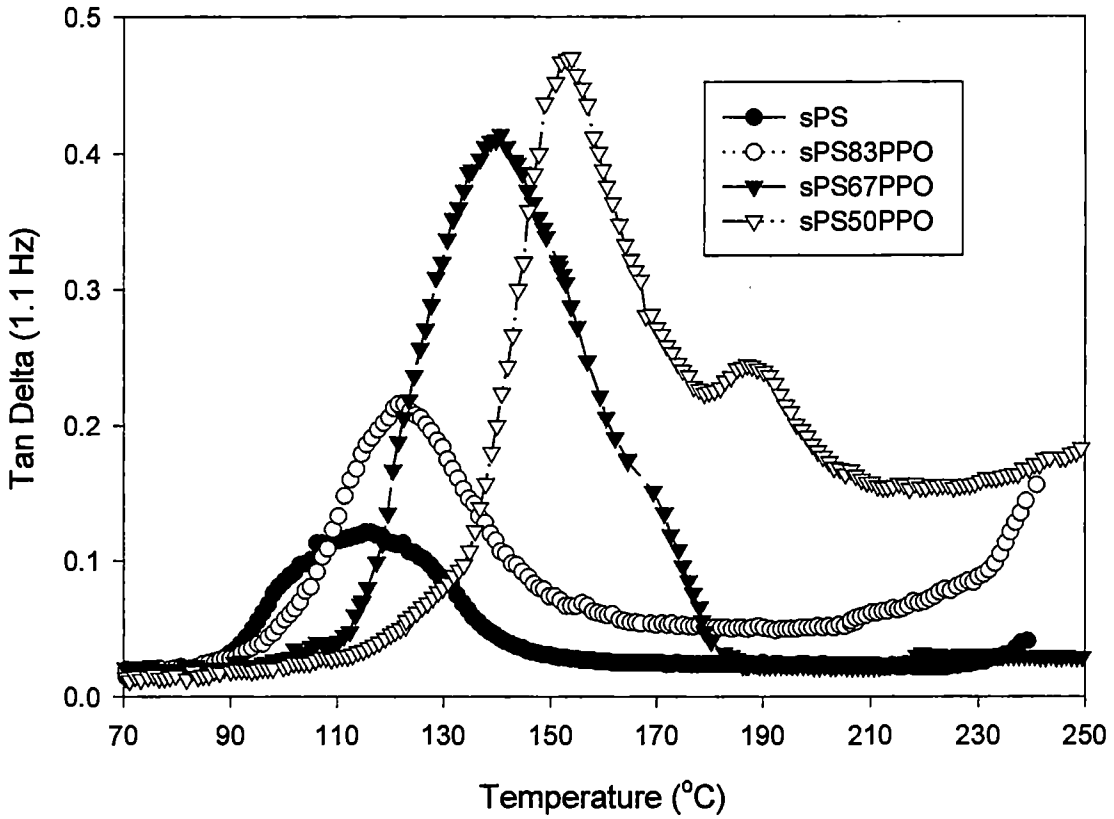

Figure 4.9. **DMA loss tangent (tanδ) of sPS/PPO blends melt crystallized at 255°C.**

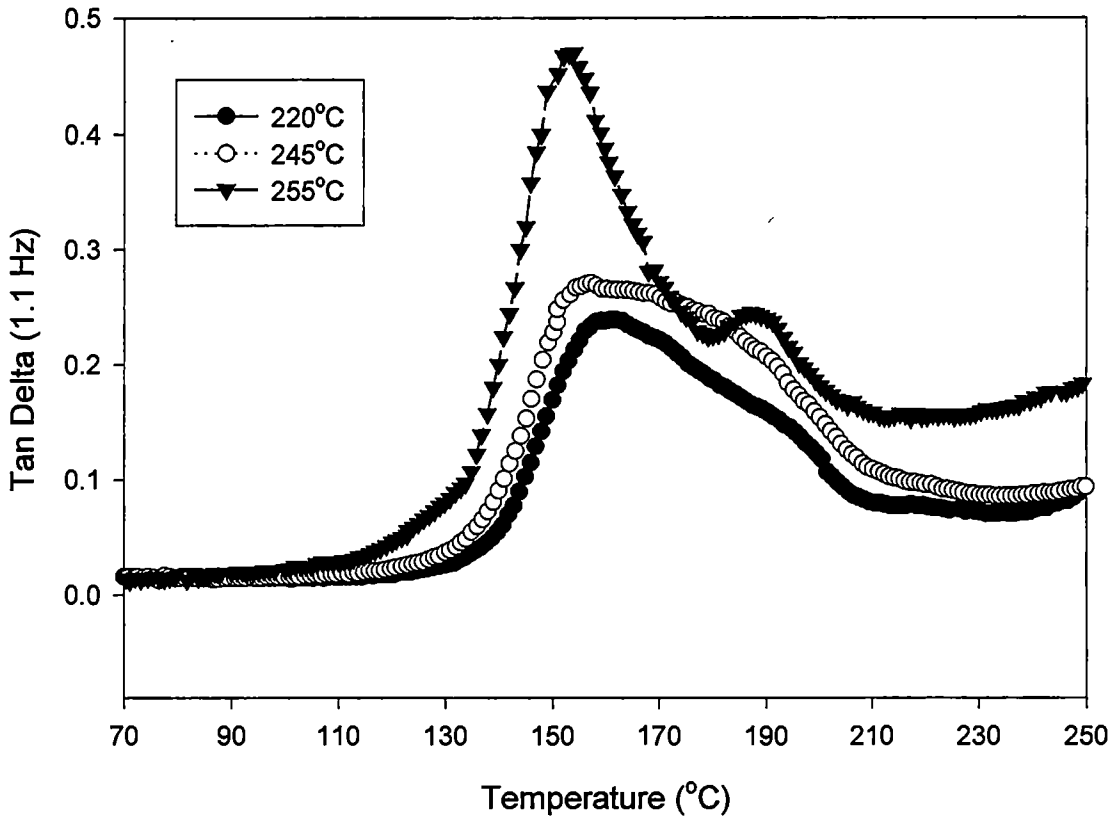

Figure 4.10. DMA loss tangent (tanδ) of melt crystallized sPS50PPO blends.

its blends [51] have listed the typical reflection peaks of the phases. The typical peaks for the α form are at 2θ angles 6.7°, 11.7°, 14.0°, 15.6° and 18.0°. The β form shows the major reflections at 2θ angles 6.1°, 12.3°, 18.6° and 21.2°. The limiting ordered form of phase α, given by α', has typical reflections at 2θ angles 6.8°, 10.3°, 14.0°, 15.6° and 17.0°. Since all these reflections are quite close to each other it is not easy to assign all of them definitely to a particular phase. Among all these reflections the reflections at 2θ angles of 15.6° for the phases α/α', and 21.2° for the β phase are most important and easy to follow.

4.3.1.1 Melt Crystallized Blends

The WAXD patterns for neat sPS, sPS67PPO and sPS50PPO blends melt crystallized at 220°C, 245°C and 255°C are shown in Figures 4.11 through 4.13. The reflection peaks are at 2θ angles slightly higher than the listed typical peaks. More interestingly, a change in the composition of the phases is indicated. At high PPO compositions almost all the β phase reflections are present. Most important among them are the peaks at 2θ angles 13° and 19°. The characteristic α/α' peak around 16° is suppressed. At a particular crystallization temperature, with the decrease in the PPO content from 50% to 33%, there is a clear shift from β phase reflections to α and α' phase reflections. There are several indications to this effect. The typical α/α' peaks around 16° and 7° increase in intensity, reflections around 18-21° occur at lower 2θ angles and the shoulder to the maximum intensity peak around 21° disappears with the increasing sPS (or decreasing PPO) content. In pure sPS WAXD patterns all α/α'

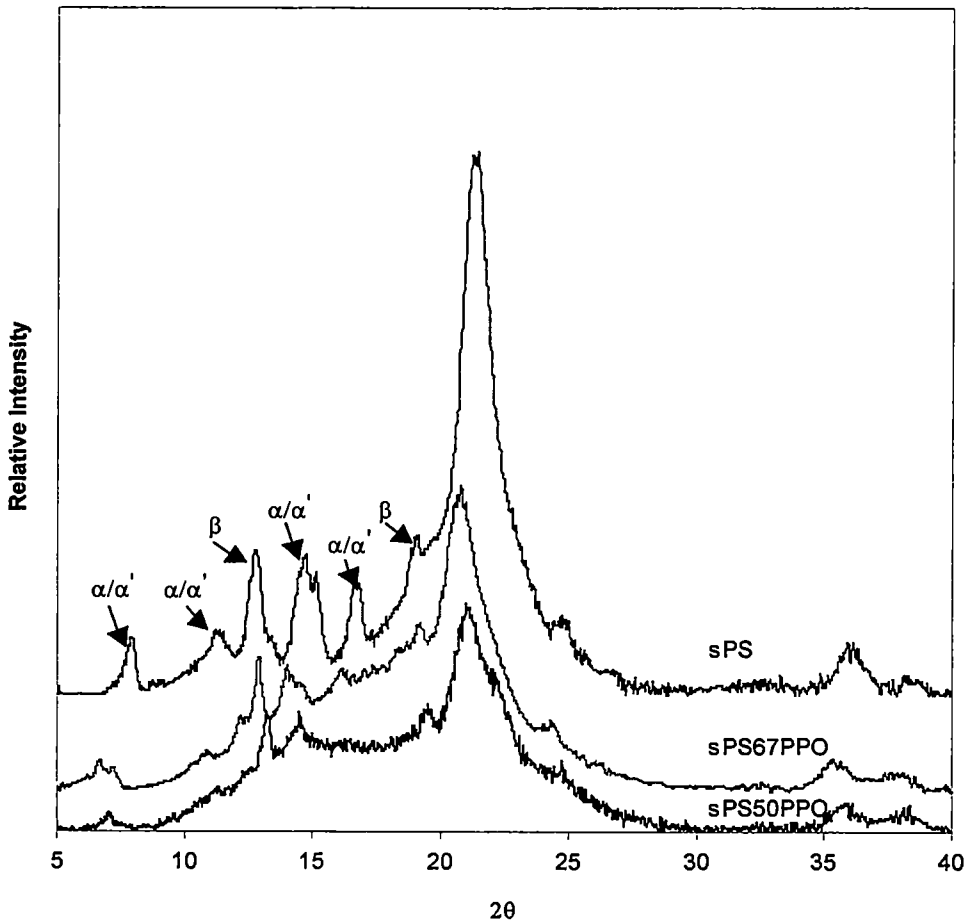

Figure 4.11. WAXD pattern of sPSPPO blends melt crystallized at 220°C.

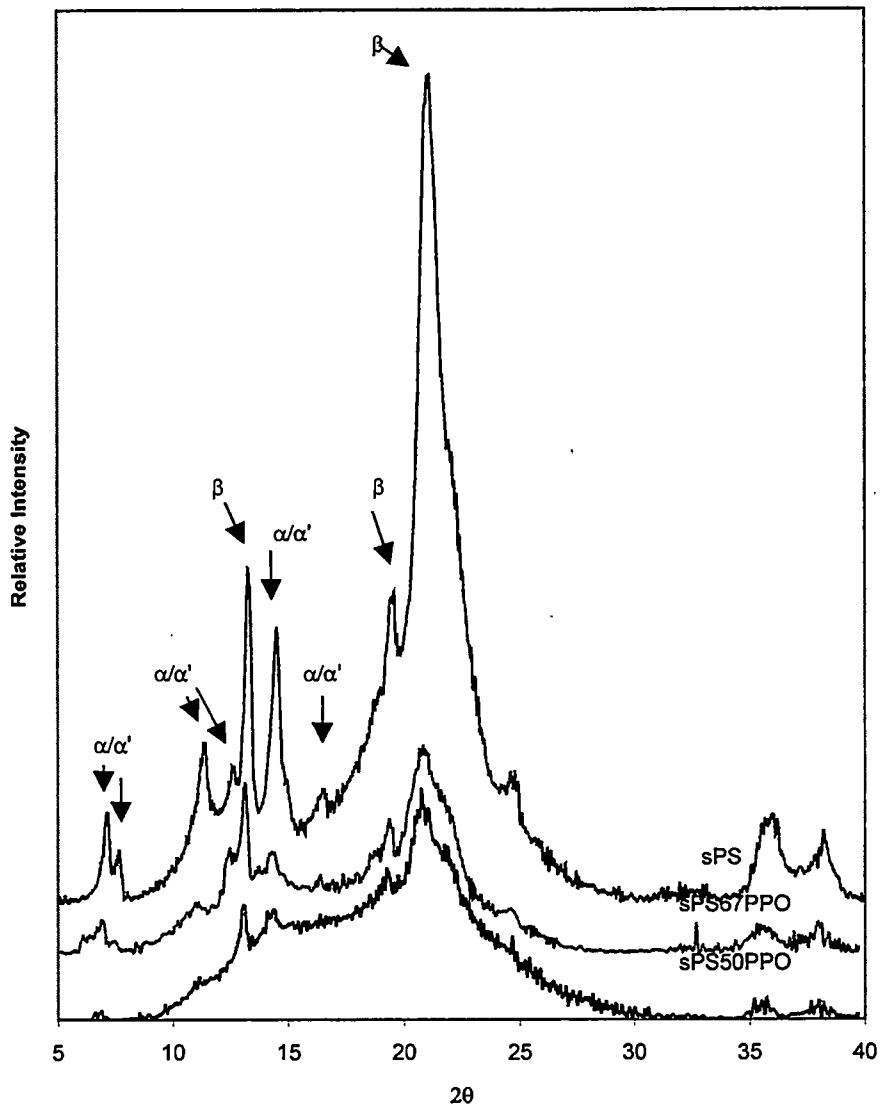

Figure 4.12. WAXD patterns of sPS/PPO blends melt crystallized at 245°C.

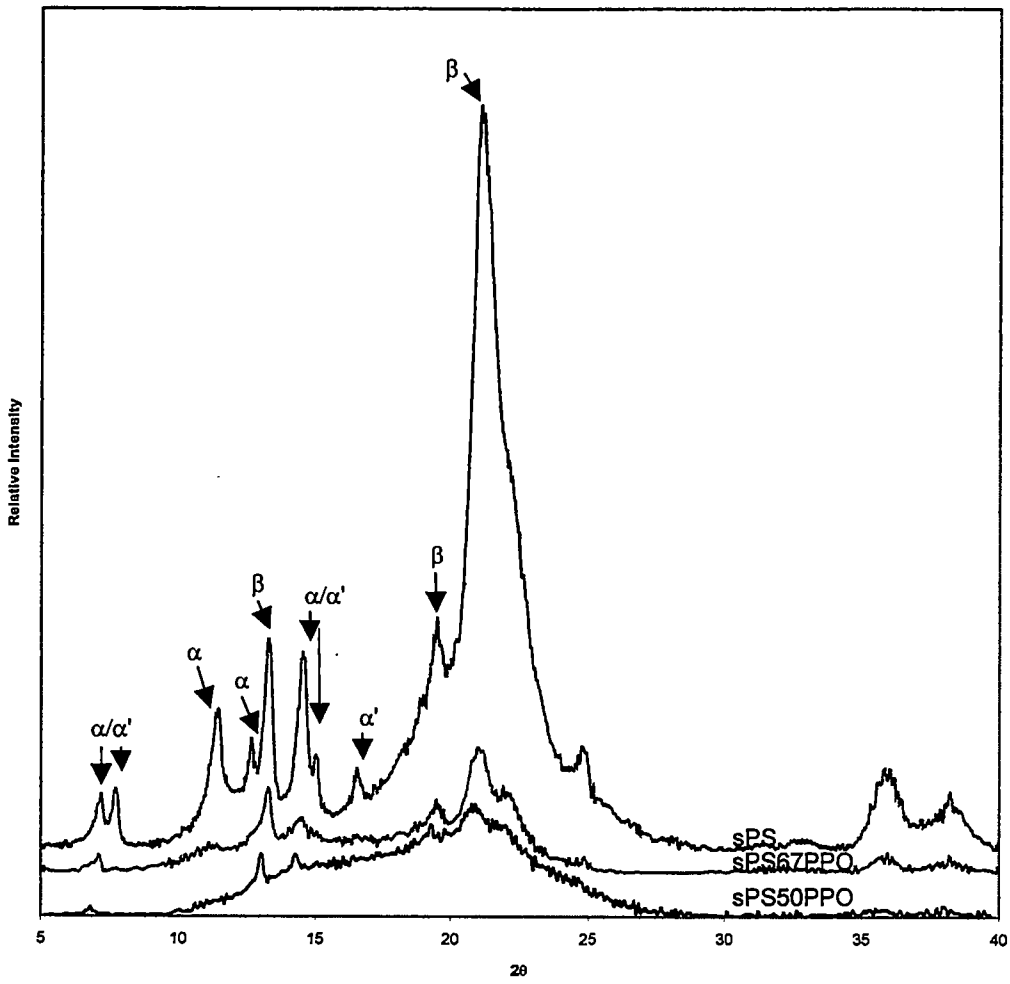

Figure 4.13. WAXD patterns of sPS/PPO blends melt crystallized at 255°C.

peaks are present. WAXD patterns of sPS50PPO blends melt crystallized at different temperatures are shown in Figure 4.14. The change in crystallization temperature does not seem to induce any phase changes. All the peaks suggest predominant presence of β/β' forms.

4.3.1.2 Cold Crystallized Blends

The WAXD patterns of the different composition sPS/PPO blends cold crystallized from the quenched state are shown in the Figures 4.15 through 4.17. The effect of blend composition on the change in phase composition is again indicated. In sPS50PPO blends, almost all the reflections present can be attributed to the β phase. With a decrease in PPO content in sPS67PPO blends, typical α/α' peaks around 2θ angles 7°, 14°-16.5° peaks increase in intensity. Also there is a decrease in the 2θ angles of peaks around 19°. In pure sPS pattern, no shoulders to the major β reflection around 21° are seen. Figure 4.18 shows the effect of crystallization temperature on crystal forms in sPS50PPO blends. With decrease in crystallization temperature (slower crystallization), while the β phase reflections around 2θ angles 13° and 19.5° are depressed, the α/α' phase reflections at approximate 2θ angles 7° and 15° increase in intensity. This trend suggests that, unlike for the melt-crystallized blends, the crystallization temperature also influences the polymorphic behavior of the sPS; the α/α' crystal form being favored more than the β form.

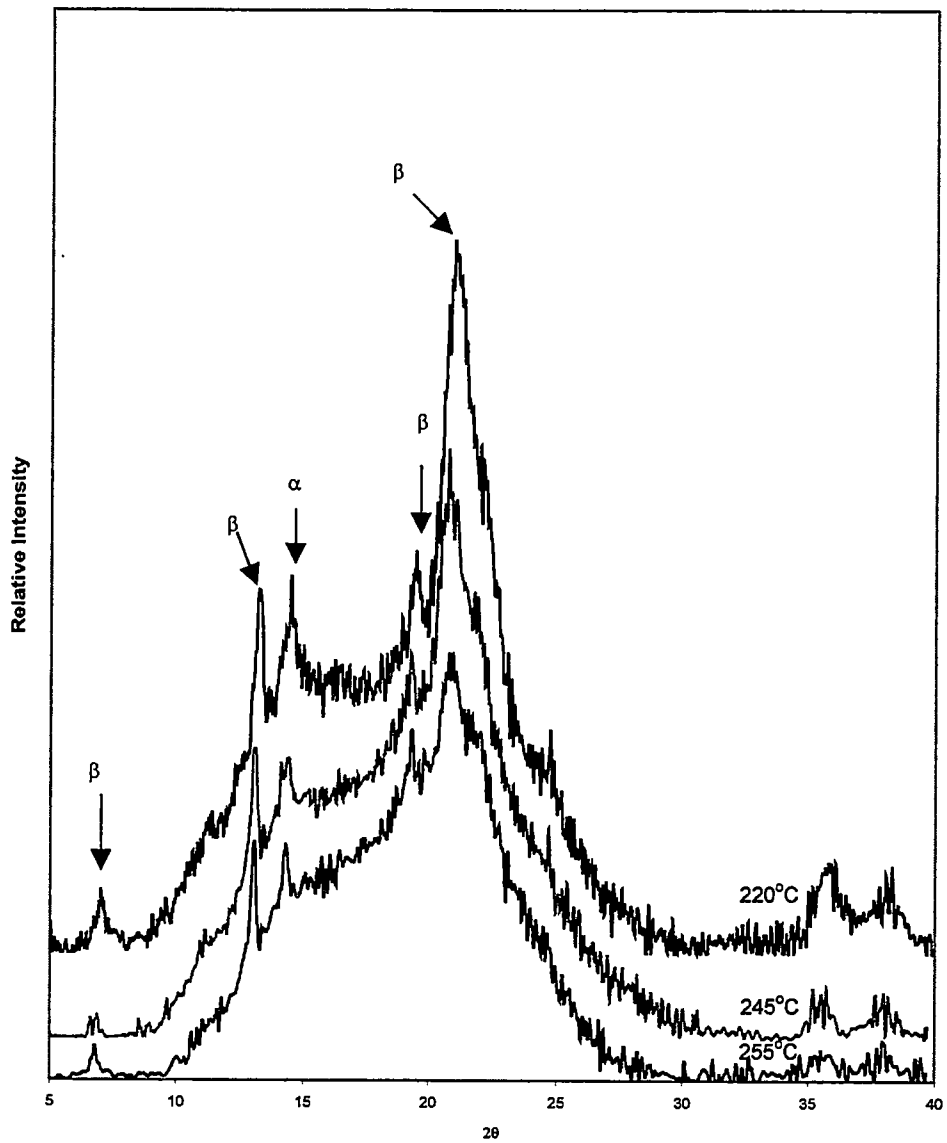

Figure 4.14. WAXD patterns for melt crystallized sPS50PPO blends.

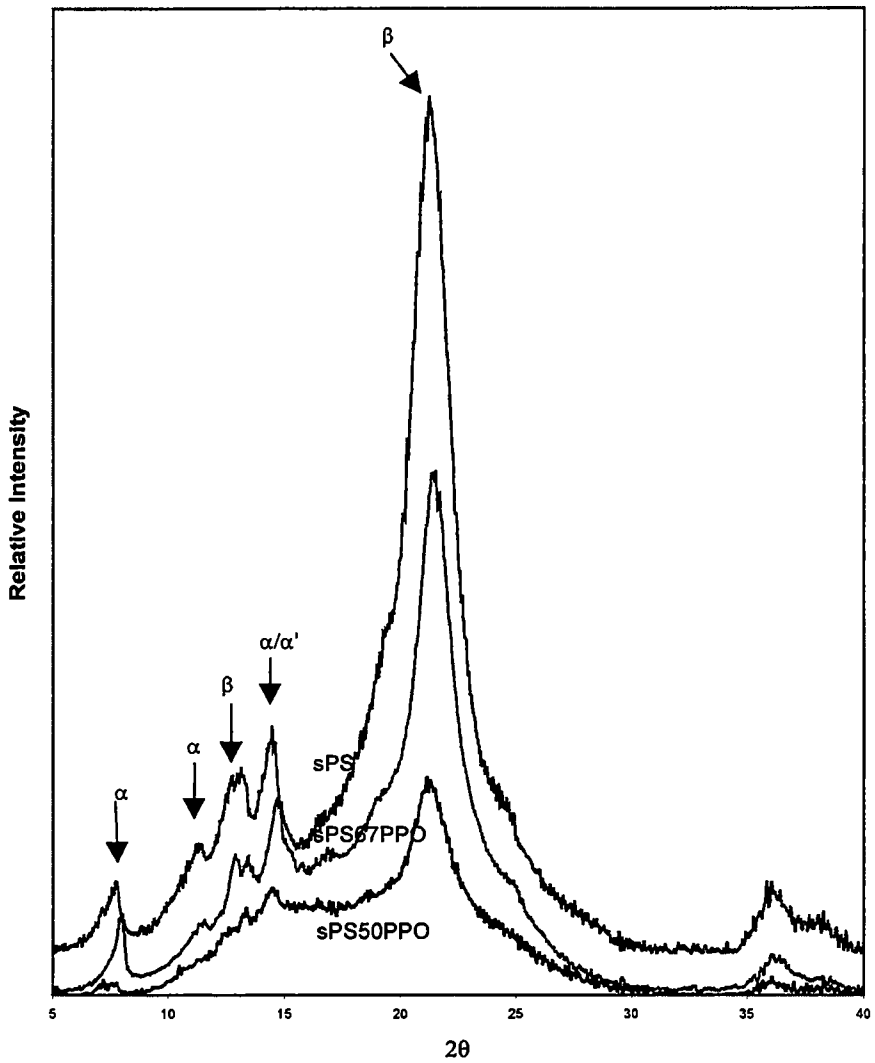

Figure 4.15. WAXD patterns of sPS/PPO blends cold crystallized at 180°C.

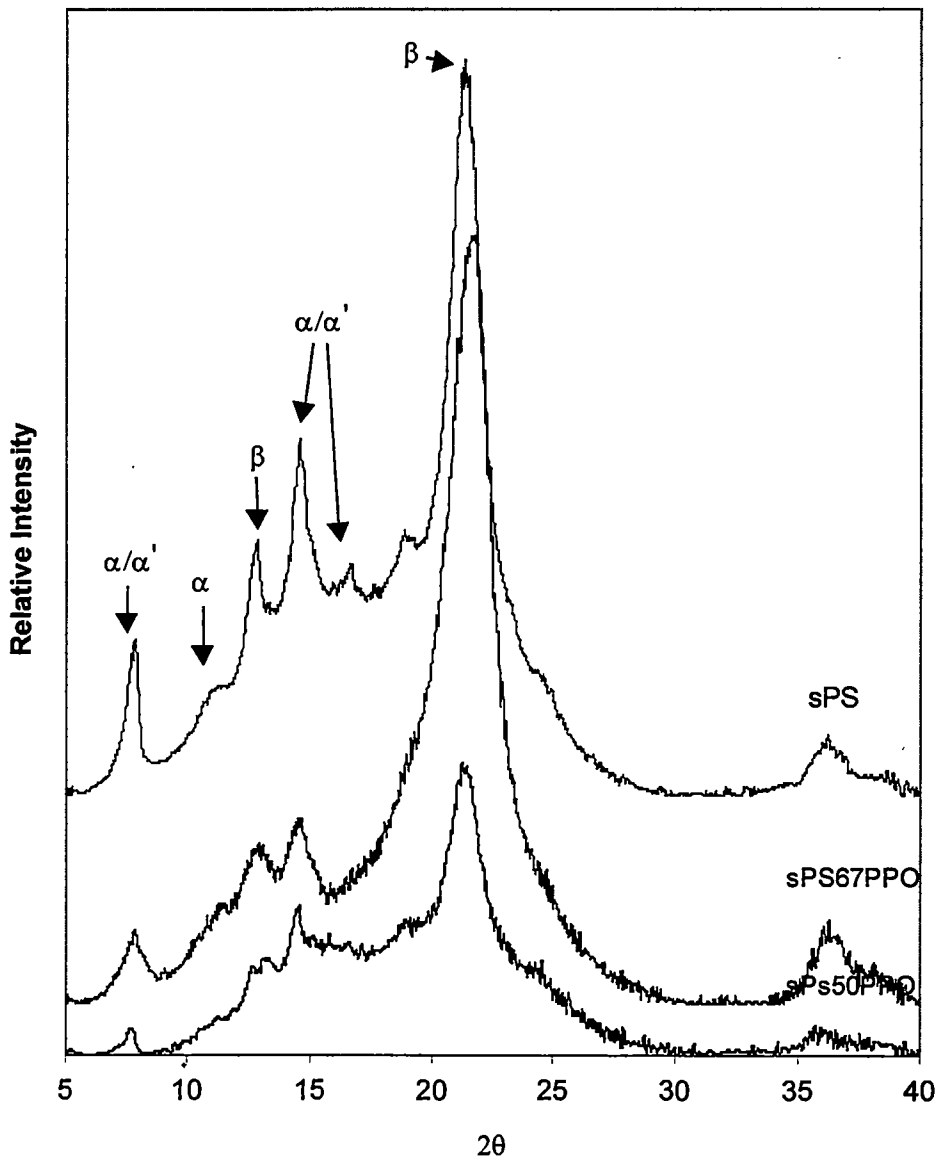

Figure 4.16. WAXD patterns of sPS/PPO blends cold crystallized at 190°C.

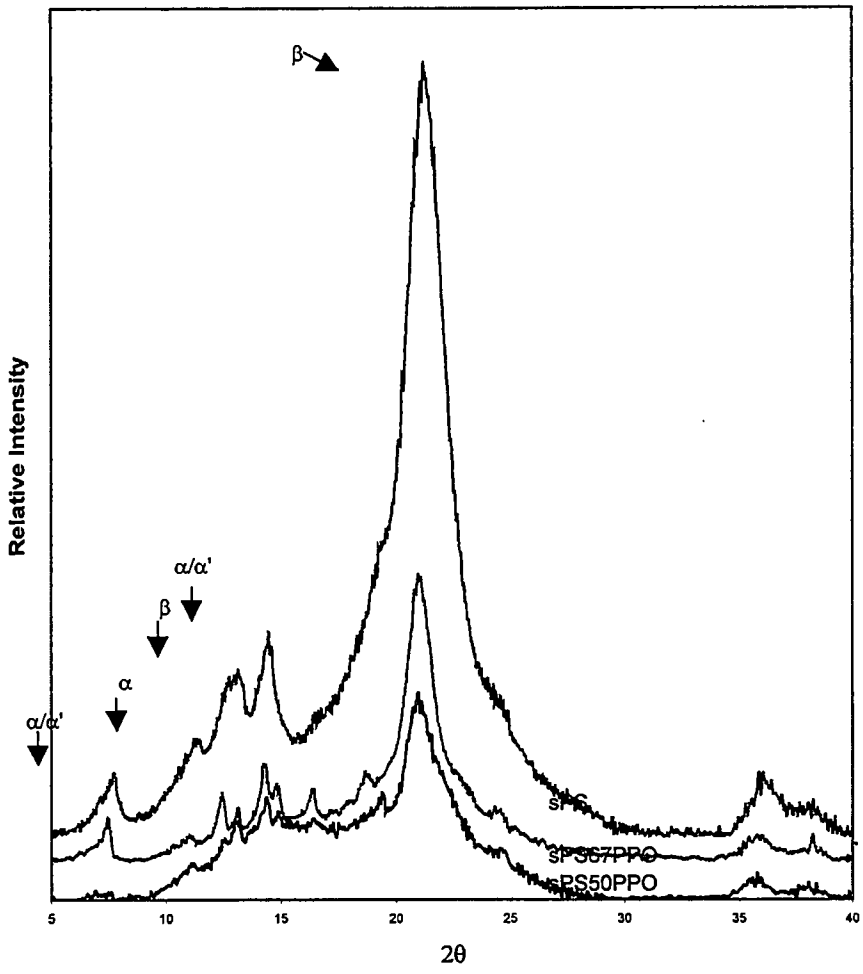

Figure 4.17. WAXD patterns of sPS/PPO blends cold crystallized at 220°C.

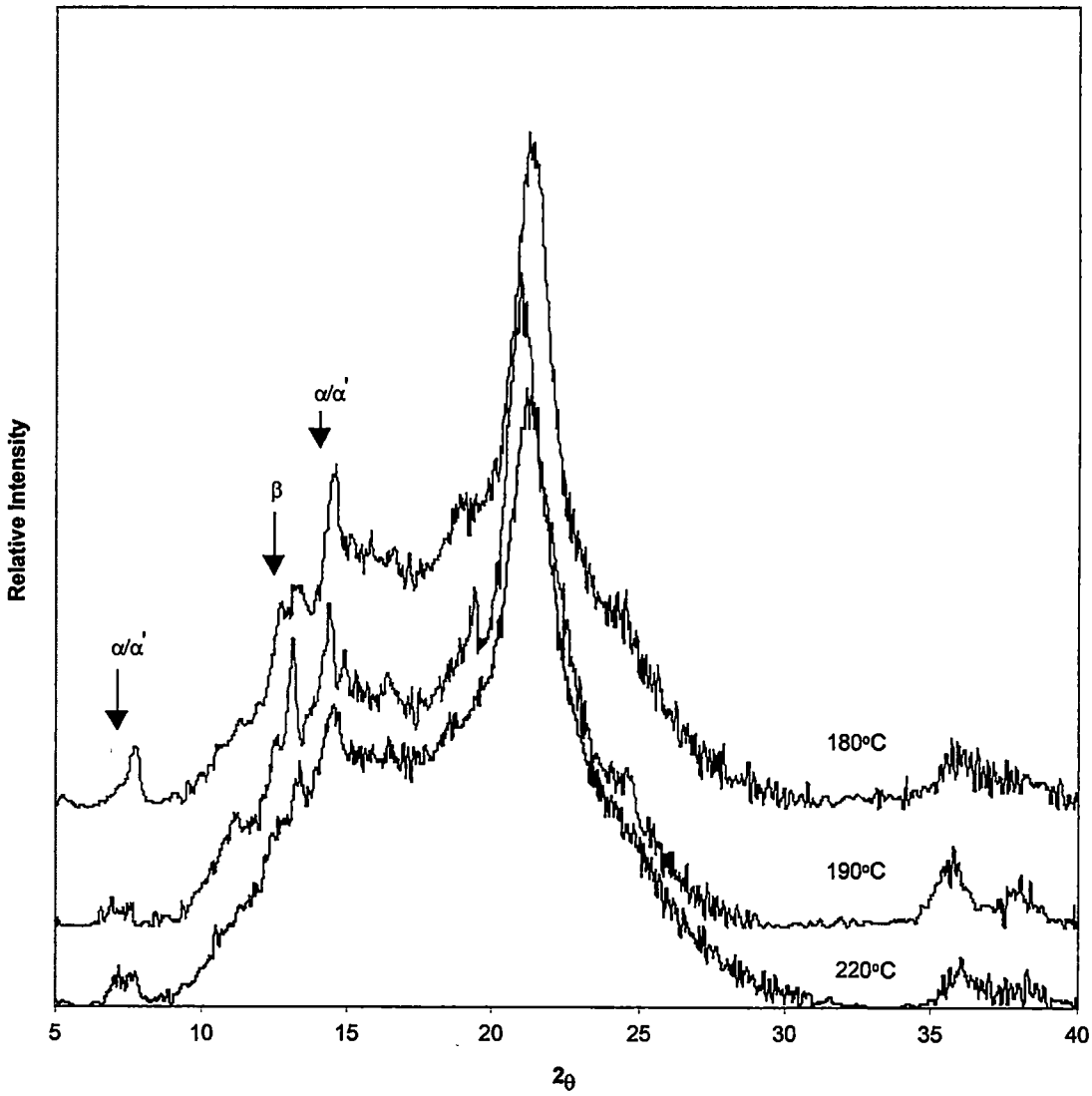

Figure 4.18. WAXD patterns for cold crystallized sPS50PPO blends.

4.3.2 WAXD Crystallinity

The bulk weight percent crystallinity for the cold and melt crystallized sPS/PPO blends was calculated by using the Peak-Fit program. This bulk weight percent crystallinity, when divided by the sPS weight fraction, gives the actual weight percent of the sPS crystallized in the blend and is shown in Figure 4.19. The crystallinity seems to be dictated by the crystallization kinetics for all the blends. For both melt and cold crystallized blends, crystallinity is lowest for the blends crystallized fastest at 220°C. Slower crystallization leads to an increase in crystallinity.

4.4 Density Measurement Results

Density of the cold and melt crystallized blends is shown in Figures 4.20 and 4.21 respectively. The right vertical axes in the figures show the density of the quenched blends. For each composition, change in density of the blends crystallized at different temperatures is very small. It is interesting to note that density of melt crystallized blends is higher than the density of the quenched blends, while that of the cold crystallized blends is lower. In case of the cold crystallized blends (Figure 4.20), no definite trend can be observed with change in crystallization temperature. The samples crystallized at 220°C have the lowest density. There is a slight increase at 190°C followed by decrease at 180°C. In the melt crystallized blends (Figure 4.21), an increase in crystallization temperature (slower crystallization) leads to an increase in the density. This effects is more pronounced for the sPS83PPO and sPS67PPO blends as compared to the sPS50PPO blends.

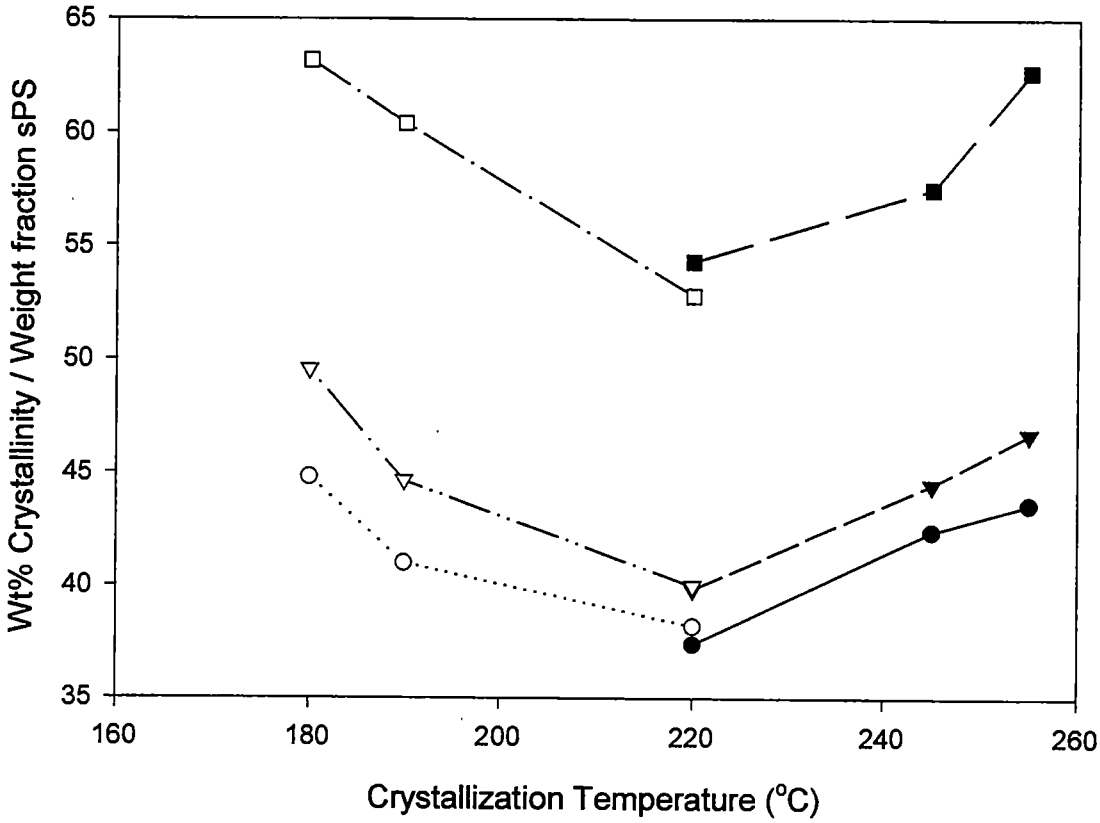

Figure 4.19. **WAXD crystallinity of cold and melt crystallized sPS/PPO blends on the basis of sPS content. Circles represent sPS50PPO blend, triangles sPS67PPO and squares neat sPS. Open data points are for cold crystallized samples, and the closed ones are for melt crystallized samples.**

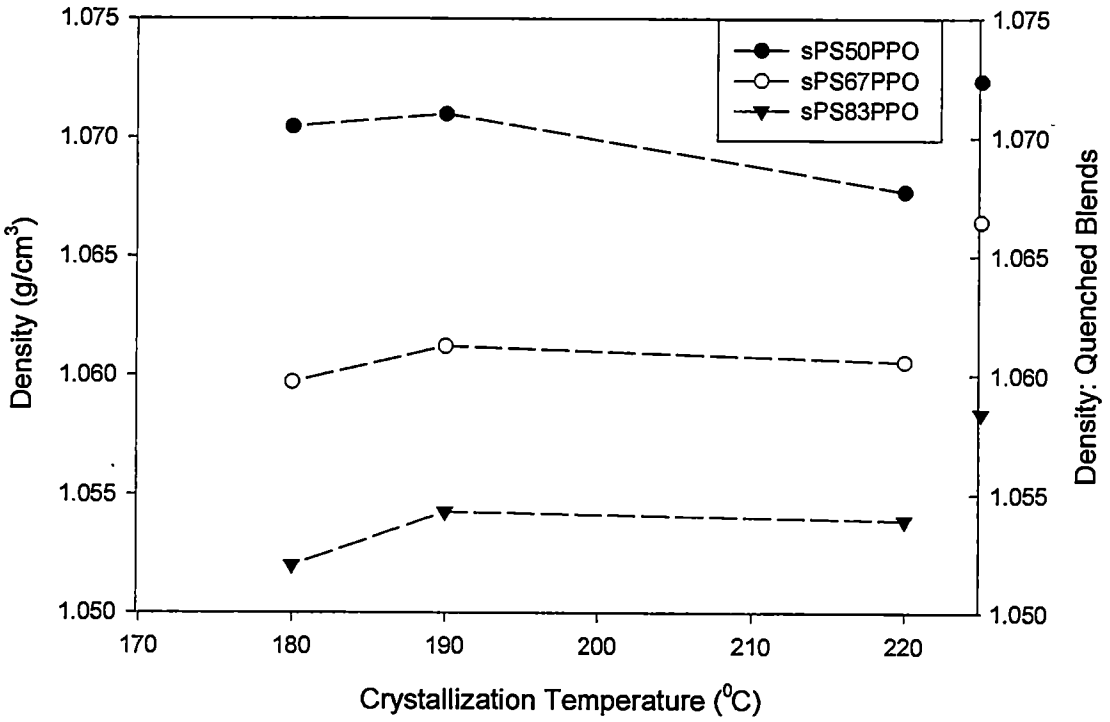

Figure 4.20. DGC measured densities of cold crystallized sPS/PPO blends. The vertical axis on the right shows comparison with the density of quenched blends.

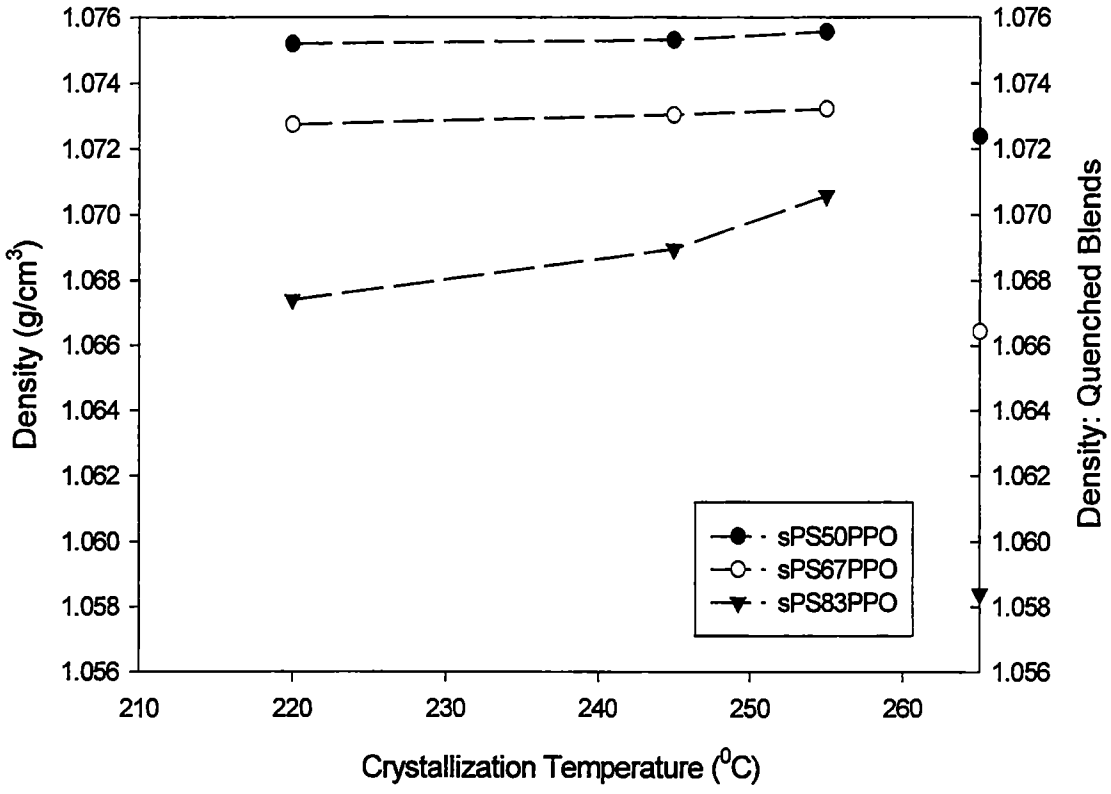

Figure 4.21. DGC measured densities of melt crystallized sPS/PPO blends. The vertical axis on right (different scale) shows comparison with the density of quenched blends.

4.5 Tensile Testing

4.5.1 Cold Crystallized Blends

The tensile strength and strain at break for the cold crystallized sPS50PPO and sPS67PPO blends are shown in Figure 4.22 and 4.23 respectively. The individual scatter points on these plots represent the data values recorded from tensile testing of one sample. These average mechanical properties and the corresponding tensile toughness for these blends and the neat sPS are given in Tables 4.1 through 4.3. For the cold crystallized sPS50PPO blends (Figure 4.22), the values of tensile strength and strain at break are quite scattered. In case of the blend samples crystallized at 180°C and 190°C these values are roughly equal. The blend samples crystallized at 220°C (highest temperature and highest crystallization rate) show lower tensile strength and strain at break. In case of sPS67PPO (Figure 4.23), again, no definite trend is observed. Decrease in PPO content significantly decreases the tensile strength and the strain at break. These values, in general, also seem to increase with decreasing crystallization temperature (slower crystallization).

The representative engineering stress-strain curves, closest to the average for the sPS50PPO blends, are shown in Figure 4.24. These curves clearly show that decreasing crystallization temperature (thereby decreasing crystallization rate) rate leads to higher tensile strength and strain at break.

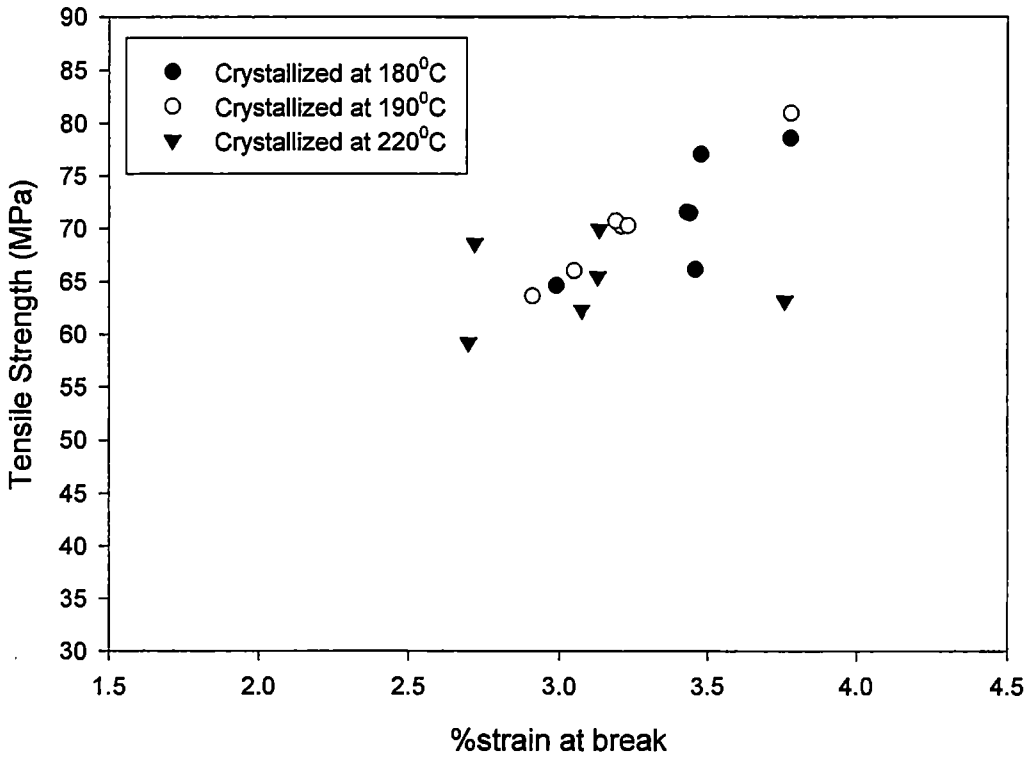

Figure 4.22. Tensile strength and percent strain at break for cold crystallized sPS50PPO blends.

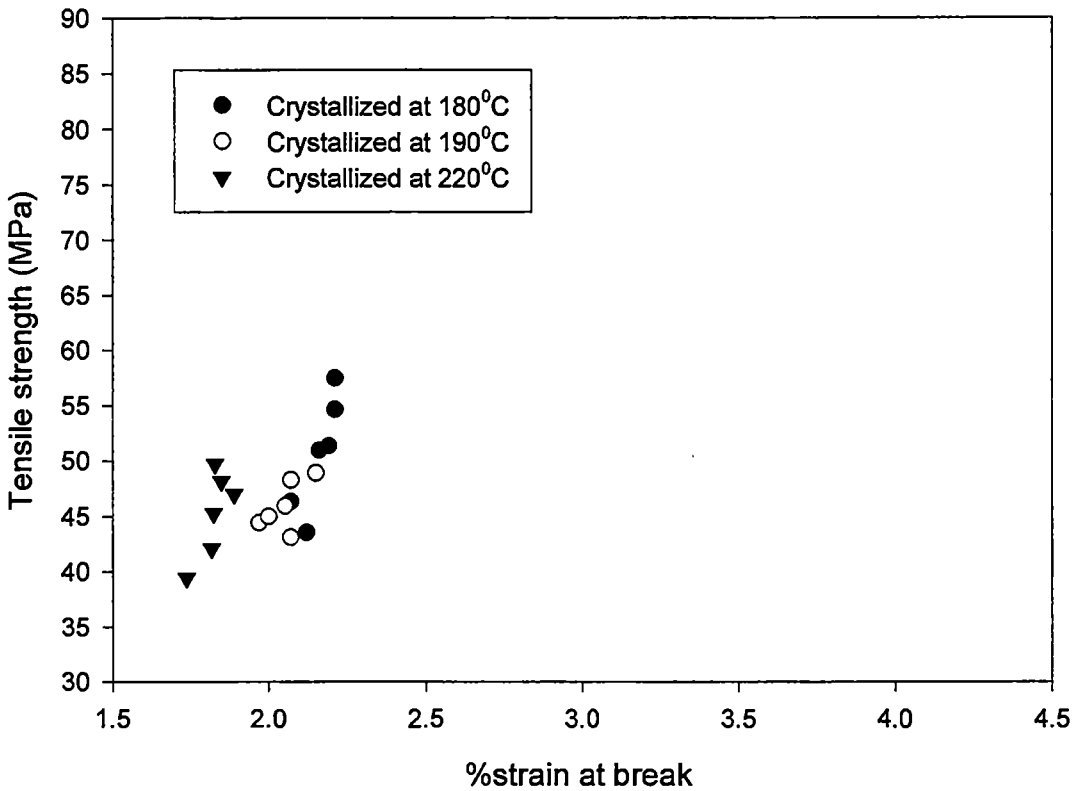

Figure 4.23. Tensile strength and percent strain at break for cold crystallized sPS67PPO blends.

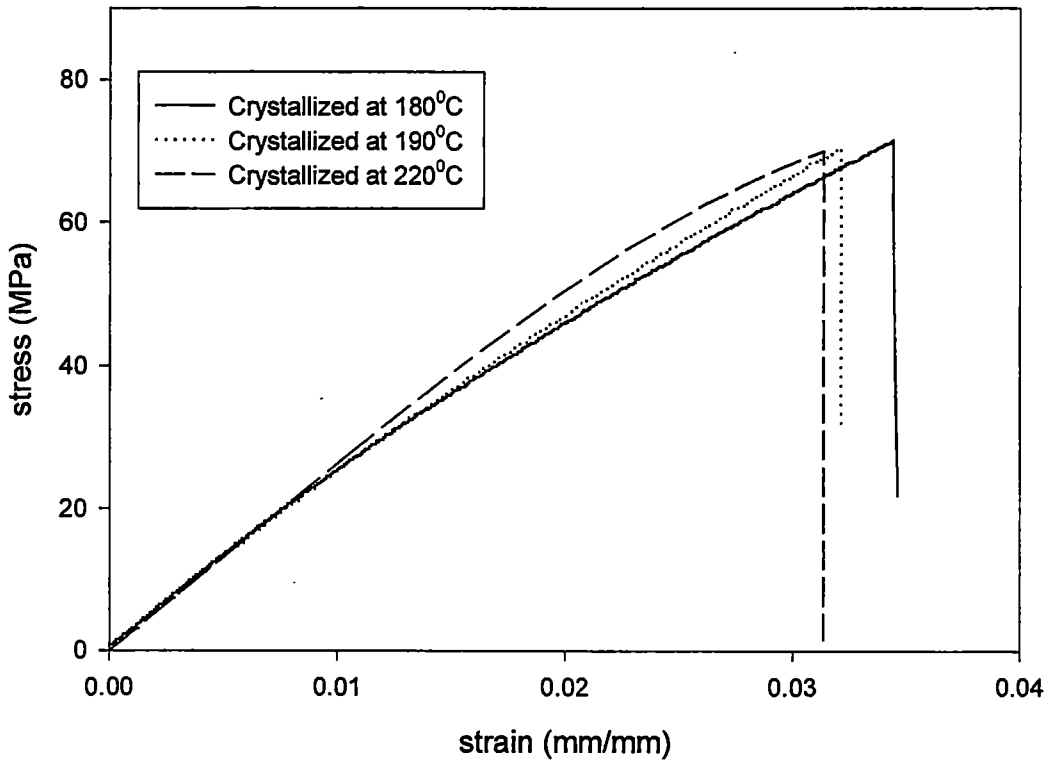

Figure 4.24. Representative stress-strain curves for cold crystallized sPS50PPO blends.

Table 4.1. Tensile properties of cold crystallized sPS50PPO blends.

Crystallization Temperature (°C)	Tensile Strength (MPa)		Strain at Break (mm/mm)		Tensile Toughness (MJ/m^3)	
	Observed	Linear Rule of mixtures	Observed	Linear Rule of mixtures	Observed	Linear Rule of mixtures
220	65.46	55.36	3.13	4.80	1.03	2.06
190	70.32	56.85	3.23	4.85	1.23	2.09
180	71.6	60.51	3.43	4.90	1.32	2.17

Table 4.2. Tensile properties of cold crystallized sPS67PPO blends.

Crystallization Temperature (°C)	Tensile Strength (MPa)		Strain at Break (mm/mm)		Tensile Toughness (MJ/m^3)	
	Observed	Linear Rule of mixtures	Observed	Linear Rule of mixtures	Observed	Linear Rule of mixtures
220	45.26	49.84	1.83	3.18	0.44	1.29
190	45.93	51.83	2.05	3.24	0.49	1.19
180	50.96	56.74	2.16	3.31	0.58	1.16

Table 4.3. Tensile properties of cold crystallized neat sPS.

Crystallization Temperature (°C)	Tensile Strength (MPa)	Strain at Break (mm/mm)	Tensile Toughness (MJ/m^3)
220	39.13	1.93	0.337
190	42.10	2.02	0.389
180	39.13	2.12	0.540

The tensile strength and strain at break for the cold crystallized samples of neat sPS are shown in Figure 4.25. A definite increase in tensile strength and strain at break is observed with decreasing crystallization temperature. Finally, the representative stress-strain curves for the neat sPS, cold crystallized at same temperatures, are shown in Figure 4.26. Neat sPS tensile bars cold crystallized at lowest temperature (180°C - corresponding to lowest crystallization rate) have the highest tensile strength and the strain at break. In general, increase in the annealing temperature decreases the ultimate tensile properties. The stress-strain curves for the neat sPS are very linear unlike the curves for the blend samples.

4.5.2 Melt Crystallized Blends

The tensile properties of the melt crystallized sPS/PPO blends and the neat sPS are stronger function of crystallization temperature than the cold crystallized blends. The tensile strength and strain at break for the melt crystallized sPS50PPO and sPS67PPO blends are shown in Figures 4.27 and 4.28 respectively. These ultimate mechanical properties and the corresponding tensile toughness for these blends and the neat sPS are also given in Tables 4.4 through 4.6. In case of melt crystallized sPS50PPO blends a definite trend is observed with the change in crystallization temperature. Blends crystallized at 255°C (highest crystallization temperature and lowest crystallization rate) consistently show much higher tensile strength and strain at break. Blends crystallized at 245°C have higher tensile strength than the blends crystallized at 220°C, but the strain at break is comparable. The melt crystallized

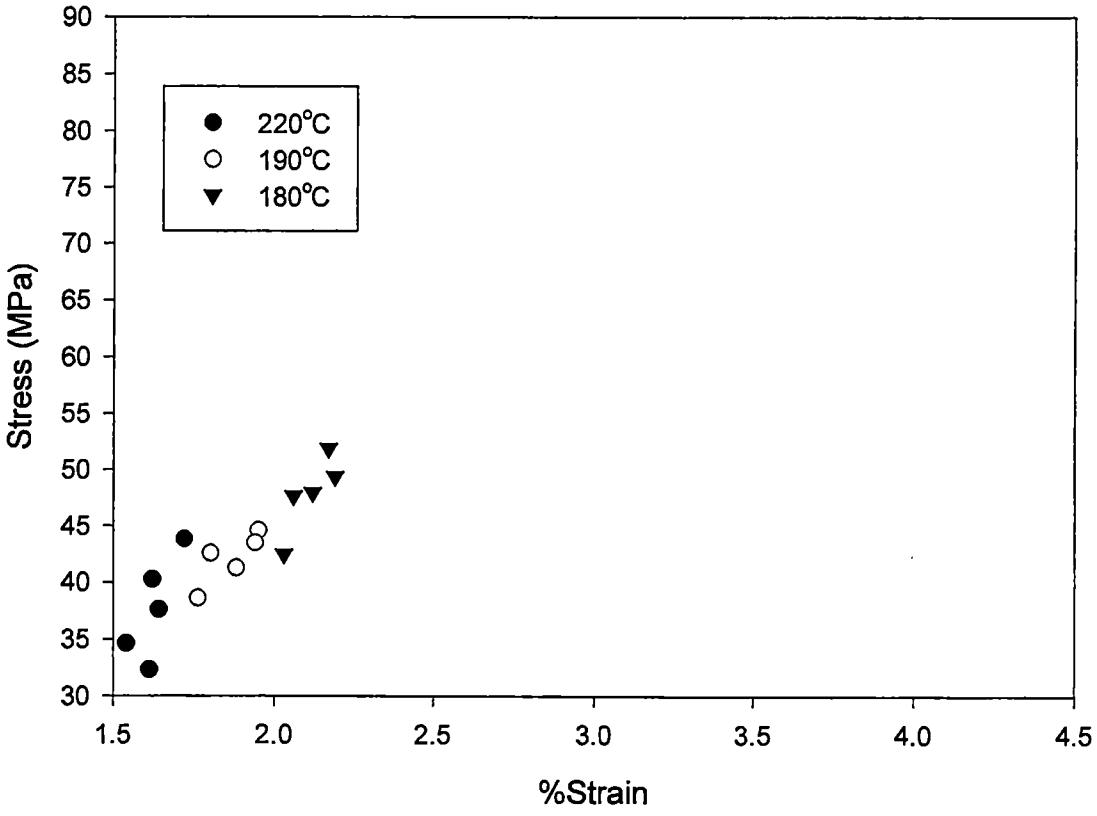

Figure 4.25. Tensile strength and percent strain at break for cold crystallized neat sPS.

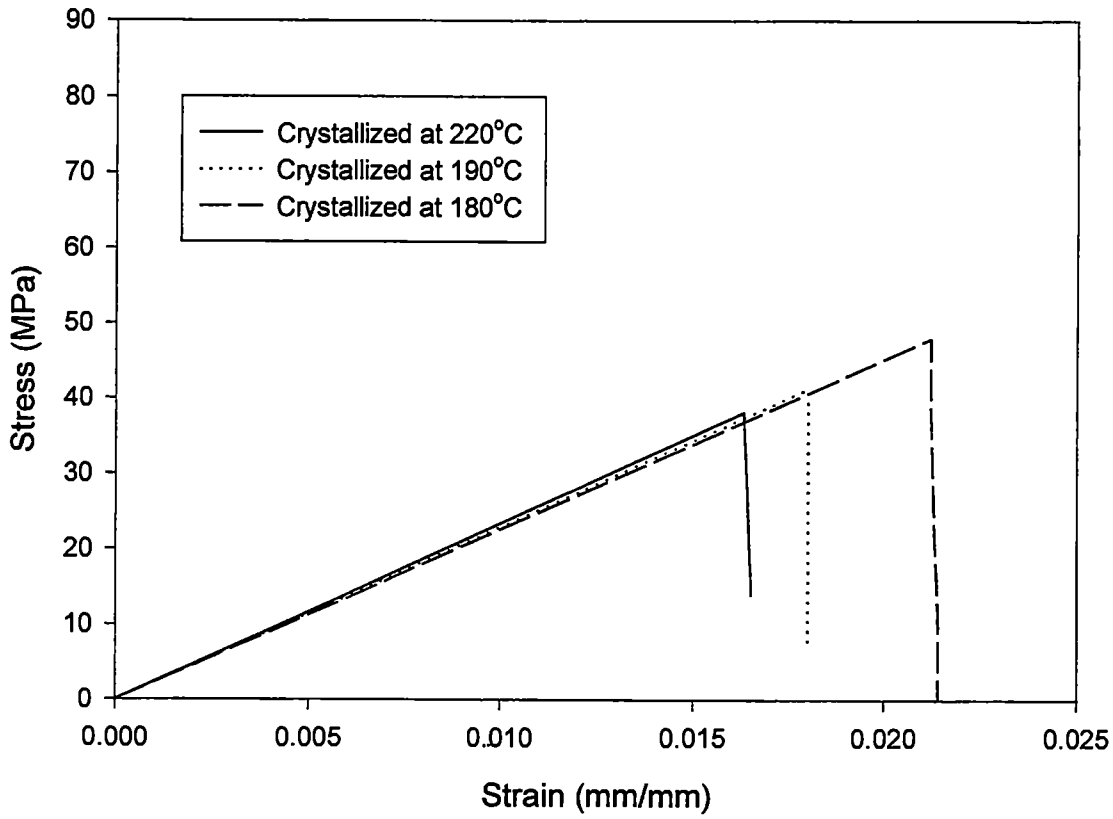

Figure 4.26. Representative stress-strain curves for cold crystallized neat sPS.

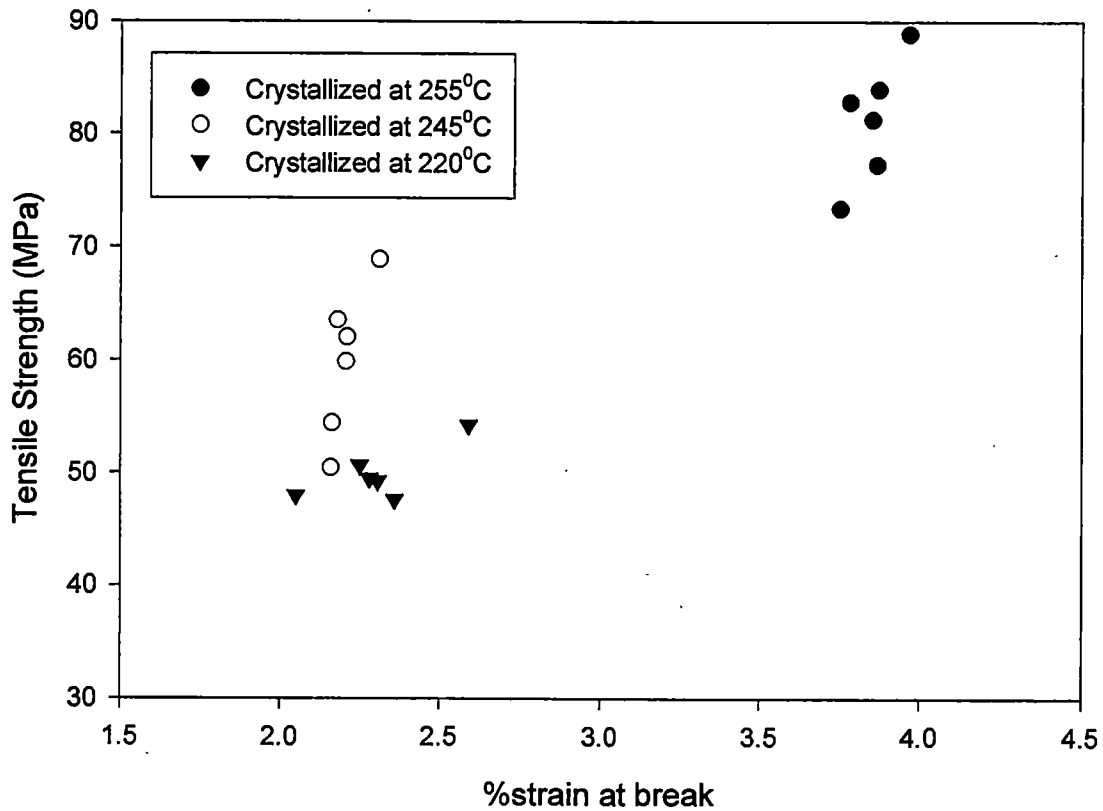

Figure 4.27. Tensile strength and percent strain at break of melt crystallized sPS50PPO blends.

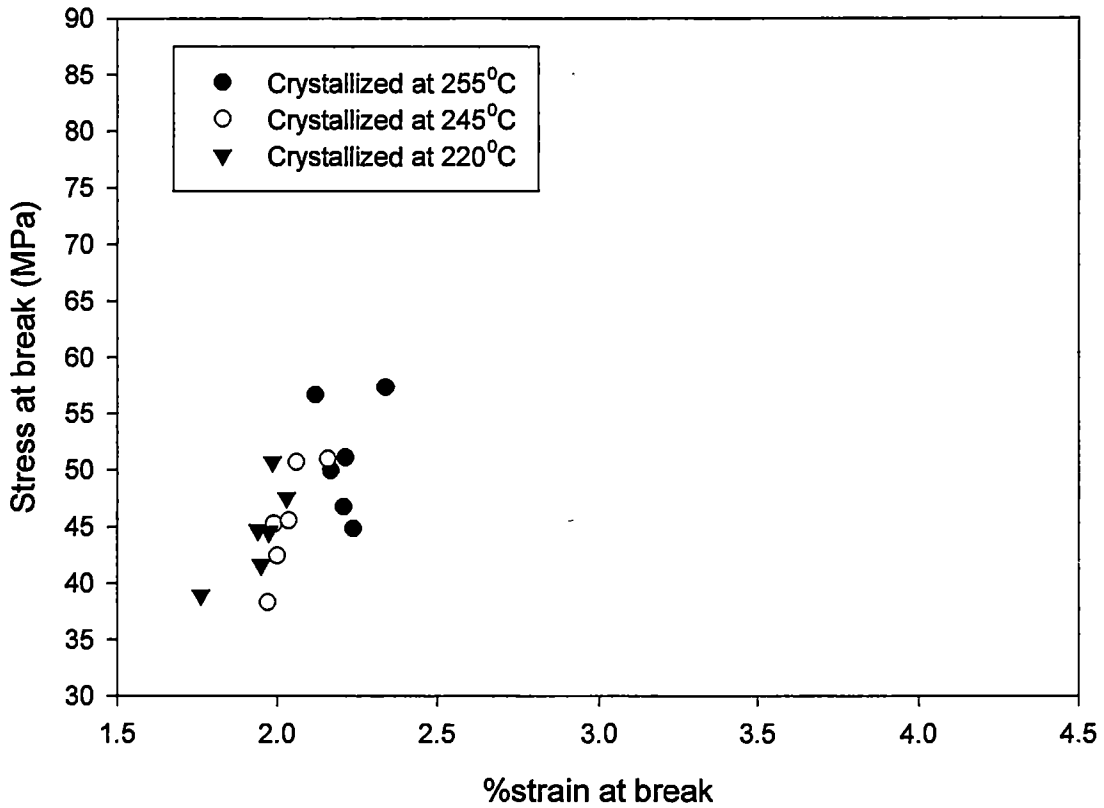

Figure 4.28. Tensile strength and percent strain at break for melt crystallized sPS67PPO blends.

Table 4.4. Tensile properties of melt crystallized sPS50PPO blends.

Crystallization Temperature (°C)	Tensile Strength (MPa)		Strain at Break (mm/mm)		Tensile Toughness (MJ/m^3)	
	Observed	Linear Rule of mixtures	Observed	Linear Rule of mixtures	Observed	Linear Rule of mixtures
220	49.23	69.07	2.31	4.59	0.61	1.98
245	59.85	61.66	2.21	4.23	0.69	1.78
255	81.28	59.33	3.85	4.10	1.71	1.71

Table 4.5. Tensile properties of melt crystallized sPS67PPO blends.

Crystallization Temperature (°C)	Tensile Strength (MPa)		Strain at Break (mm/mm)		Tensile Toughness (MJ/m^3)	
	Observed	Linear Rule of mixtures	Observed	Linear Rule of mixtures	Observed	Linear Rule of mixtures
220	44.67	68.22	1.94	4.20	0.45	1.68
245	45.53	58.29	2.04	3.73	0.49	1.41
255	51.07	55.16	2.21	3.55	0.59	1.33

Table 4.6. Tensile properties of melt crystallized neat sPS.

Crystallization Temperature (°C)	Tensile Strength (MPa)	Strain at Break (mm/mm)	Tensile Toughness (MJ/m^3)
220	66.55	3.46	1.12
245	51.73	2.74	0.72
255	47.06	2.48	0.60

sPS67PPO blends do not show the clear trend observed in sPS50PPO blends. The change in tensile strength with the crystallization temperature is almost negligible while the strain at break shows a small increase with increasing temperature.

The representative engineering stress-strain curves for the melt-crystallized sPS50PPO blends are shown in Figure 4.29. In case of sPS50PPO blends the sample crystallized at 255°C has exceptionally high tensile strength and strain at break. It also shows a slight convex curvature to the stress-strain curve. The stress-strain characteristics of the samples crystallized at 245°C and 220°C are similar to each other, with the ultimate strength and strain at break being slightly higher for the blends crystallized 245°C.

The ultimate tensile strength and strain at break for melt crystallized neat sPS samples are shown in Figure 4.30. The samples crystallized at 220°C show the highest values for these ultimate tensile properties. The values for the samples crystallized at 245°C are slightly higher than the samples crystallized at 255°C. Finally, engineering stress-strain curves for the neat sPS samples melt crystallized at these temperatures are shown in Figure 4.31. Again neat melt crystallized sPS shows mechanical behavior opposite to that of the melt crystallized blends. The sample crystallized at 220°C has the highest tensile strength and strain at break. These values decrease with increasing crystallization temperature and decreasing crystallization rate. Moreover, the stress-

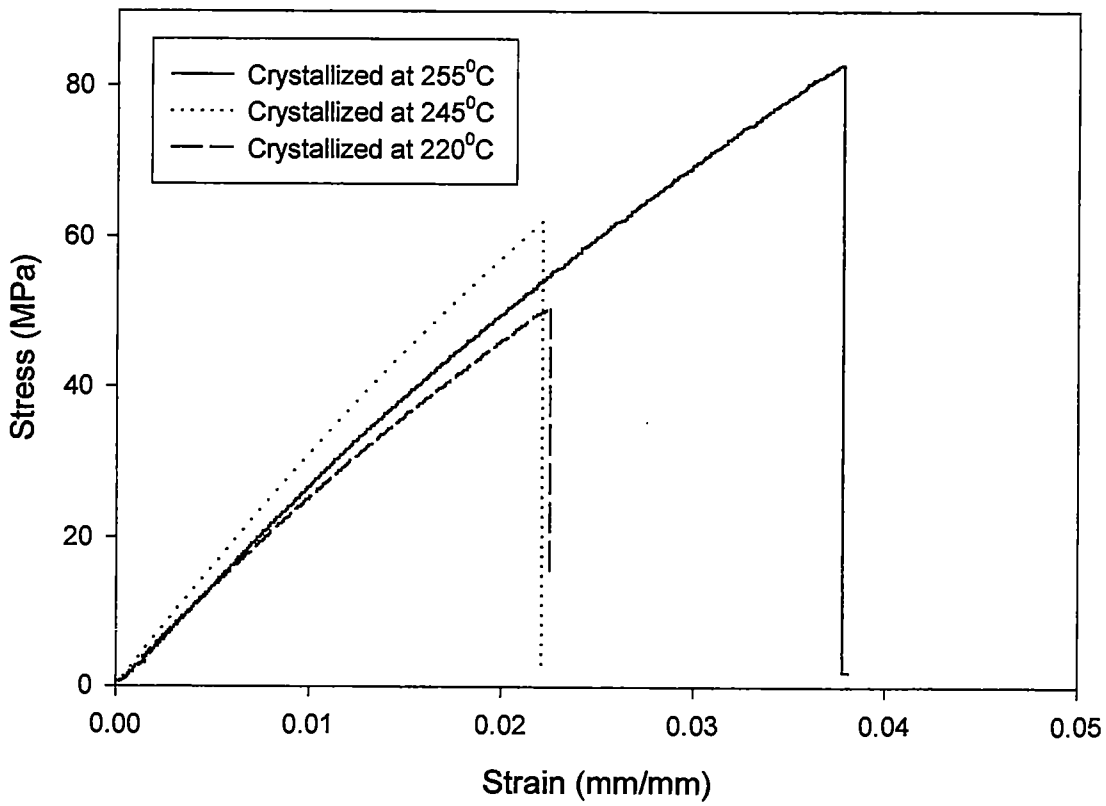

Figure 4.29. Representative stress-strain curves for melt crystallized sPSS50PPO blends.

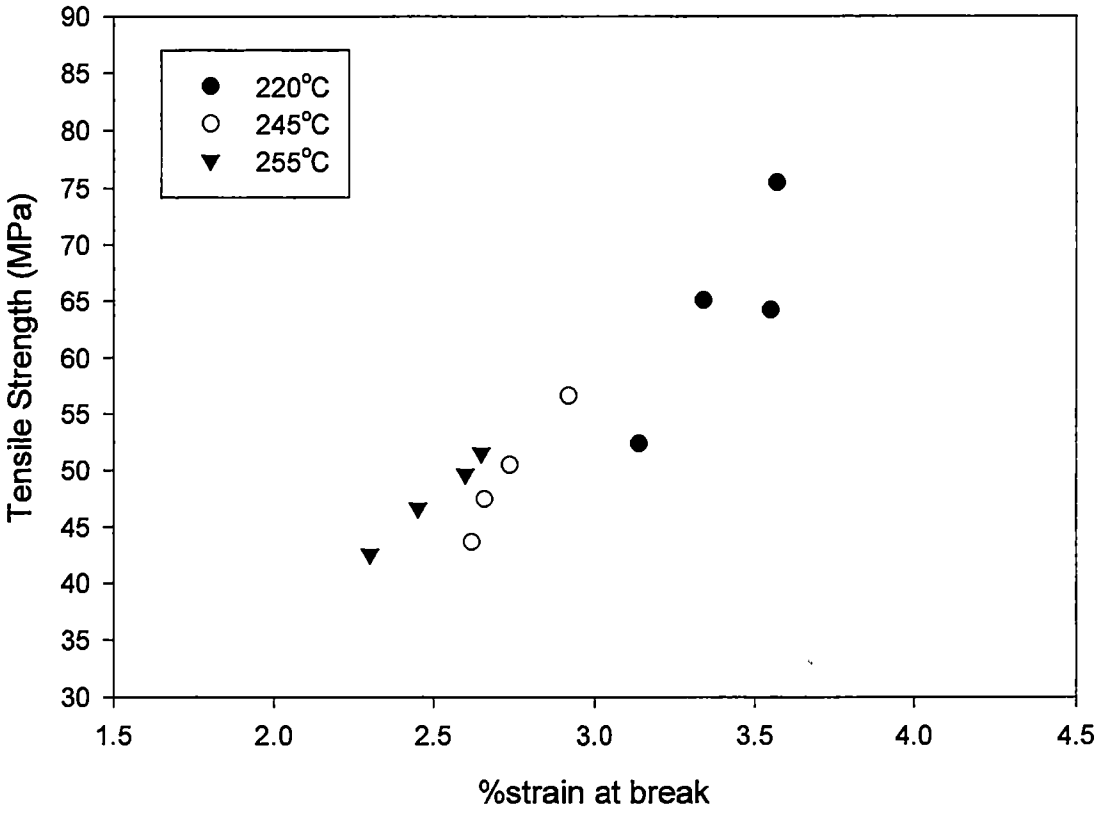

Figure 4.30. Tensile strength and strain at break for neat melt crystallized sPS.

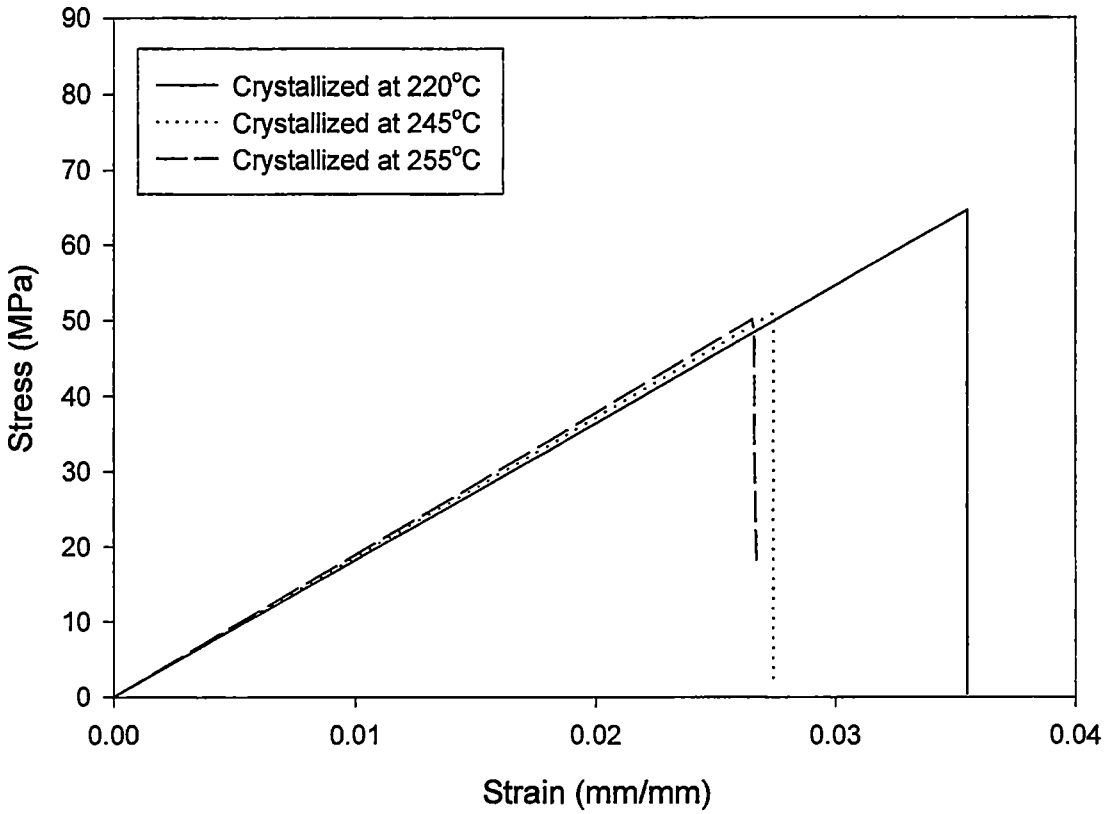

Figure 4.31. Representative stress-strain curves for melt crystallized neat sPS.

strain curves for the neat sPS are very close to linear, while similar curves for the blends show some curvature.

4.6 Scanning Electron Microscopy

4.6.1 Cold Crystallized Blends

SEM micrographs of etched sPS50PPO films cold crystallized at 220°C, 190°C and 180°C are shown in Figures 4.32 through 4.34. These micrographs have been taken at different magnifications.

All these micrographs show lamellar bundles forming a mesh like structure. The holes in the mesh may be either regions between the small spherulites or amorphous regions formed after branching of the bundles. No complete or identifiable sections of spherulites are seen. Except for the blend crystallized at 220°C, it is very difficult to see the removed amorphous regions between these layered crystalline bundles. The thickness of these bundles varies with the crystallization temperature. Decreasing crystallization temperature leads to a systematic decrease in bundle thickness. The measurement of other texture features like bundle spacings, compactness and the dimensions of the ellipsoidal amorphous domains in the SEM micrographs of these cold crystallized blends is not possible.

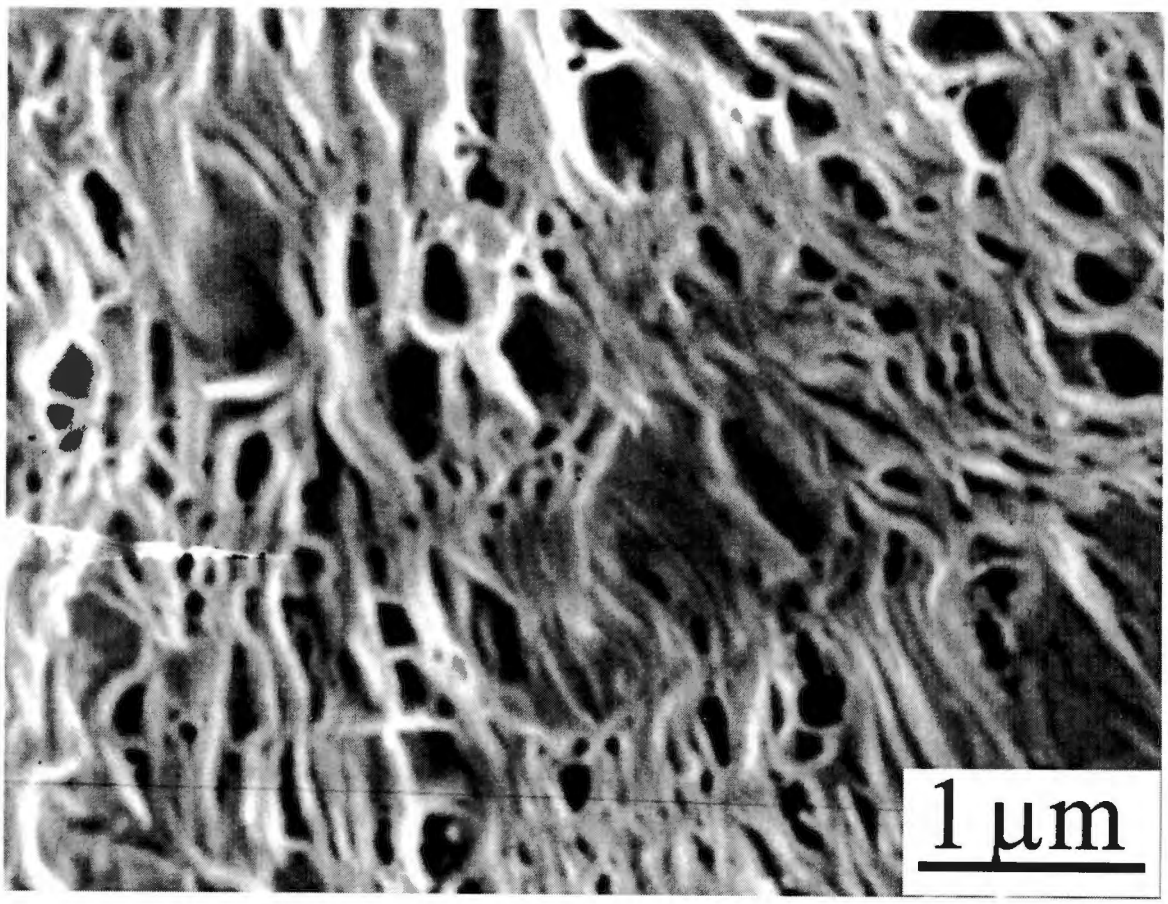

Figure 4.32. SEM micrograph of sPS50PPO blend cold crystallized at 220°C.

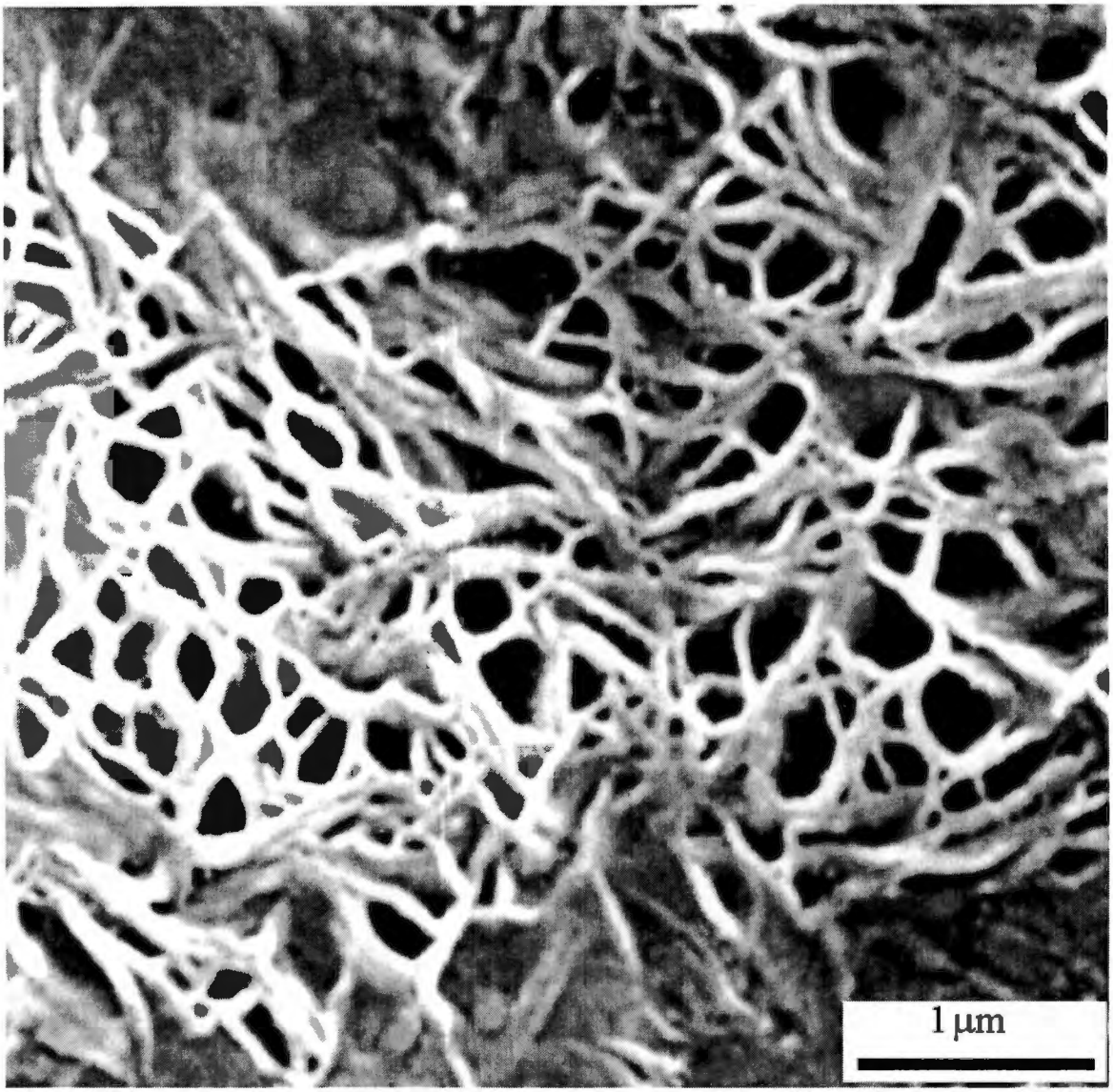

Figure 4.33. SEM micrograph of sPS50PPO blend cold crystallized at 190°C.

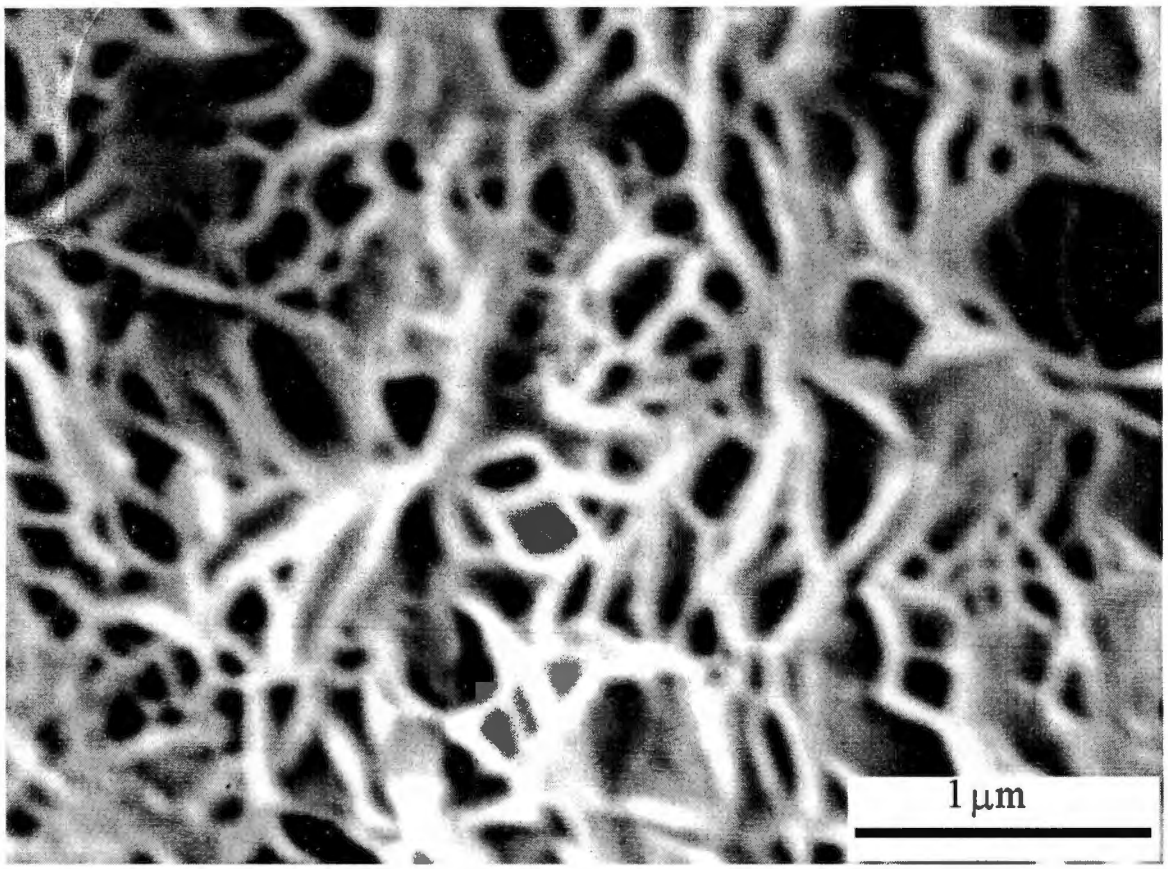

Figure 4.34. SEM micrograph of sPS50PPO blend cold crystallized at 180°C.

4.6.2 Melt Crystallized Blends

SEM micrographs of etched sPS50PPO melt crystallized at 220°C, 245°C and 255°C are shown in Figures 4.35 through 4.37. The micrographs of etched sPS67PPO and sPS83PPO blends melt crystallized at 245°C are shown in Figures 4.38 and 4.39. All these micrographs have been taken at 7kX magnification. The etched samples of neat melt-crystallized sPS did not reveal any features in the SEM.

These micrographs show complete or partial sections of etched spherulites. These spherulitic sections consist of ribbon-like fibrous units radiating from a center. These ribbon-like structures, known as bundles, are stacks of 5-50 lamellae, being viewed edge-on. Isolated bundles, whose lateral dimensions can be easily measured, are seen at the periphery of the spherulites. The spaces between these bundles are amorphous regions known as bundle spacings. As these bundles move away from the center, they branch and splay continuously to form void ellipsoid structures from which trapped amorphous material is removed by etching. The size of these ellipsoid voids increases from center to the periphery of the spherulite.

The measured thickness of these bundles and bundle spacings are shown in Table 4.8(a) through 4.8(c). Compactness, defined as the fraction of crystalline bundle thickness in the repeating bundle-bundle spacing structure, has also been calculated. The dimensions of the ellipsoid voids, measured by the major and minor axes of the ellipse formed in one plane, are also tabulated. The variation in the dimensions of the

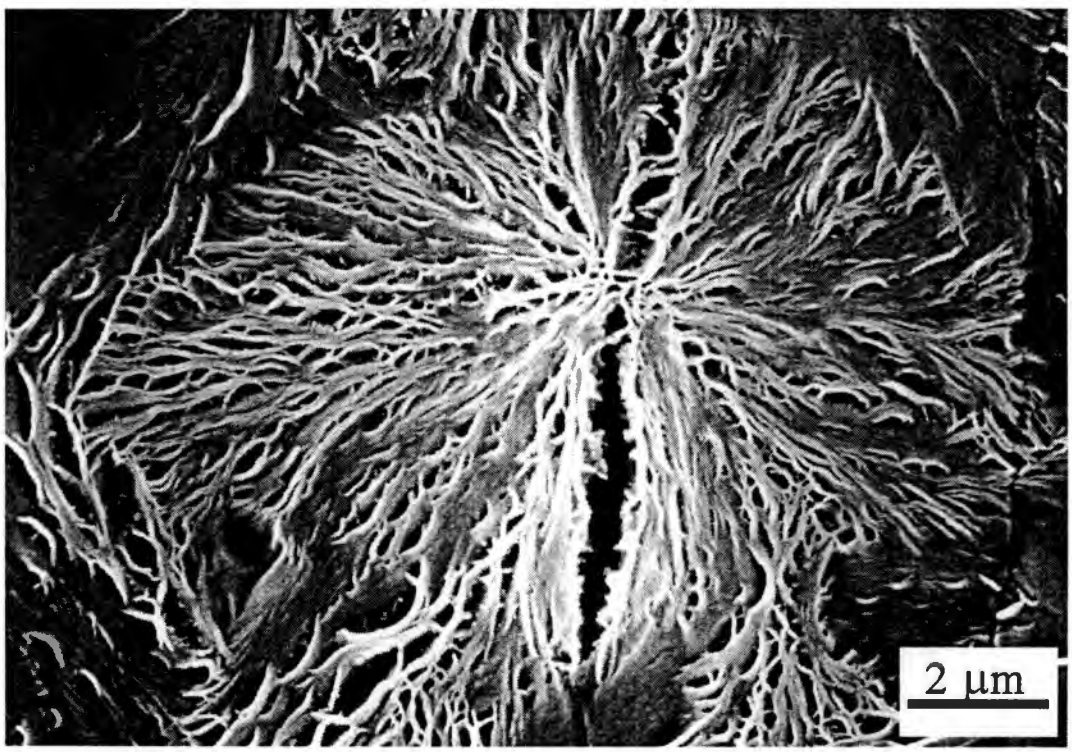

Figure 4.35. SEM micrograph of sPS50PPO blend melt crystallized at 220°C

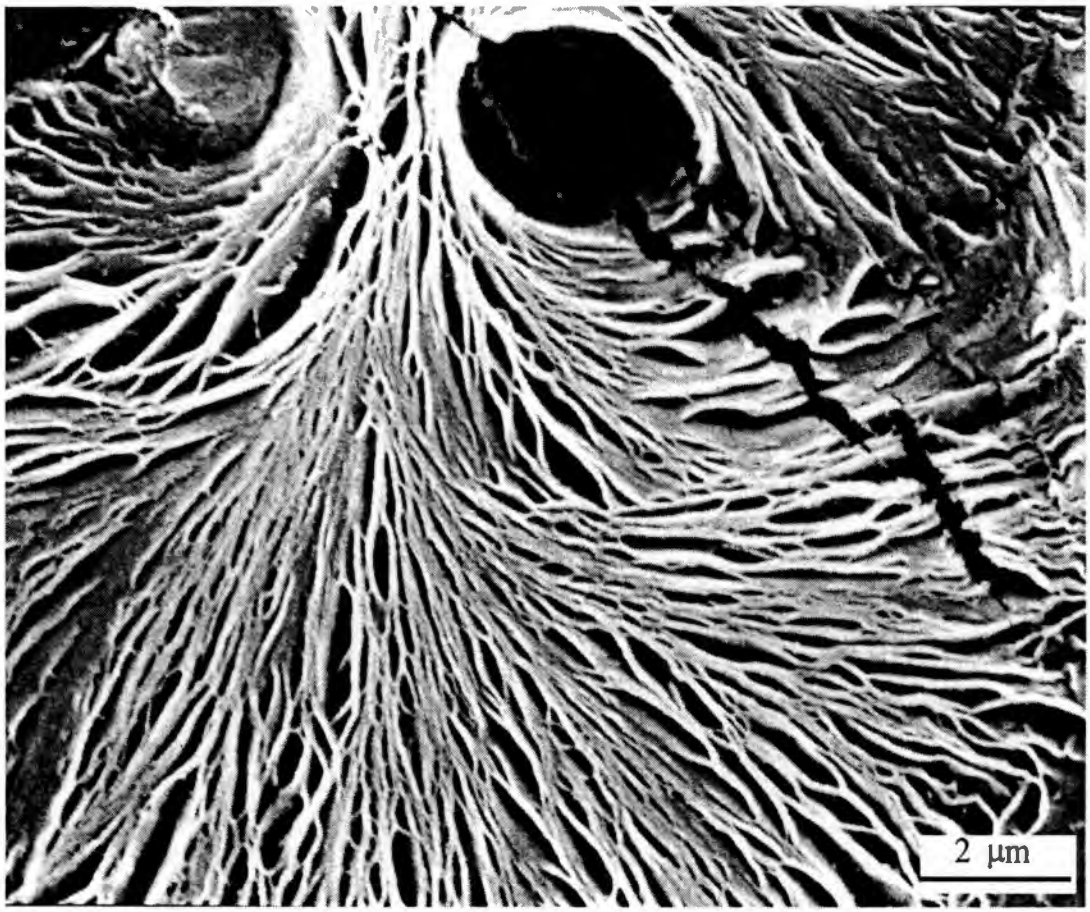

Figure 4.36. SEM micrograph of sPS50PPO blend melt crystallized at 245°C.

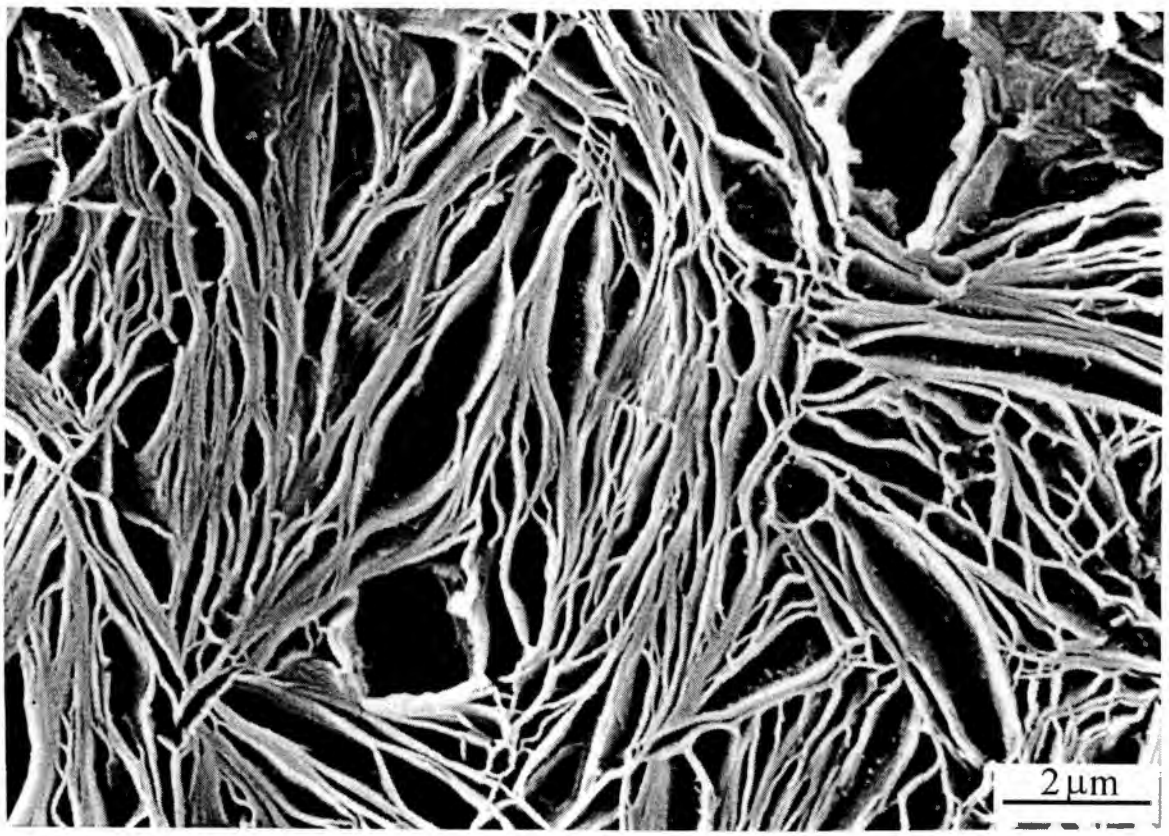

Figure 4.37. SEM micrograph of sPS50PPO blend melt crystallized at 255°C

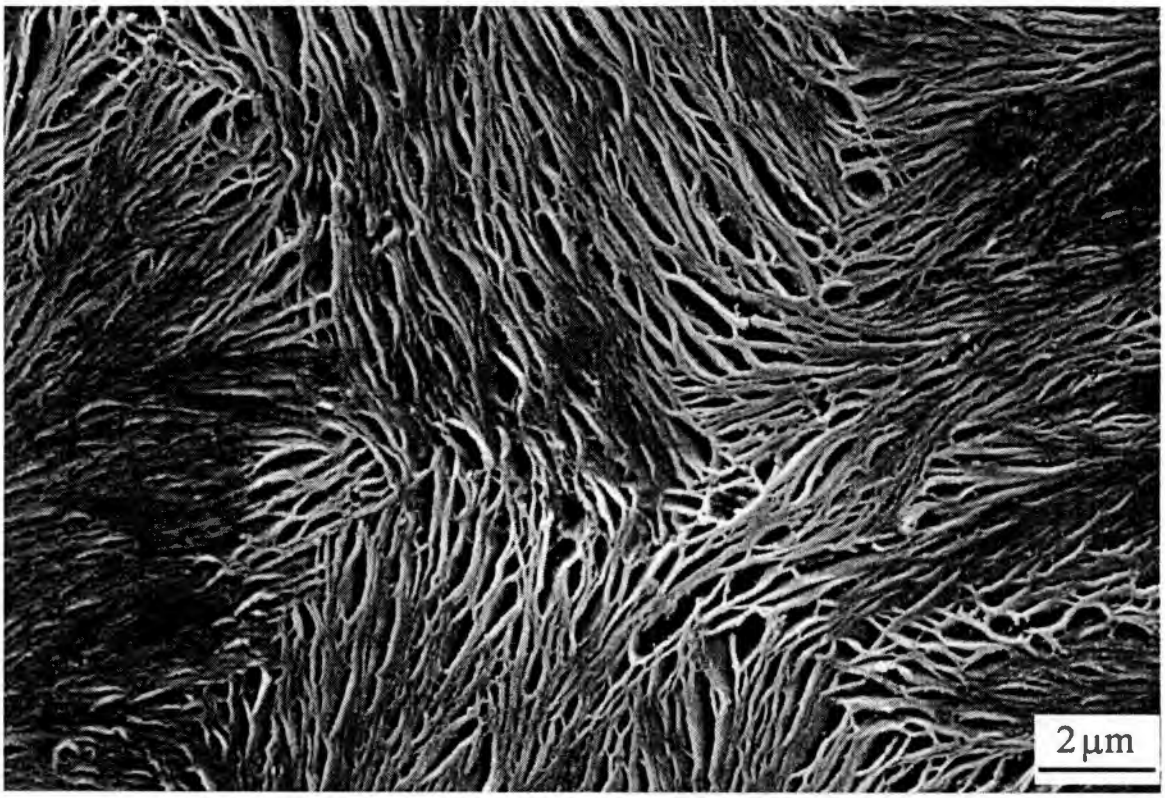

Figure 4.38. SEM micrograph of sPS67PPO blend melt crystallized at 245°C.

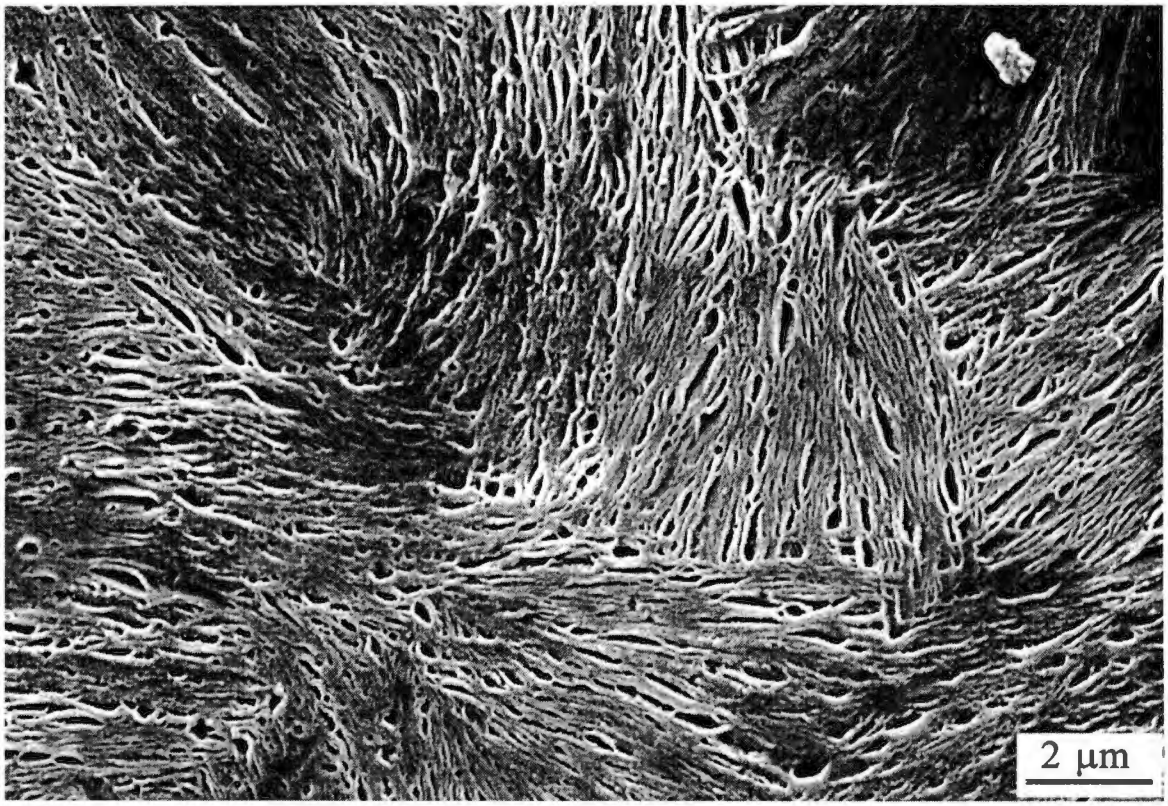

Figure 4.39. SEM micrograph of sPS83PPO blend melt crystallized at 245°C.

Table 4.7. Bundle Thickness of cold crystallized sPS50PPO blends.

Crystallization Temperature (°C)	Bundle Thickness (nm)
220	65.4
190	58.8
180	55.3

Table 4.8. Measurements from SEM micrographs of melt crystallized sPS/PPO blends.

(a) sPS50PPO

Crystallization Temperature (°C)	Bundle Thickness (nm)	Bundle Spacing (nm)	Compactness (Bundle Fraction)	Ellipsoid Voids Dimensions (nm)	
				Major Axis	Minor Axis
220	46	22	0.676	370	119
245	67	32	0.677	456	120
255	78	37	0.678	562	196

(b) sPS67PPO

Crystallization Temperature (°C)	Bundle Thickness (nm)	Bundle Spacing (nm)	Compactness (Bundle Fraction)	Ellipsoid Voids Dimensions (nm)	
				Major Axis	Minor Axis
220	45	19	0.703	258	92
245	66	28	0.702	408	104
255	80	33	0.708	477	146

(c) sPS83PPO

Crystallization Temperature (°C)	Bundle Thickness (nm)	Bundle Spacing (nm)	Compactness (Bundle Fraction)	Ellipsoid Voids Dimensions (nm)	
				Major Axis	Minor Axis
220	47	19	0.712	211	79
245	65	25	0.722	347	93
255	75	27	0.735	417	119

ellipsoidal dimensions and the bundle spacings at the corresponding crystallization temperatures is also plotted in Figure 4.40.

Coarseness, which is the measure of absolute size of these bundles, is increasing with increasing crystallization temperature (lower supercoolings and slower crystallization). It, however, varies little for different composition blends crystallized at same temperature.

For each blend composition, bundle spacing increases with crystallization temperature. Increase in PPO concentration, on the other hand, increases the bundle spacing. Compactness does not vary much with change in crystallization temperature for sPS50PPO blends. With decreasing PPO concentration it increases slightly with increasing crystallization temperature.

Finally, for each blend composition, the dimensions of the ellipsoidal voids (both major and minor axes) increase with increasing crystallization temperature. Decrease in PPO content decreases these dimensions.

4.6.3 Fracture Surfaces

The tensile fracture surfaces of the melt crystallized blends sPS50PPO blends crystallized at 220°C and 255°C were observed under the SEM. Etching of these samples was also done to reveal the effect of strain to the spherulitic morphology.

(a)

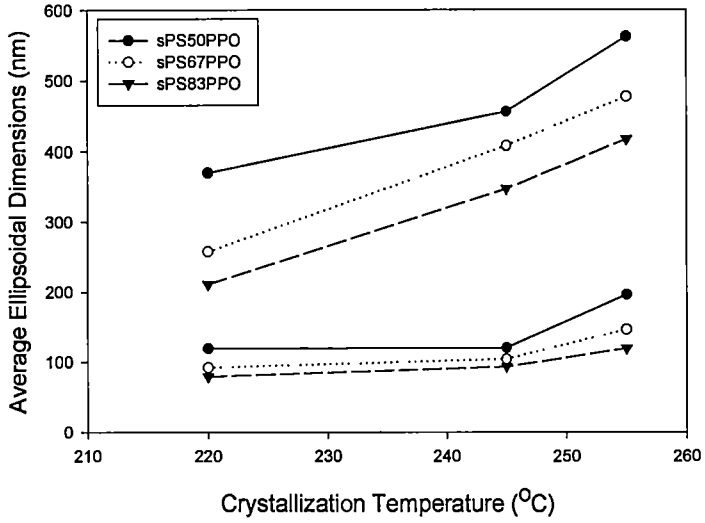

(b)

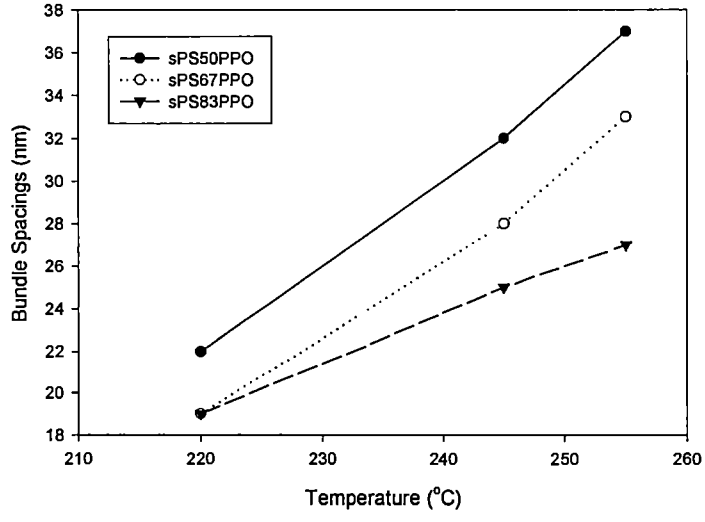

Figure 4.40. Variation of spherulitic texture with crystallization temperature in melt-crystallized sPS/PPO blends. (a) Ellipsoidal domains dimensions and (b) Bundle Spacing.

The SEM micrographs of non-etched tensile fracture surfaces of the melt crystallized sPS50PPO blend samples are shown in Figures 4.41 and 4.42. Figure 4.41 shows fracture surface of the sPS50PPO sample melt crystallized at 255°C. The structure shows few pits or corrugations and is characterized by highly elongated fibrils ejecting out of the fractured surface. The fracture surface of the sPS50PPO sample, melt crystallized at 220°C, is shown at same magnification in Figure 4.42. In this figure pits of various depths with protruding pyramidal structures can be seen. Chu and Schultz have observed similar structures in poly(ether ether ketone) (PEEK) [64]. They have suggested that knobby apexes of these pyramidal structures consist of a hard nucleus to which loose lamellae bundles are attached. The voids formed are the impressions of the nuclei that remained with the other fracture surface during the crack growth.

The SEM micrographs of fracture surfaces of melt crystallized neat sPS are shown in Figures 4.43 and 4.44. Figure 4.43 shows a layered structure of the fractured surface of neat sPS melt crystallized at 255°C. These layered structures are mainly internal micro-cracks and voids. Figure 4.44 shows the fracture surface of neat sPS melt crystallized at 220°C. The structure observed here is very similar to the one observed in blends crystallized at 220°C. The spherulitic nuclei at the crack surface are evident from the uneven pyramidal structures coming out of the matrix.

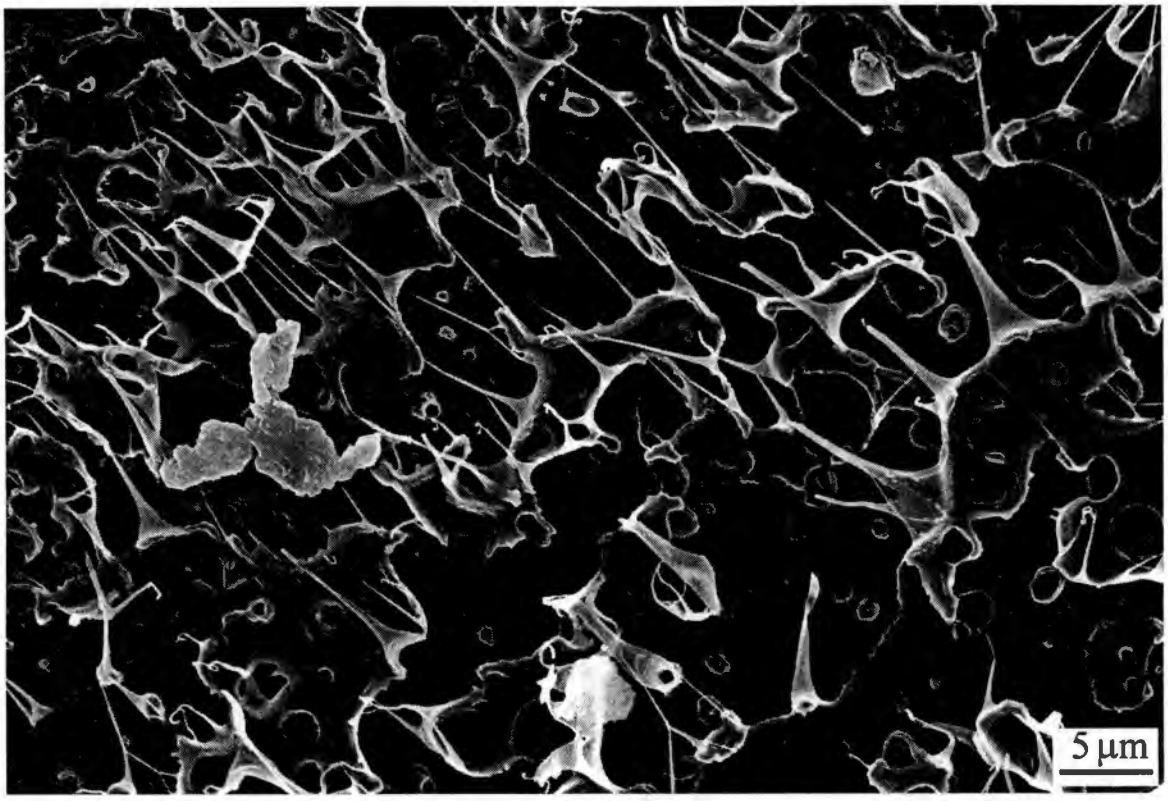

Figure 4.41. SEM micrograph of non-etched fracture surface of sPS50PPO blend melt crystallized at 255°C showing highly drawn fibrils.

Figure 4.42. SEM micrograph of non-etched fracture surface of sPS50PPO blend melt crystallized at 220°C showing intraspherulitic fracture.

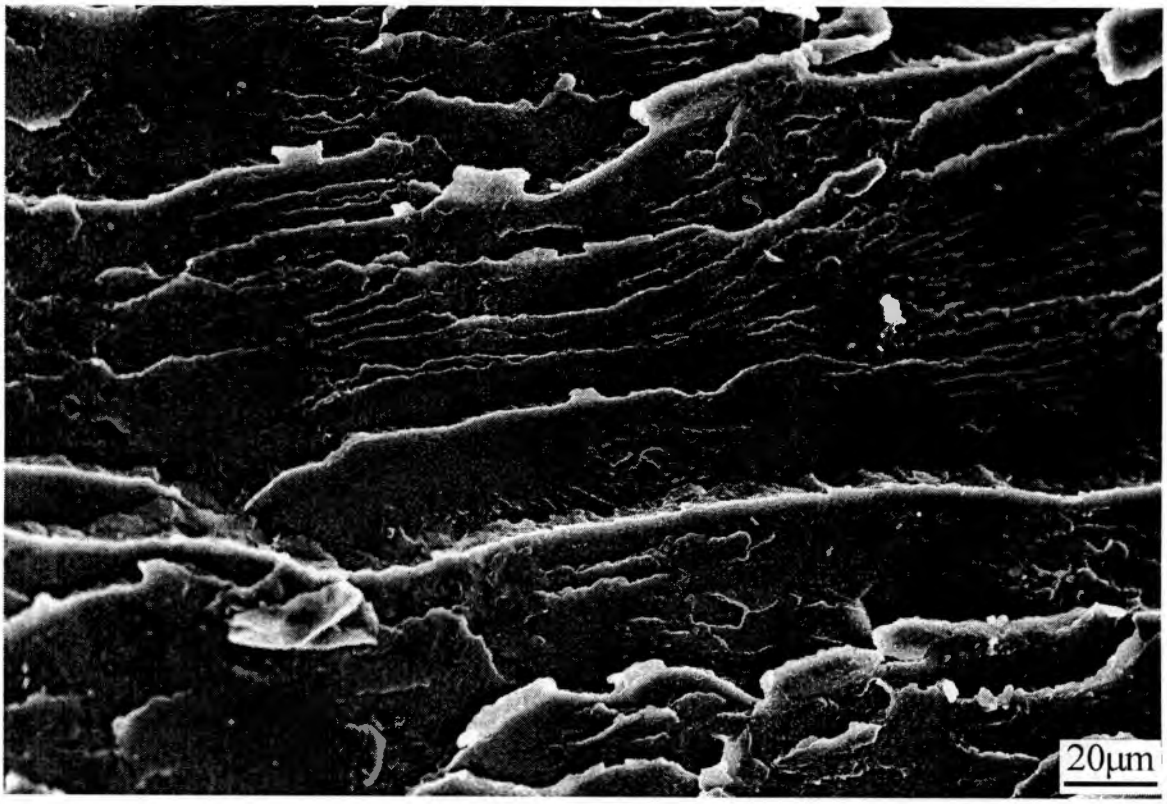

Figure 4.43. SEM micrograph of non-etched fracture surface of neat sPS melt crystallized at 255°C showing multi-layered micro-cracks.

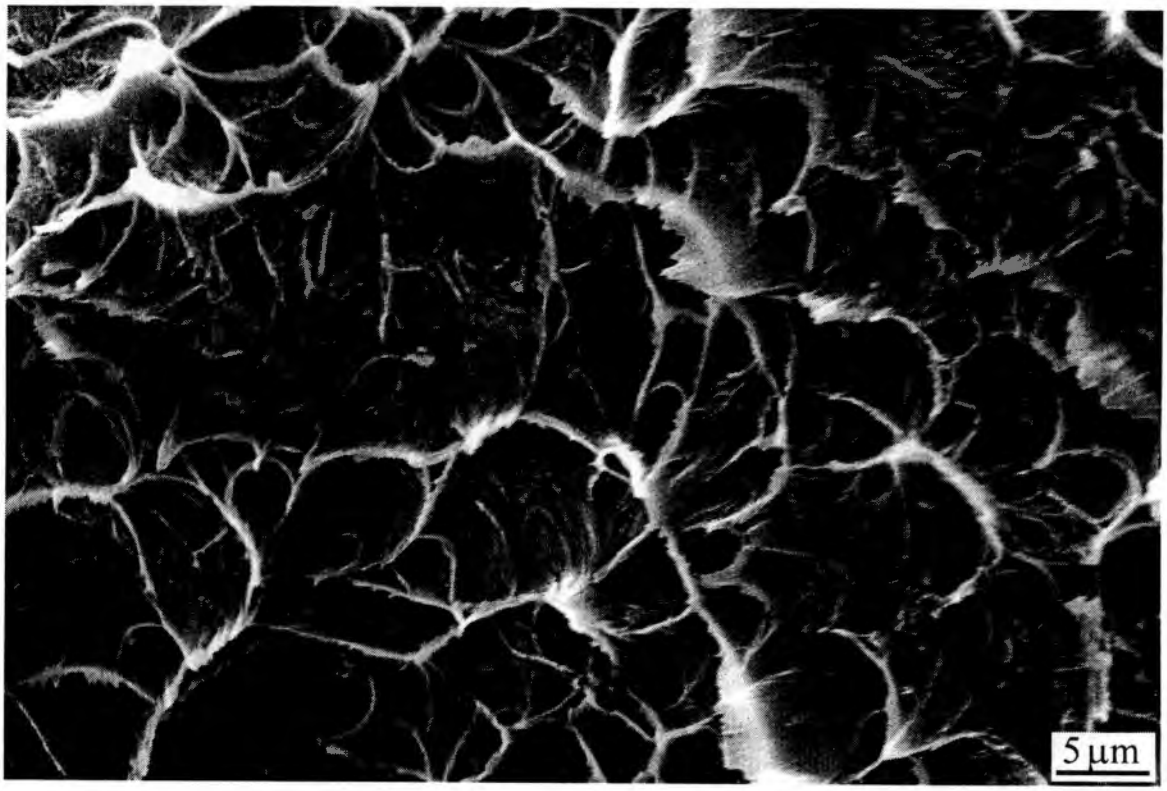

Figure 4.44. SEM micrograph of non-etched fracture of neat sPS melt crystallized at 220°C showing nucleus intraspherulitic fracture.

Figure 4.45 shows a low magnification micrograph of etched tensile fracture surface of sPS50PPO blend sample crystallized at 255°C. The uneven surface shows spherulites protruding out of the matrix. The depressed regions are the impressions of the spherulites pulled out from the fracture surface with the other section of the tensile specimen. One spherulite of the same sample imaged at high magnification is shown in Figure 4.46. In this micrograph the amorphous domains appear elongated and irregular in shape after fracture. Similar etched fracture surface micrograph for the sPS50PPO blend sample crystallized at 220°C is shown in Figure 4.47. The fracture surface consists of etched spherulites impinged with each other. These spherulites are very similar to the ones seen in the non-fractured films imaged before (Figures 4.35 through 4.39).

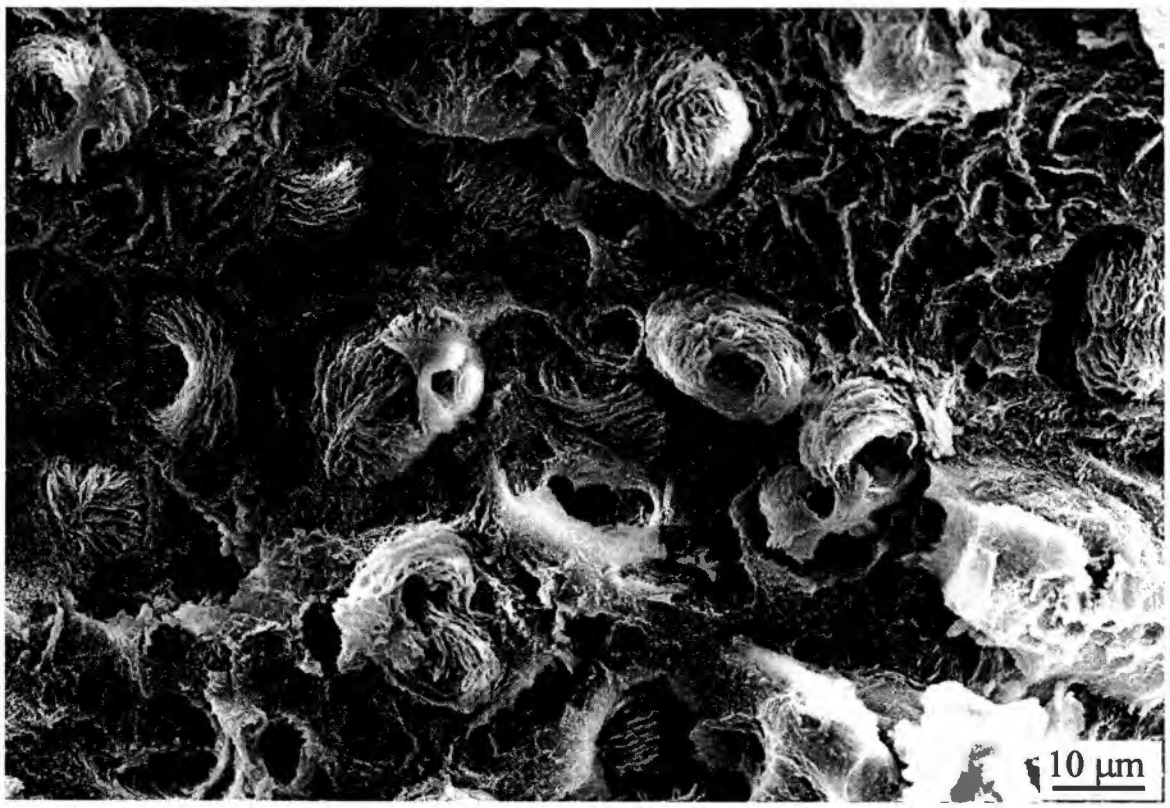

Figure 4.45. SEM micrograph of etched fracture surface of sPS50PPO blend crystallized at 255°C showing interspherulitic fracture.

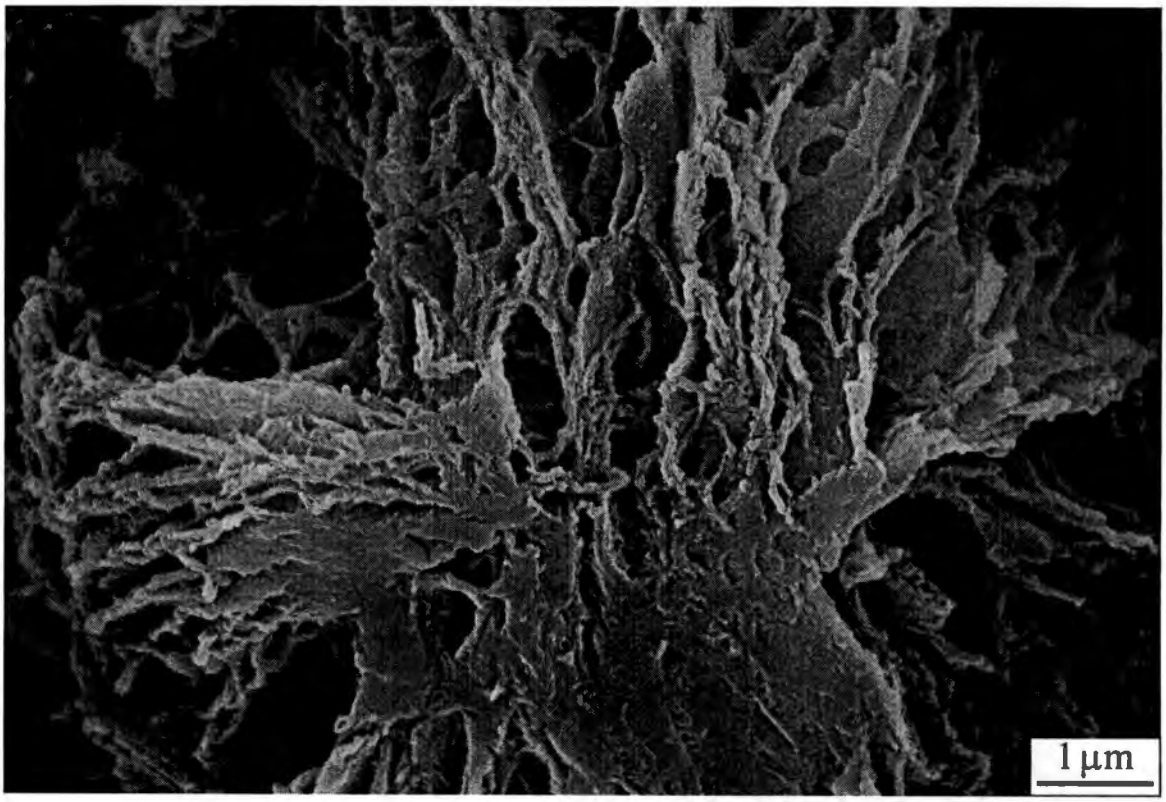

Figure 4.46. SEM micrograph of etched fracture surface of sPS50PPO blend melt crystallized at 255°C showing deformed amorphous regions.

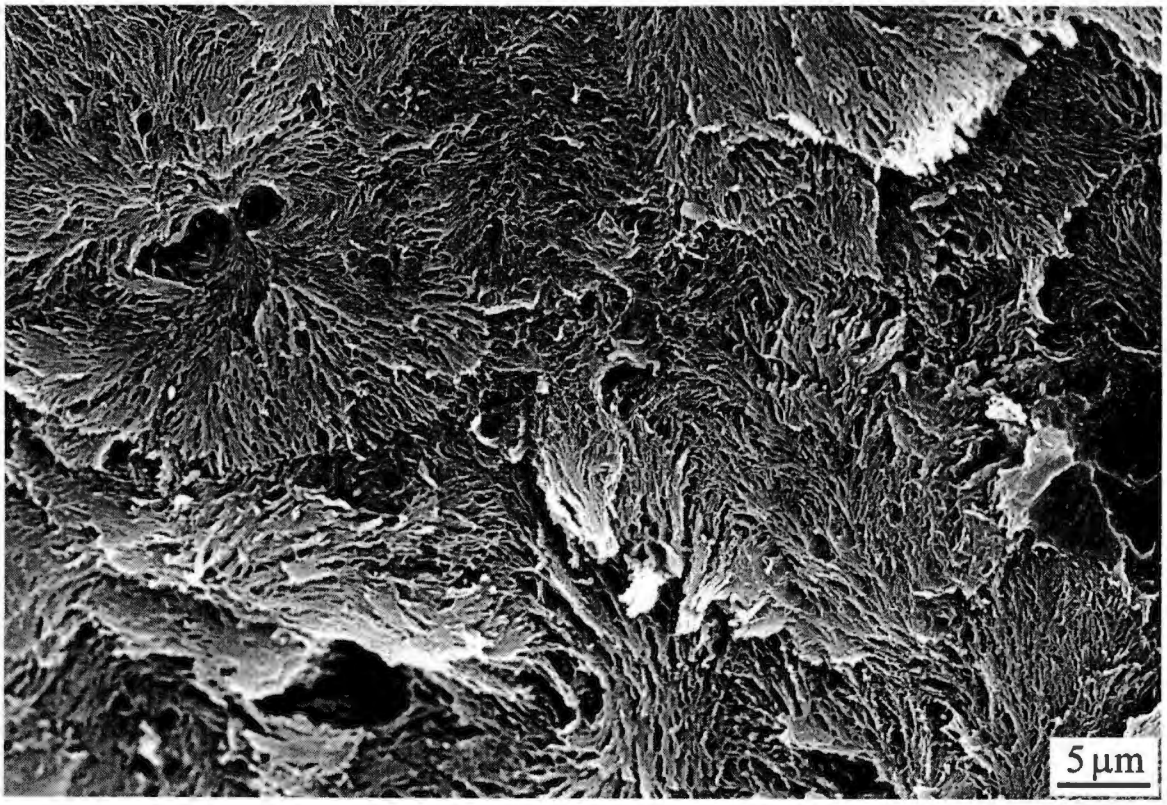

Figure 4.47. SEM micrograph of etched fracture surface of the sPS50PPO blend melt-crystallized at 220°C showing unstrained impinged spherulites.

Chapter 5

DISCUSSION

5.1 Differential Scanning Calorimetry

In all the DSC scans of different composition quenched sPS/PPO blends (Figure 4.1), a single, well-defined, composition-dependent glass transition is observed. It clearly suggests that, at all compositions, the blend is miscible to the segmental level in the melt.

The pronounced effect of the PPO on the crystallization and melting of the sPS is also evident. With the increase in the PPO content, the crystallization exotherm, during the heating scan, becomes smaller and occurs at higher and over a wider range of temperatures. Depression in the melting point of sPS increases with increase in PPO composition. The corresponding melting endotherm also becomes smaller. In the sPS50PPO blend, the crystallization exotherm on heating is not seen at all. The increase in crystallization temperatures (T_c) and decrease in melting temperatures (T_m), with the increasing PPO content, suggest that PPO strongly interferes with the sPS crystallization from the amorphous phase. These effects also indicate segmental miscibility. Guerra *et al* [48] have also reported the same trend for the quenched sPS/PPO. They have also shown that the behavior of the miscible sPS/aPS (atactic polystyrene) is completely different; in this system the T_c values and the degrees of crystallinity of the sPS component remain almost unchanged. They have suggested that the increase in T_c may be due to the increase in glass transition temperature on

the addition of PPO. The glass transition temperatures of the sPS/aPS blends, of course, remain practically unchanged.

5.2 Dynamic Mechanical Analysis

5.2.1 Quenched Blends

The mechanical loss tangent (tanδ) scans of different composition quenched sPS/PPO blends show a single, well-defined, composition dependent amorphous phase relaxation corresponding to the glass transition. It indicates true segmental homogeneity in the amorphous phase.

Several T_g-composition analysis relations were used to fit the temperature of the relaxation to the composition and the relaxation temperatures of the quenched, neat sPS and PPO. The composition dependent T_g predicted by Kelly-Bueche equation [17], Flory-Fox equation [20] and Couchman-Karasz relation [18] are compared with the relaxation temperatures obtained from the DMA in Figure 5.1. The linear Gordon-Taylor equation [19] has also been used to fit the transition temperatures recorded by the DMA. The parameter k, which is the ratio of change in thermal expansion coefficients of the neat polymers, between their rubbery and the glassy states was found to be 0.83 for the best fit to the experimental data. This value of the parameter k was then used to predict the compositions of the amorphous phases of the crystallized blends also. It is interesting to note that, using $\alpha_{PPO} = 0.69\alpha_{sPS}$ [61], where

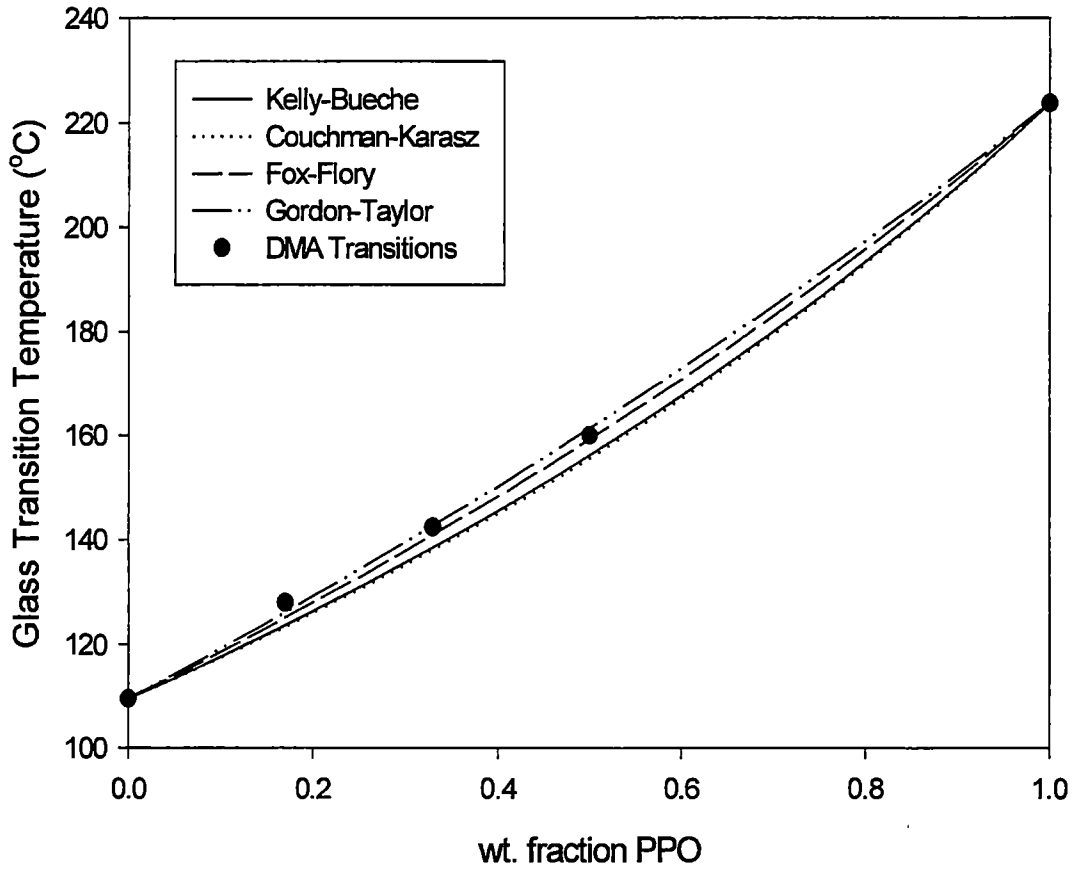

Figure 5.1. Composition dependence of glass transition temperatures of quenched blends by different relations.

α is thermal coefficient of expansion, both Kelly-Bueche equation and Couchman-Karasz relation give identical predictions for the T_g of the miscible sPS/PPO system. The DMA transition temperatures for the pure, quenched sPS, PPO and blends are higher than the ones obtained from the DSC. Guerra *et al* [51] have also obtained very similar results. The difference is reasonable in view of the tensile strain applied to the samples in the DMA, at the frequency of 1.1 Hz, simultaneously with the temperature sweep. Moreover, since the thermocouple in the sample chamber is not in direct contact with the sample, the transition temperatures obtained are only relative. Any inadvertent change in the thermocouple position may have also affected the peak temperatures.

The shoulders to the primary relaxation peaks in the quenched blends are due to the crystallization of the sPS and reorganization of smaller crystals during the annealing of predominantly amorphous samples from the quenched state. That these shoulders do not constitute a relaxation from a different amorphous phase is confirmed by the behavior of the storage modulus with the change in temperature. The crystallization during heating leads to the modulus recovery in the modulus-temperature curve as shown for the sPS50PPO blend in the Figure 5.2. The shoulder is broader at higher PPO content, which is a result of slower crystallization at these compositions. The smaller intensity, and increased width of the relaxations in blends, as compared to the neat polymers are evidently due to the crystallites formed in the cold crystallization during heating.

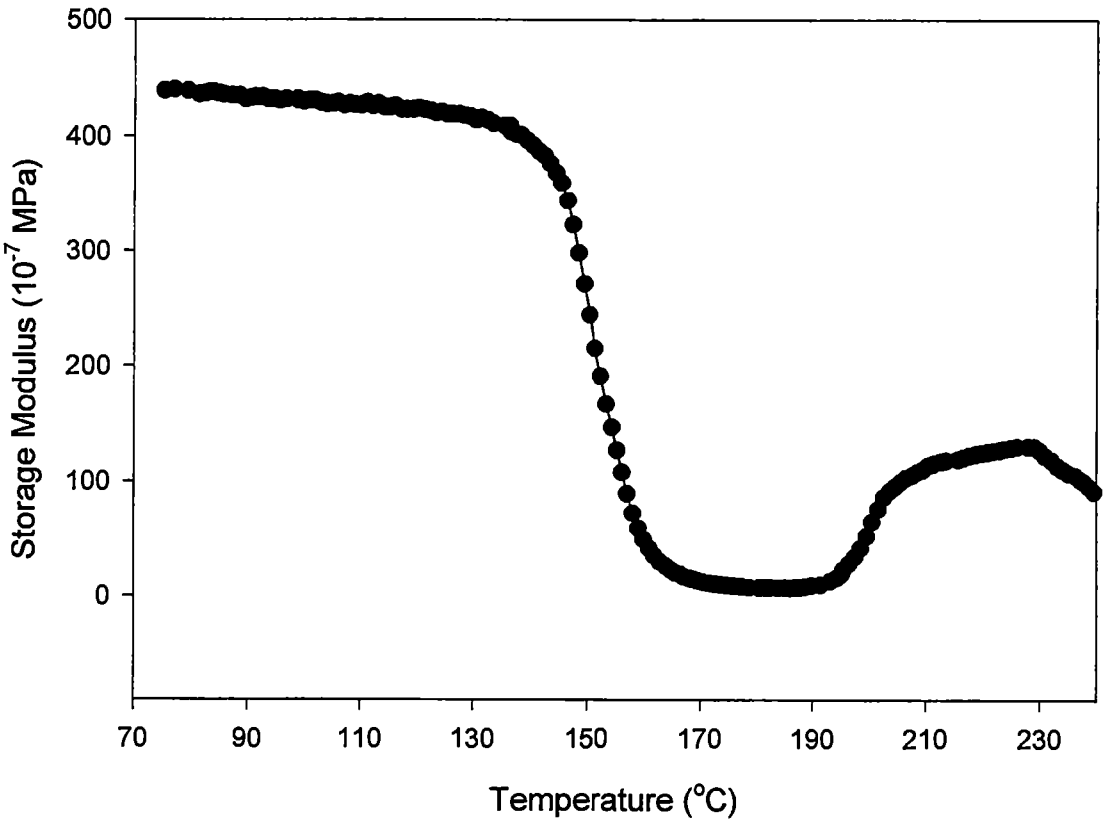

Figure 5.2. DMA storage modulus for quenched sPS50PPO blend.

5.2.2 Cold Crystallized Blends

As shown in the Figures 4.3 through 4.5, all cold crystallized blends (except some sPS83PPO blends) show a distinct shoulder to the major relaxation peak observed in the quenched amorphous blends. The storage modulus for the sPS50PPO blend cold crystallized at 180°C is shown in the Figure 5.3. Although the shoulder to the primary relaxation peak is most prominent at this temperature in the loss tangent scan, no modulus recovery can be seen after transition from the glass to the rubbery state in the storage modulus scan. This behavior strongly suggests that the shoulder is not due to the crystallization during the temperature sweep. Hence it can be concluded that the shoulders to the primary relaxation peaks indicate segregation of the uniform amorphous phase in the quenched blends into two distinct, but homogeneous, amorphous phases of different compositions. The intensity of the shoulder is much smaller than that of the primary relaxation. It indicates that the relative amount of the second phase is much smaller. No evidence of pure sPS or PPO amorphous domains is observed. Broader peaks at lower temperatures (lower crystallization rates) may be result of combined effect of segregation on a larger scale and the constraining effect of the crystallites on the relaxation of the amorphous regions. These smaller crystallites have a large number of amorphous domains of similar compositions, which give a broad amorphous peak. This effect is more pronounced at higher sPS content because of the higher crystallinity obtained at these compositions.

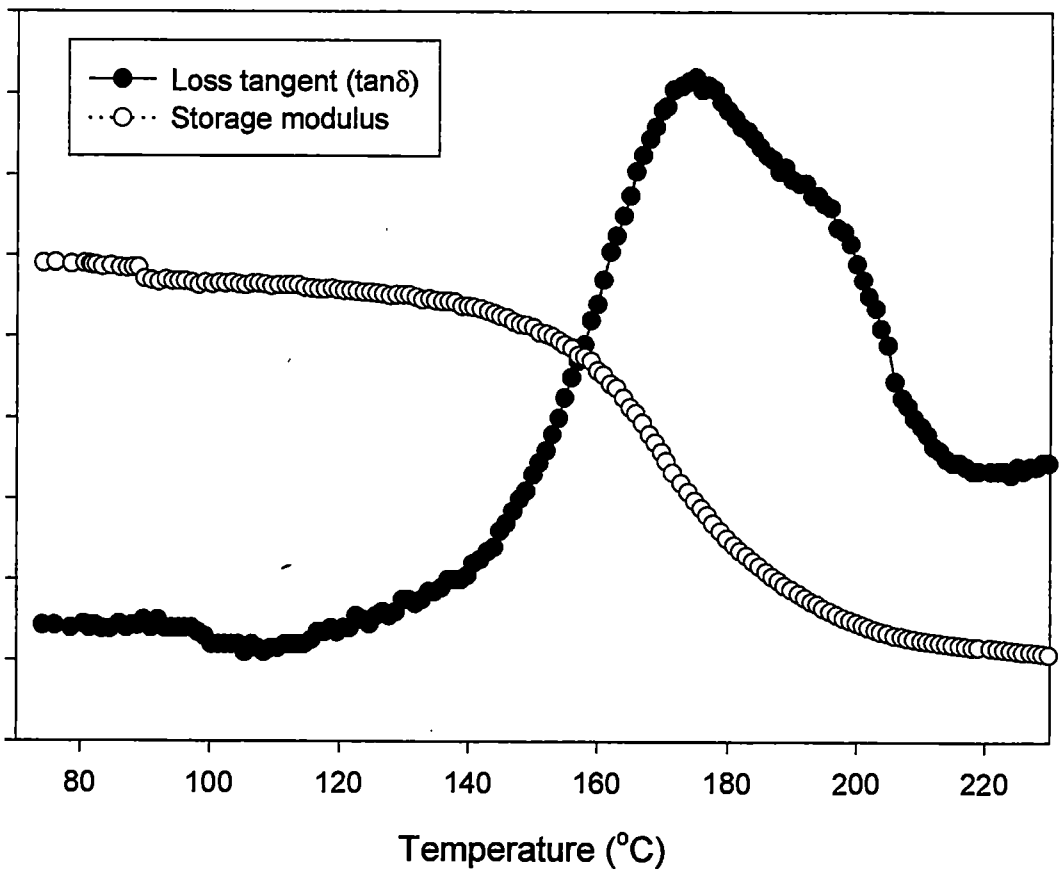

Figure 5.3. **Storage Modulus and loss tangent for sPS50PPO blend cold crystallized at 180°C.**

As stated before, given the transition temperatures of the neat homopolymers and the blend compositions, temperatures of relaxations for the blends can be substituted into a suitable T_g-composition to back calculate the composition of the phases. Several authors have reported the results of such studies [27,30]. In this study, the compositions of homogeneous amorphous phases, developed after crystallization, have been calculated using the Gordon Taylor equation (k = 0.83). Since the transition temperatures in the crystallized blends are higher because of the constraining effect of the crystallites on the amorphous domains, these calculated compositions are not very accurate and, at best, qualitatively indicate the relative composition variations in the two phases with changes in crystallization temperatures. The variation in amorphous phase compositions, with change in crystallization temperatures, of the sPS50PPO and sPS67PPO blends is shown in Figures 5.4.

For all the blend compositions, crystallization at 220°C results in both the amorphous phases with the highest sPS contents. Since among all the temperatures, the crystallization rate is highest at this temperature, small, less perfect sPS crystals are formed and overall crystallinity is low. With decreasing temperature (and decreasing crystallization rate), the sPS concentration in both the amorphous phases decreases. It can be directly correlated to the increase in crystallinity. The crystallinity index of these cold and melt crystallized blends, calculated from WAXD spectra, is shown in Figure 4.19. The changes in the slope of the sPS concentration lines between different crystallization temperatures can be followed with the crystallinity changes. The

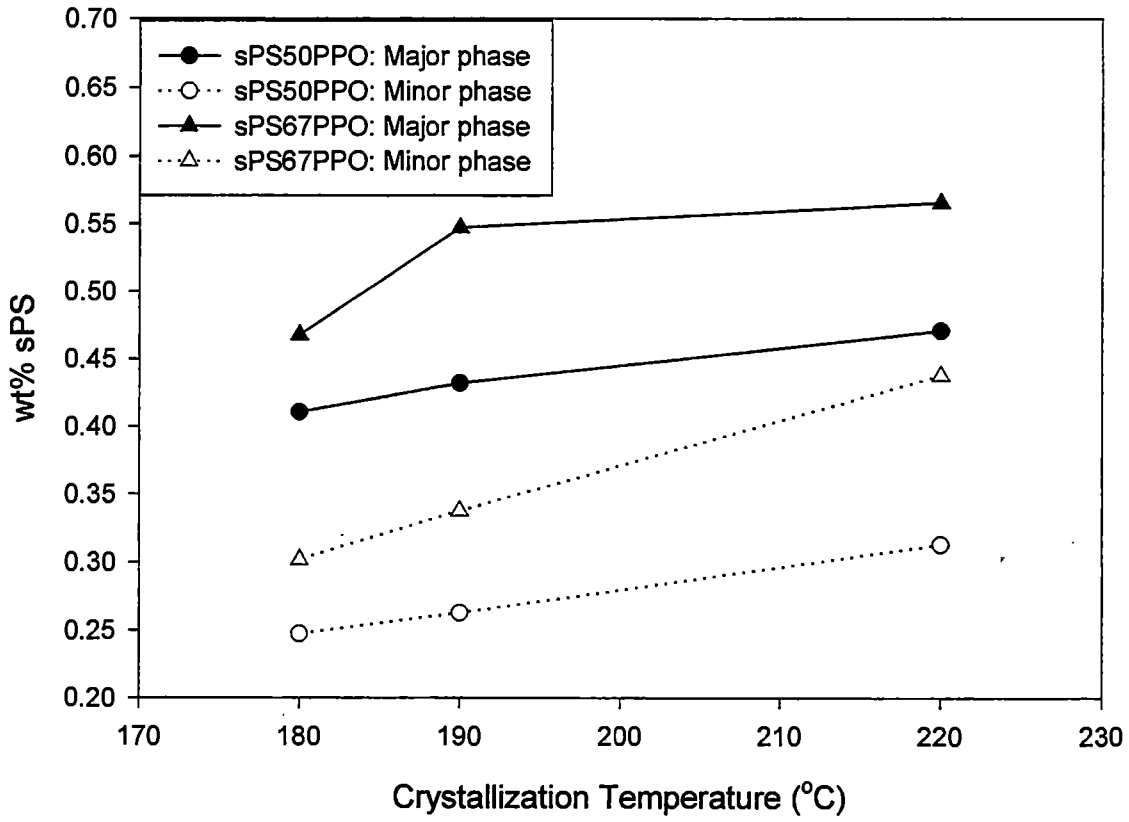

Figure 5.4. **Variations in the amorphous phase compositions for cold crystallized blends, as calculated from DMA transition temperatures and Gordon-Taylor relation.**

higher slope between the temperatures 190°-180° is reflected in the sharper decrease in crystallinity (especially for the sPS67PPO blends). This effect is more pronounced in sPS67PPO blends. Higher crystallinity reduces the sPS concentration and results in PPO rich amorphous phases.

The identification of these amorphous phases as interspherulitic or inter/intra-lamellar is difficult. Crystallization of quenched sPS/PPO blends at large supercoolings results in large number of nuclei, which grow into relatively small, imperfect spherulites on cold crystallization. In these spherulites, it becomes difficult to distinguish between the inter/intra-lammellar regions. Still the SEM micrographs suggest that these spherulites are space-filling, which indicates that the interspherulitic segregation is minimal.

5.2.2 Melt Crystallized Blends

All melt crystallized blends, except sPS83PPO, show a primary relaxation peak followed by a small shoulder or a peak. The second peak is most visible for the sPS50PPO blend melt crystallized at 255°C. The corresponding behavior of the storage modulus for this sample is shown in Figure 5.5. No evidence of crystallization during the temperature sweep is seen. It suggests that the second peak is due to the segregation of the initially homogeneous phase into two different phases, which consist of both the polymers dispersed uniformly in different compositions. Increase in PPO content increases the glass transition temperature and pushes the relaxations

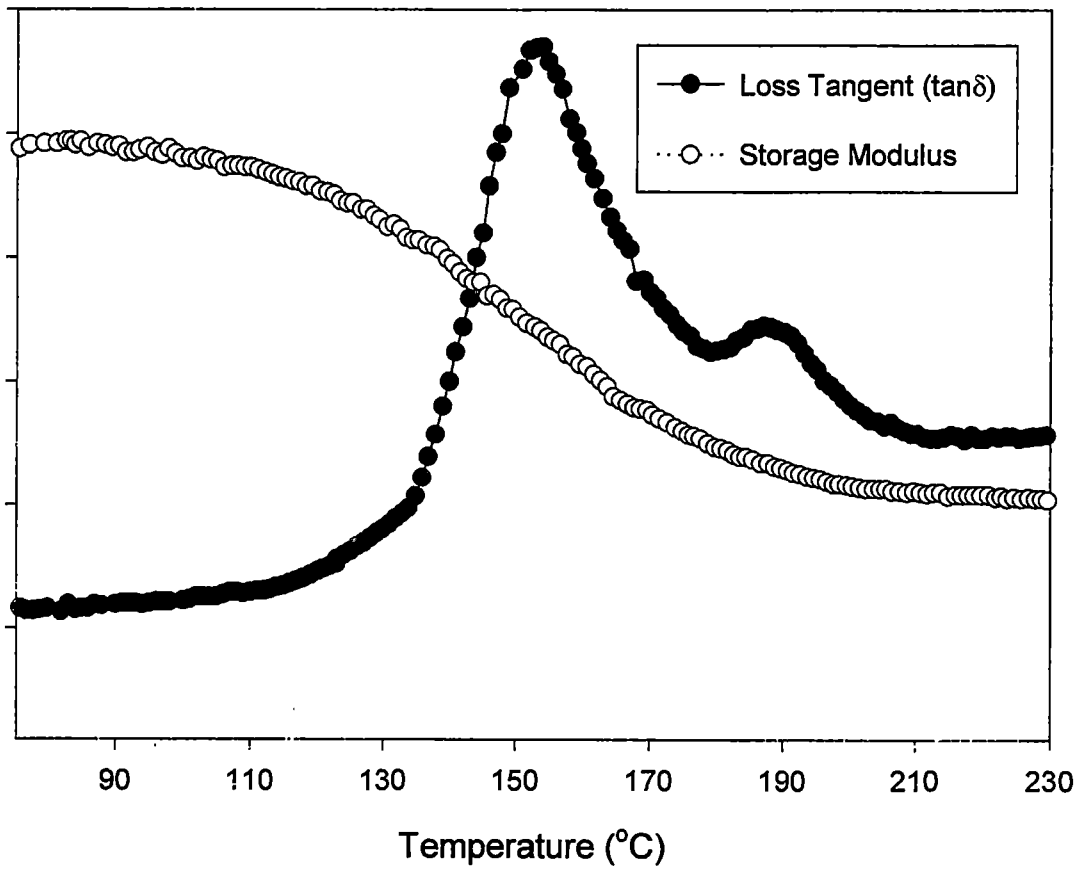

Figure 5.5. **Storage modulus and loss tangent for sPS50PPO melt crystallized at 255°C.**

to higher temperatures. For a fixed composition, increase in crystallization temperature increases the difference between the temperatures of the primary and secondary relaxations. It suggests that slower crystallization facilitates the formation of phases of increasingly different compositions. The decreasing temperature of the primary relaxation suggests an increase in the sPS (lower glass transition temperature (T_g) component), in the major phase at the cost of the minor second phase. Crystallization from melt provides lesser constraints on the diffusion of the low T_g amorphous part, as there are fewer nuclei than the cold crystallization.

As in case of the cold crystallized blends, the composition of the phases corresponding to the primary and the secondary relaxations have been calculated using the Gordon Taylor relation (k = 0.83). The variation in the composition of the phases with the change in crystallization temperature is shown in Figure 5.6. For both sPS50PPO and sPS67PPO blends, with the increase in the crystallization temperature, the concentrations of the major and minor phases diverge away from each other. While the major phase becomes sPS rich, the minor phase is depleted of the sPS and becomes PPO rich. Therefore, crystallization at higher temperatures leads to increased degree of segregation.

The concentration profile of the amorphous sPS in the minor phase also corresponds with an increasing relative crystallinity with the increase in crystallization temperature. The growing sPS crystal front absorbs the amorphous sPS and rejects

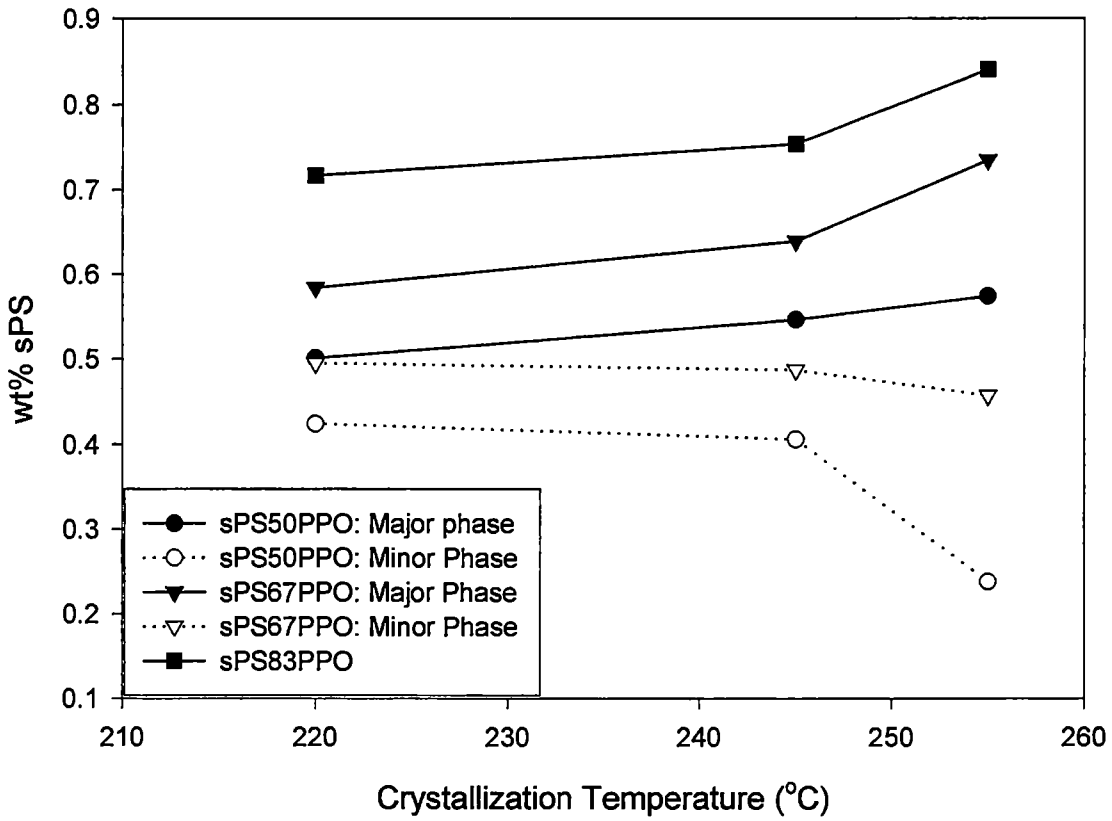

Figure 5.6. **Variations in the amorphous phase compositions for melt crystallized blends, as calculated from the DMA transition temperatures and Gordon-Taylor relation.**

the PPO. As a result, the sPS concentration is smallest near the growing crystal front and increases at longer distances. The concentration of PPO changes in the reverse manner. It is highest near the growing crystal front and decreases with the increase in distances. These observations follow closely with the expected concentration profiles of the interlamellar and interfibrillar regions. A schematic diagram of the growing lamellar fronts in a bundle and corresponding interlamellar and interfibrillar regions is shown in Figure 5.7. The fine interlamellar regions constitute minor sinks of the amorphous regions and due to their proximity to the crystal growth front should have lowest sPS and hence the highest T_g. Since the interspherulitic segregation of the amorphous material is not seen, the interfibrillar regions should then form the major sinks of the amorphous sPS and non-crystallizable PPO. These regions should have high amorphous sPS and low PPO concentration, and hence lower T_g. Therefore it can be concluded that the high intensity peak at lower temperature is due to the relaxation of the amorphous material present in the interfibrillar regions. The smaller intensity shoulder at higher temperatures is due to the relaxation of the amorphous interlamellar regions.

5.3 Wide-Angle X-ray Diffraction

The WAXD results prove that blending with PPO alters the polymorphic behavior of sPS. Cold crystallization of the blend, from the quenched state, results in varying degree of disordered α and β forms. For the pure cold crystallized sPS polymorphic forms very close to the α phase are formed. Blending leads to the disordering of the α

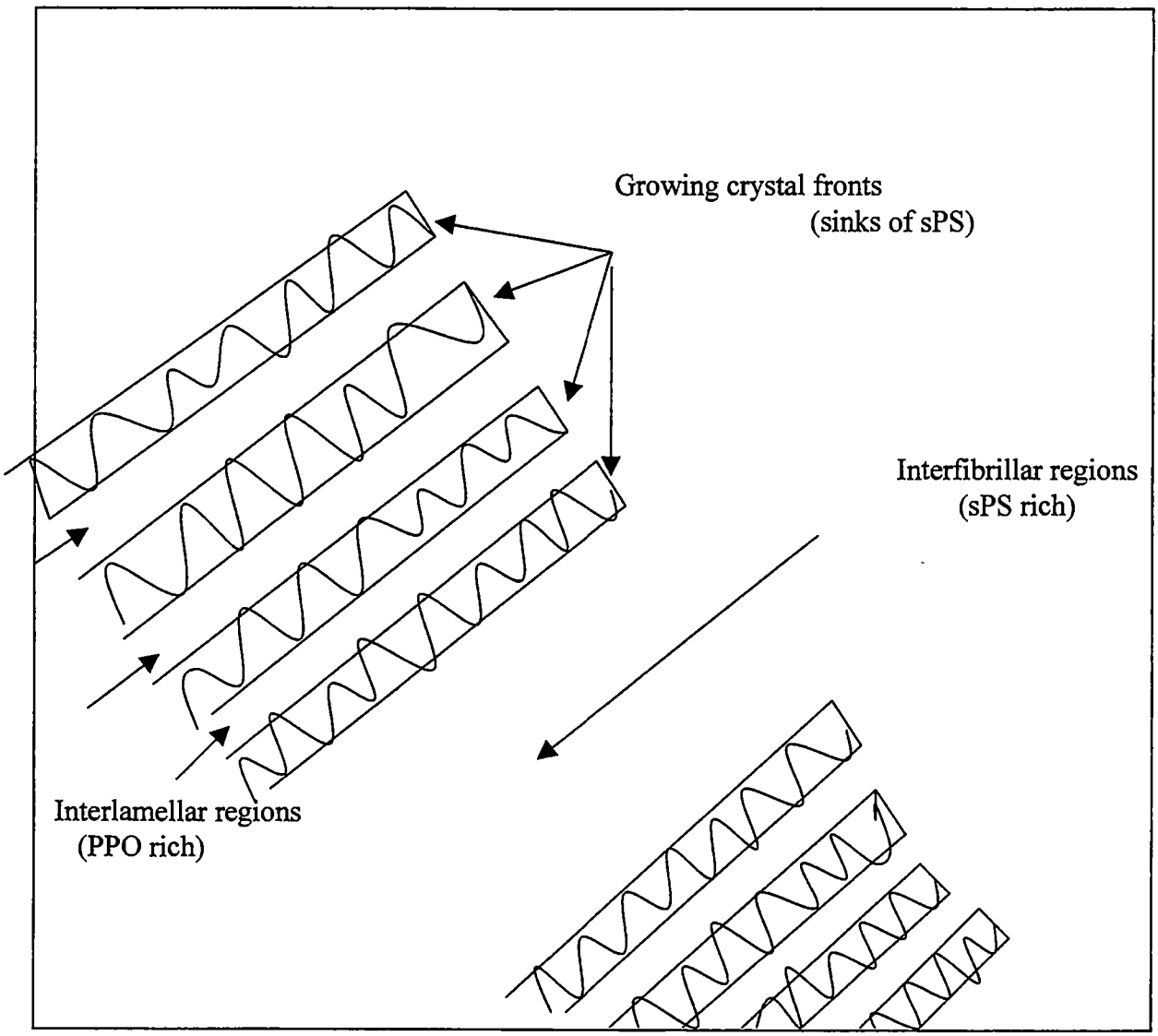

Figure 5.7. Schematic diagram of interlamellar and interfibrillar amorphous regions and their expected compositions.

phase into α' or β phases depending upon low and high content of the PPO respectively. In case of melt crystallized blends, the formation of β phase is favored. Neat, melt crystallized sPS exists in both α and β forms. Blending with PPO and melt crystallization results in increasing β content, which increases with increasing PPO content.

In general, for both melt and cold crystallization, slower crystallization results in higher crystallinity (Figure 4.19). Slower crystallization leads to formation of more perfect crystals and leads to higher crystallinity.

The crystallinity of the sPS/PPO blends depends greatly upon the PPO content. The ratio of WAXD crystallinity of the blend to the corresponding weight fraction of the sPS gives the actual weight percentage of the sPS crystallized in the blend. The WAXD crystallinity on the basis of weight fraction of the sPS is plotted against the blend composition in Figure 5.8. The continuous decrease in the actual content of the sPS crystallized clearly shows the retarding effect of the PPO on sPS crystallization.

It is difficult to explain the drastic changes in the polymorphic forms and crystallization behavior of the sPS. A possible reason might be the difference in the glass transition temperatures of the two constituent polymers. Increase in PPO content increases the glass transition and crystallization temperatures and reduces the melting point (T_m). Hence the temperature range between the T_g and T_m is considerably

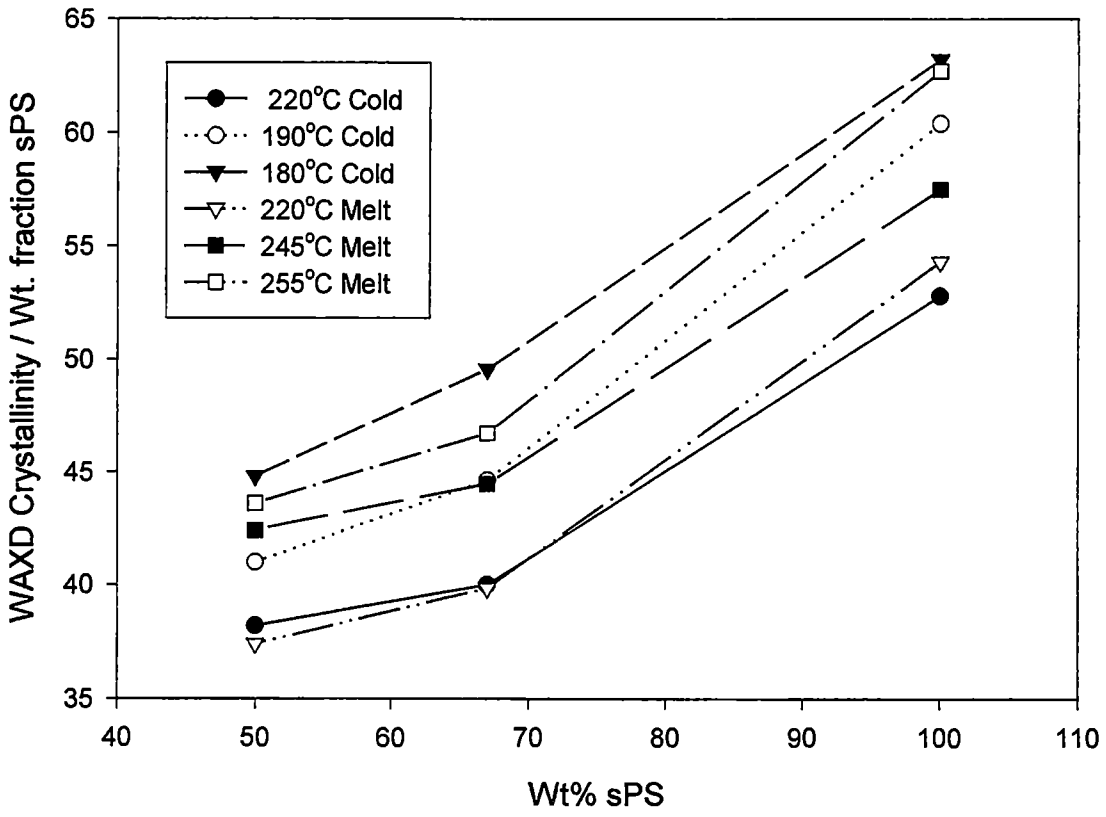

Figure 5.8. **WAXD crystallinity calculated on the basis of sPS wt. fraction against blend composition.**

reduced. This change is reflected in phase changes and reduced crystallinity. It is relevant to note that these changes are not observed in the miscible sPS/aPS system [50]. Both blend components have very close T_gs and the crystallization temperature and crystallinity of the sPS remain practically unchanged.

5.4 Density Measurement

Density readings from the Density Gradient Column (DGC) show very small differences in the blends crystallized at different temperatures. The density of the neat sPS, quenched from the melt was found to be 1.048 g/cm^3, while that of the quenched PPO was 1.073 g/cm^3. Therefore, density values of the blends seem to depend, to a large extent, on the PPO content in the blend. The change in density for the sPS83PPO blends, both melt or cold crystallized at different temperatures, is much more than the other composition blends.

In case of melt crystallized blends, increase in density with increasing crystallization temperature is accompanied by an increase in crystallinity. It suggests that the crystal structure formed has higher density than the amorphous phase. This result is in good agreement with the increase in the content of high-density (1.08 g/cm^3) β form as shown by the WAXD patterns.

The cold crystallized blends show a decrease in the density with increasing crystallinity. This decrease is more visible in the blends with high crystallinity and

sPS content. This result is also in good agreement with the WAXD patterns, which show that at low PPO content cold crystallization leads to the formation of slightly disordered, low-density (1.033 g/cm^3) α' forms.

5.5 Tensile Testing

5.5.1 Cold Crystallized Blends

The mechanical properties measured for the cold crystallized sPS/PPO blends vary substantially only with the change in composition. High PPO content blends (as in sPS50PPO) have higher tensile strength and strain at break as compared to the sPS67PPO blends. But, for a constant composition, although slower crystallization leads to better properties, change in crystallization temperature has a minor effect on these values (Tables 4.1 and 4.2).

The variation in mechanical properties with the PPO composition, at different crystallization temperatures, is plotted in Figures 5.9 through 5.11. The tensile data for the neat PPO has been taken from a reference [60] in which the testing was done at the same strain rate. For comparison, based upon the ultimate tensile properties of the crystallized neat polymers, changes in properties of the blends linearly with composition have been calculated. This linear composition dependence of the mechanical properties can be termed as *linear rule of mixtures*.

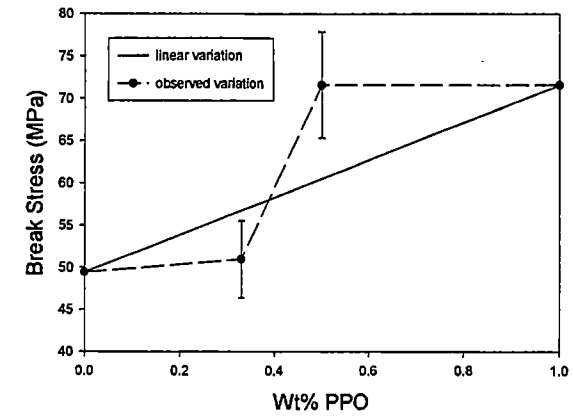

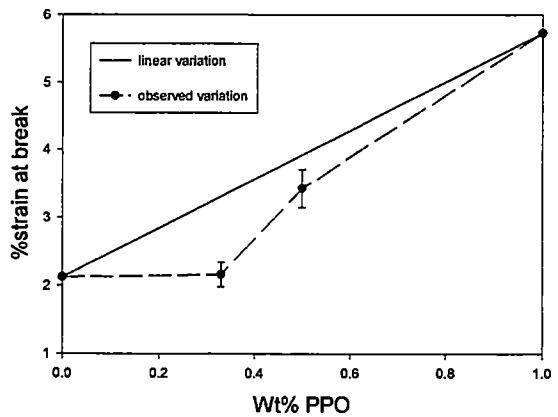

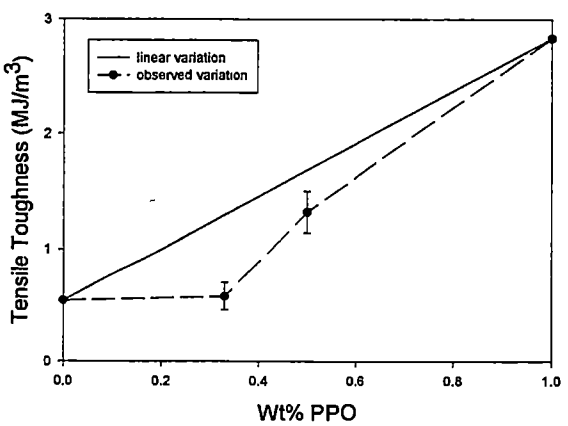

Figure 5.9. Tensile properties of sPS/PPO blends cold crystallized at 180°C.

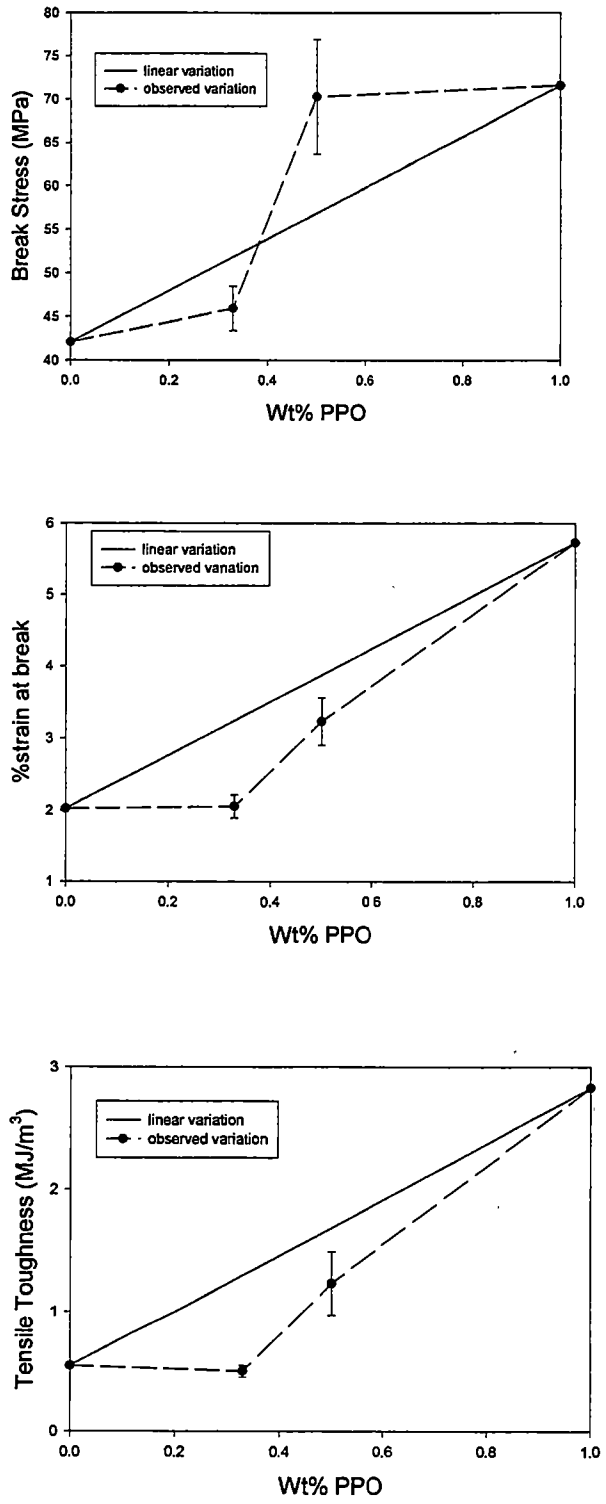

Figure 5.10. Tensile properties for sPS/PPO blends cold crystallized at 190°C.

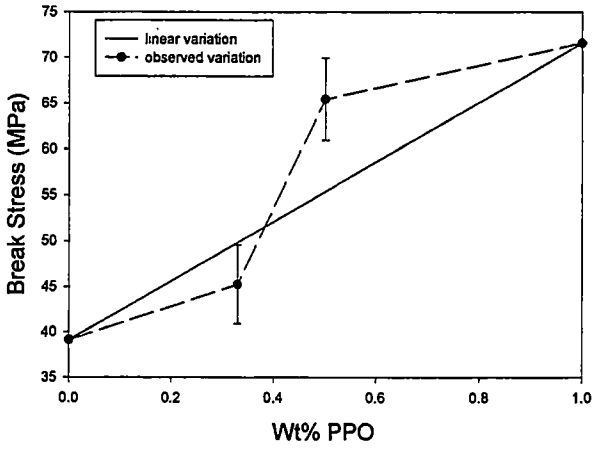

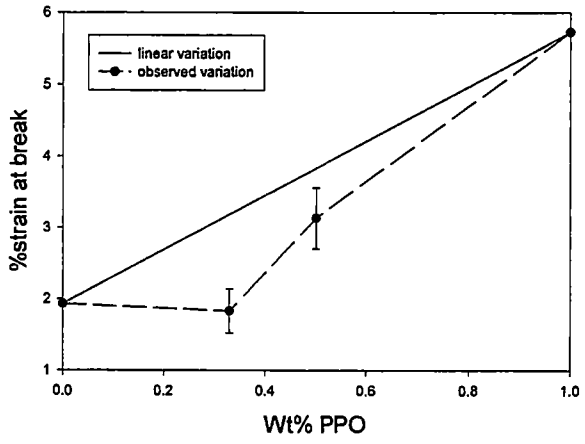

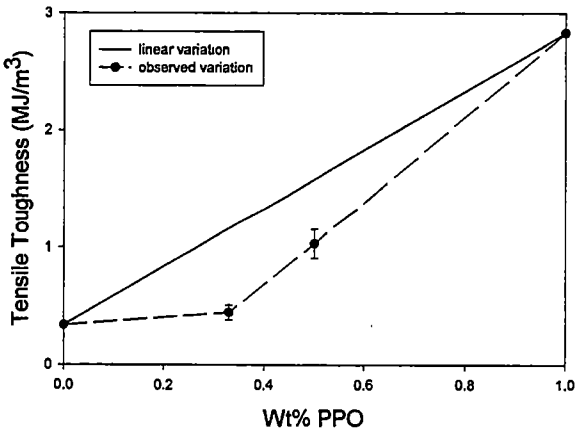

Figure 5.11. Tensile properties of sPS/PPO blends cold crystallized at 220°C.

The tensile strength of sPS50PPO blends, cold crystallized at different temperatures, is higher than that calculated by the linear rule of mixtures. In case of sPS67PPO blends, these values are quite comparable. So there appears to be a synergism in the tensile strength for the blends having PPO content at least near 50%. For the strain at break and tensile toughness, the values obtained for both the blend compositions are always much lower than the ones calculated by the linear rule of mixtures.

These comparisons of the results suggest that although blending increases the tensile strength the sPS still remains inherently brittle. As seen from the DMA scans, even after crystallization the blends predominantly consist of one amorphous phase only. The second minor phase, if present, is very small in mass fraction, and usually has composition close to that of the major phase. This phase behavior suggests formation of a uniform rigid matrix. There seem to be no stress concentrators to nucleate crazes or initiate some other mechanism to relieve the hydrostatic tension.

5.5.2 Melt Crystallized Blends

In case of the melt crystallized blends, there is a substantial change in the measured mechanical properties with the change in the composition. For sPS50PPO blends, there is a strong variation in these properties with the change in crystallization temperature also (Tables 4.4 and 4.5).

The variation in mechanical properties with the PPO composition, at different crystallization temperatures, is plotted in Figures 5.12 through 5.14. An interesting trend is observed from these figures and the Tables 4.4 and 4.5. The ultimate mechanical properties for the melt-crystallized blends, as calculated by the linear rule for mixtures, decrease with increase in crystallization temperature. The observed mechanical properties, on the other hand, show an increase in these ultimate properties with an increase in the crystallization temperature. However, the observed values are, in general, much lower than the ones predicted by the linear rule for mixtures. The only exception is the SP50PPO blend melt crystallized at 255°C. The ultimate tensile strength for this blend is much higher than the linear rule, while the strain at break is quite close to the calculated value. This outstanding synergistic behavior is not shown by any other blend.

As in case of the cold crystallized blends, these blends are essentially brittle. The changes in the mechanical properties, with the processing temperatures, can not be explained on the basis of the changes in crystallinity. The cold crystallized blends also follow a very similar trend in crystallinity. The data for ultimate mechanical properties suggests that the spherulitic morphology plays an important role. The change in crystallization temperatures, and the corresponding changes in amorphous phase compositions and distribution of amorphous domains in the spherulite, has profound effect on these properties. The energy absorption mechanisms in most of these blend samples in not clear. It has also been suggested [65] that cold drawing of

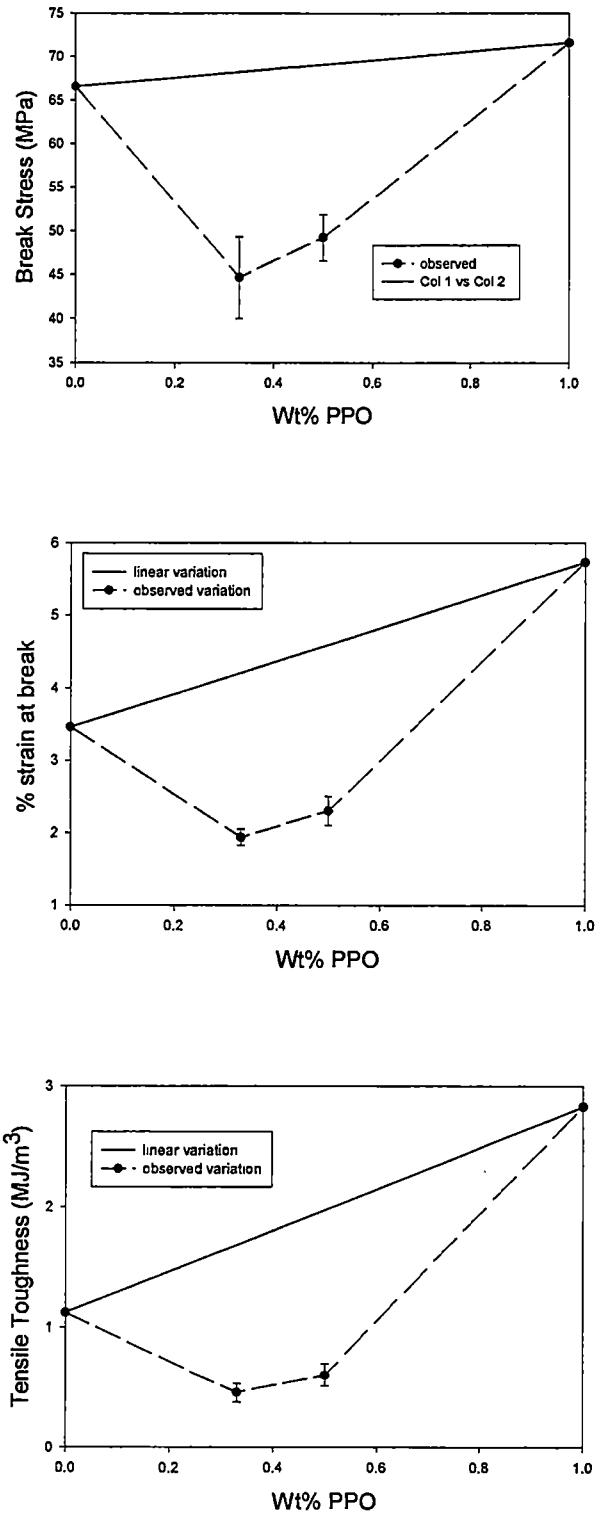

Figure 5.12. Tensile properties of sPS/PPO blends melt crystallized at 220°C.

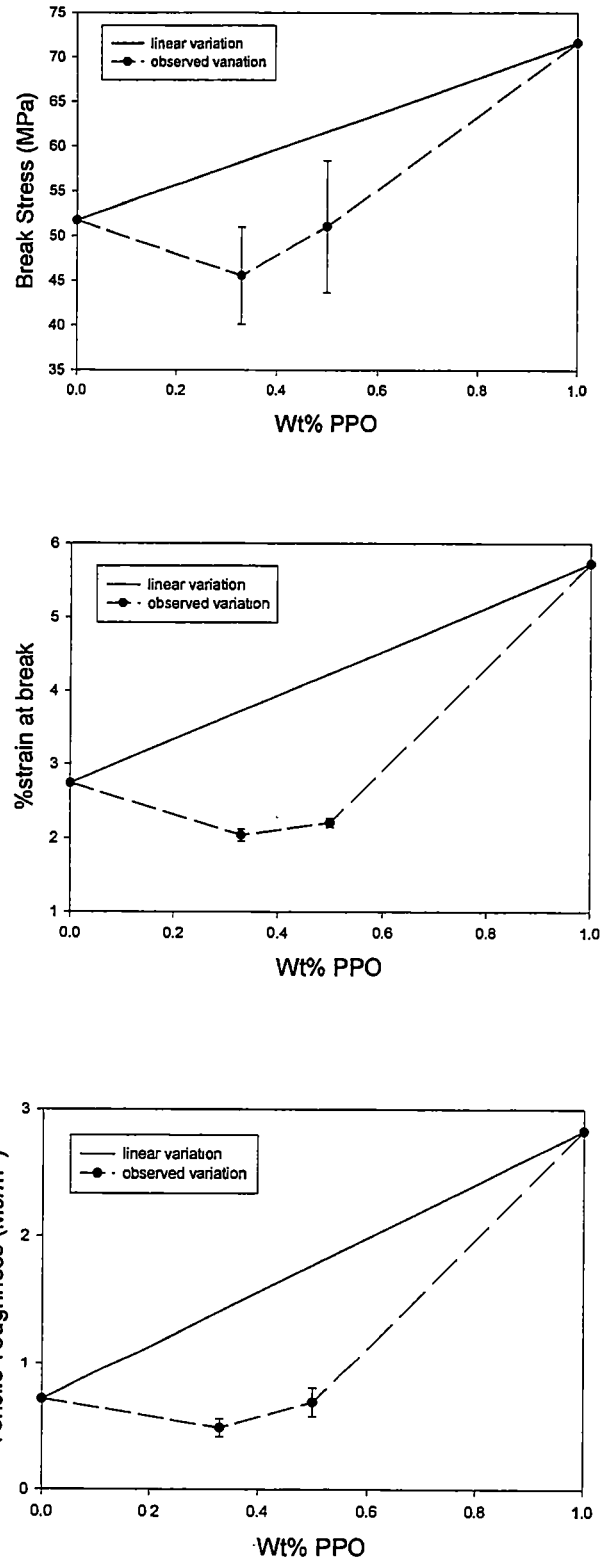

Figure 5.13. Tensile Properties of sPS/PPO blends melt crystallized at 245°C.

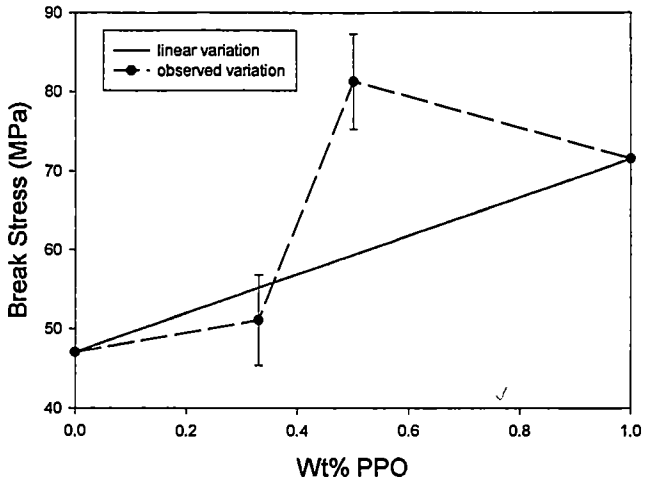

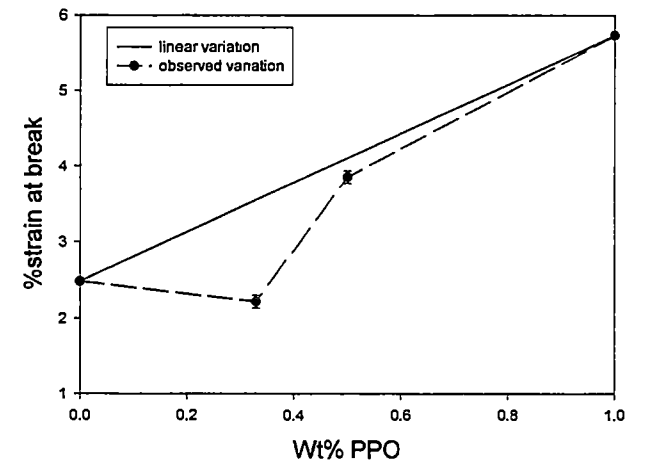

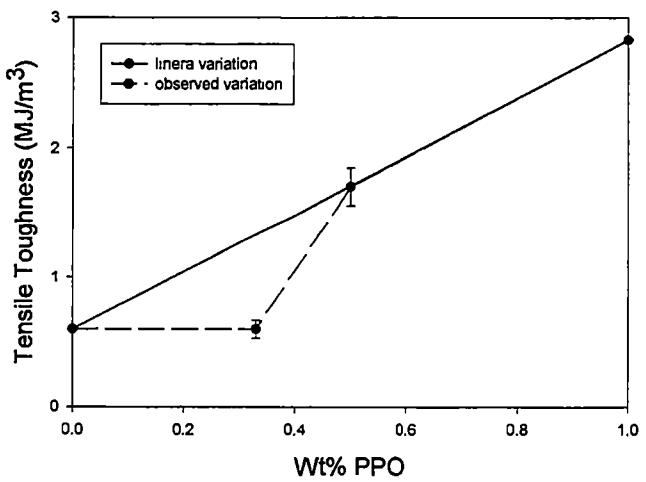

Figure 5.14. Tensile properties of sPS/PPO blends melt crystallized at 255°C.

the more rigid phase should occur to facilitate the absorption of energy. The SEM micrographs of non-etched fracture surfaces of the sPS50PPO melt crystallized at 255°C do show highly drawn fibrils.

5.6 Scanning Electron Microscopy Micrographs

5.6.1 Cold Crystallized Blends

The cold crystallized blends show very fine lamellar bundles whose dimensions do not vary substantially with the change in crystallization conditions (Table 4.7). It might be attributed to the quenching step in the processing of these blends. A sharp drop in the temperature from the melt-state to the room temperature (below the glass transition temperature of the blend), and further annealing at high supercoolings results in the formation of large number of nuclei. These nuclei are almost contiguous to each other. When the blend is crystallized, small, imperfect spherulites are formed which impinge very quickly, resulting in a mesh like structure. Longer annealing times cause secondary crystallization, but it makes little changes in the morphology. The corresponding changes in the measured ultimate mechanical properties are also small.

5.6.2 Melt Crystallized Blends.

Melt crystallized blends show appreciable changes in the morphology with the change in blend composition and crystallization temperature. All the melt crystallized blends show well developed spherulites grown from the melt. The spherulite size,

bundle thickness and the dimensions of the elliptical amorphous regions increase with increase with crystallization temperature (Table 4.8). The bundle spacings, on the other hand, show a small decrease with increase in temperature.

As per the theory of spherulitic crystallization of Keith and Padden [24], the change in the bundle thickness with the change in crystallization temperature can be qualitatively correlated to the diffusion length δ, which is the ratio of diffusion rate of the rejected species to the crystalline growth rate. At temperatures close to the melting point (like 255°C and 245°C), the crystal growth rate is very small and the corresponding diffusion coefficient is very large. Both these factors result in a large value of δ and hence, large bundle thickness. At crystallization temperature of 220°C, there is an exponential decrease in the diffusion coefficient. The crystalline growth rate, for the sPS50PPO blend, increases by an at least an order of magnitude [52]. The result is a much smaller diffusion length δ and is reflected in the smaller measured bundle thickness.

The corresponding changes in the ultimate mechanical properties, at least for the melt crystallized sPS50PPO blends, are also substantial. The dimensions of the amorphous ellipsoids for the sPS50PPO blend melt crystallized at 255°C are much larger than that of the other blends. This correlation suggests that these less rigid amorphous domains might be initiating some energy absorbing process during tensile rupture.

5.6.3 Fracture Surfaces

The etched fractured surface for the sPS50PPO blend crystallized at 255°C at low magnification shows (Figure 4.45) protruding spherulites with hollow surfaces in between. These features strongly indicate that complete spherulites have been pulled out of the fracture surface (interspherulitic fracture). The high magnification image of one of these spherulites (Figure 4.46) suggests that there was a great amount of localized strain also. The bundles appear relaxed after the release of the strain. The voids, which consisted of the amorphous material before etching, have undergone deformation and at some points joined with each other to form larger irregular domains. Still, it may be noted that complete spherulite is preserved. The non-etched fracture surface of the same blend shows drawn fibrils protruding out of the matrix (Figure 4.41). No voids or pits are seen and the surface appears to be quite flat. All these features are consistent with the interspherulitic mode of fracture. Although the spherulite does not crack internally, the sPS-rich interfibrillar amorphous domains appear to be drawn inside. It is important to note here that this sample showed the tensile properties that were higher than the ones given by the linear rule of mixtures. In fact this was the only sample that showed any synergism. The etched micrograph for the sPS50PPO blend crystallized at 220°C (Figure 4.47) shows layers of impinged spherulites. These spherulites do not appear to be strained and suggest that spherulite boundaries did not affect the crack propagation substantially.

The non-etched micrograph for the sPS50PPO blend melt-crystallized at 220°C shows pyramid like structures with pointed heads that are separated by pits (Figure 4.42). These pits appear to be formed by the pulling out of parts of the spherulite, with the spherulite surface elevated in some parts. Chu and Schultz [64] have suggested that these elevated features are high-density nuclei that remain after intraspherulitic cracking due to strain. This intraspherulitic fracture observed can be related to the spherulite density. The density of a spherulite increases from low-density periphery to high density and high crystallnity nucleus at the center. This density gradient, steeper in smaller spherulites, can lead to propagation of the crack through the spherulite. This micrograph clearly suggests that the mode of fracture is intraspherulitic. The comparison of this micrograph with its etched counterpart proves that spherulites in the blend samples crystallized at 220°C do not undergo micro level deformation. Although the non-etched micrograph does suggest some deformation, it is not on a microlevel and can not be expected to contribute substantially to energy absorption.

The non-etched fracture surfaces of the neat sPS show features similar to the ones seen in the blends crystallized at the same temperatures. The sPS crystallized at 255°C shows a layered fracture surface (Figure 4.43). There are numerous micro-cracks and voids. This type of structure, formed from a multi-step fracture process occuring at different points (because of uneven stress points on the surface), strongly suggests craze growth. The micrograph of the fracture surface of the neat sPS

crystallized at 220°C (Figure 4.44) shows elongated ridge-like structures with pits in-between them. These structures, similar to the ones seen for sPS50PPO blend melt-crystallized at 220°C, indicate intraspherulitic fracture.

5.7 Effect of the Spherulitic Morphology on Tensile Properties

The SEM micrographs and the results of the tensile testing strongly suggest a correlation in the morphology and tensile properties. Different processing conditions resulted in vastly different spherulitic morphologies for the melt and cold crystallized blends, which in turn resulted in different properties.

In case of the cold crystallized blends, the mechanical properties and morphology weakly depend upon crystallization temperature. The SEM micrographs showed that fine lamellar bundles are formed after cold crystallization. The dimensions of these bundles and the amorphous domains varied little with the crystallization temperatures (and hence, the crystallization rates). The variation in the resulting mechanical properties was also not substantial.

For melt crystallized blends, the morphology and mechanical properties attained varied appreciably with the composition and processing temperatures. The better mechanical properties achieved than the sPS can not be explained on the basis of crystallinity. Slower crystallization resulted in coarser bundles and larger amorphous domains as well as higher crystallinity, and was accompanied by higher tensile

strength and strain at break. This trend was opposite to the one observed for neat, crystallized sPS samples having higher bulk weight crystallinity. Slowly crystallized neat sPS samples showed poor mechanical properties while the slow crystallized blends showed better tensile strength, strain at break and tensile toughness. The enhanced mechanical properties of sPS/PPO melt crystallized slowly can not be attributed to composition of the amorphous phase domains either. Phase compositions of sPS50PPO melt crystallized at 255°C are quite similar to that of sPS67PPO cold crystallized at 190°C, but the synergistic increase in the tensile strength is not observed. The mechanical properties seem to follow the trend in the sizes of the amorphous domains better. Samples with larger amorphous domains showed better tensile properties. Hence, the better mechanical properties for the blends may be attributed to the efficient re-organization of the amorphous material between the crystalline bundles.

The SEM micrographs of the etched and non-etched fracture surfaces of melt-crystallized blends suggest that the samples crystallized at low temperatures (fast crystallization) undergo predominantly intraspherulitic fracture. In this mode, the crack propagates through the spherulite boundary without inducing any large scale micro-level deformation. In this process, the energy absorption can be expected to be very small. In case of sPS50PPO blends melt crystallized slowly at 255°C, the spherulites on the fracture surfaces showed complete spherulites with deformed amorphous regions. Non-etched surfaces even revealed flat fracture surfaces with

drawn fibrils, which might be structures formed from cold drawing of the less rigid amorphous domains. These features indicate that both interspherulitic and intraspherulitic fracture modes were prevalent and contributed to the energy absorption.

Chapter 6

CONCLUSIONS AND FUTURE WORK

6.1 Conclusions

In this study it was seen that at PPO concentration near 50%, sPS/PPO blends crystallized slowly from the melt state have tensile strength higher than that of the sPS and PPO themselves. In general, strong correlations between crystallization temperature, PPO content, resulting morphology and tensile properties have been identified. Specifically, it can be concluded that:

1. SPS/PPO system forms a completely miscible system in the melt state. Phase separation that does occur is induced by crystallization of the sPS. In most cases two amorphous phases are formed. The composition of the major phase is close to the initial blend composition. The second phase is very small in mass fraction. In melt crystallized blends while the interfibrillar regions become PPO rich, the interlamellar regions become sPS rich. In cold crystallized blends, while the sPS concentration in both the phases decreases with slow crystallization at low supercoolings, the scale of segregation of the PPO is much lower

2. Blending with PPO strongly affects the polymorphic behavior of the sPS. Cold crystallization results in the formation of the disordered into α' or β phases depending upon low and high PPO content. Melt crystallization favors the

formation of the thermodynamically stable β form. Slower crystallization results in higher crystallinity for both the melt and cold crystallized samples.

3. The density of the blends varies strongly with the composition. The change with the processing temperatures, however, is very small. Increase in the content of the more dense β crystal form of the sPS increases the density, while the formation of less dense α' form decreases the density. As a result, cold crystallized samples have lower density than the quenched samples. Melt crystallized samples, on the other hand, have densities higher than that of the quenched blends.

4. Cold crystallized samples show spherulitic morphology consisting of very fine bundles forming a mesh like structure. The change in the morphology, over the range of processing temperatures, is essentially small. Melt crystallized samples, on the other hand, show complete, well developed, spherulites. The distribution of the amorphous material is mostly intra-spherulitic, the major part being in the ellipsoids formed by the branching and splaying of the bundles. The coarseness of bundles, bundle spacing, and the size of the ellipsoids increase with increasing crystallization temperatures. Increase in PPO content results in little change in the coarseness, but increases the bundle spacings and size of the ellipsoidal domains.

5. Tensile properties of cold crystallized blends are weak function of the crystallization temperature. The mechanical properties of the melt crystallized blends change substantially with crystallization temperature, at least for the

sPS50PPO blends. Samples melt crystallized slowly, having larger size ellipsoid dimensions, show higher tensile strength, strain at break and toughness. For sPS50PPO blend melt crystallized at 255°C, increase in the tensile strength for the neat sPS crystallized at the same temperature is approximately 60%, while for the PPO its more than 10%.

6. The composition of the amorphous phases formed after crystallization at different temperatures does not seem to have large influence on the mechanical properties. The effect of morphology and the redistribution of the amorphous phase appears to be more important.

7. The SEM micrographs of the etched and un-etched fracture surfaces of melt crystallized samples suggest intra-spherulitic fracture for the low crystallization temperature (220°C). The fracture surface of the blend sample crystallized slowly at the high temperature of 255°C showed deformed but complete spherulites with highly drawn fibrils suggesting inter-spherulitic fracture and drawing of the amorphous interfibrillar regions. It corresponds well with the synergistic properties achieved for this blend sample.

6.2 Future Work

Based on the interesting correlation between crystallization temperature, morphology and tensile properties observed in this work, several suggestions can be made which

may result in better understanding of the amorphous phase behavior, morphology – properties relationship and deformation processes in melt miscible blends:

1. Small-Angle X-Ray Scattering (SAXS) studies may result in better understanding of the scale of segregation and amorphous compositions rendered by crystallization.

2. The study of the sPS/PPO system over wider range of PPO content and crystallization temperatures may result in more definite understanding of the processing conditions, morphology and mechanical property relationships.

3. Similar studies on other systems, especially sPS blends with rubbery polymers may lead to a different degree of segregation and consequently different morphology – mechanical property relationships.

4. Study of the microstructural deformation behavior in the blends using Transmission Electron Microscopy (TEM) may provide better understanding of the deformation mechanisms and any energy absorbing processes.

REFERENCES

1. S. T. Wellinghoff and E. Baer, *J. Appl. Polym. Sci.*, **22**, 2025 (1978).

2. S. Wu. *J. Appl. Polym. Sci.*, **35**, 549 (1988).

3. C. B. Buckhall. *Toughened Plastics,* Applied Science Publ., London (1977).

4. G. H. Michler, *Acta Polym.*, **36**, 285 (1985).

5. R. A. Pearson and A. F. Yee. *J. Mater. Sci.*, **26**, 3828 (1991).

6. C. B. Buckhall and D. Clayton. *J. Mater. Sci.*, **7**, 202 (1972).

7. R. D. Deanin *in Encyclopedia of Polymer Science and Technology,* John Wiley and Sons, supplemental vol. **2**, 458 1977.

8. F. E. Karasz, and M. T. Shaw *in Polymer Blends and Mixtures,* NATO ASI Series, Martinus Nijhoff Publishers, 1985.

9. D. R. Paul and S. Newman in *Polymer Blends,* Academic Press, 1978.

10. O. Olabisi, L. H. Robenson and M. T. Shaw in *Polymer-Polymer Miscibility,* Academic Press, 1979.

11. D. J. Walsh and S. Rostami. *Advances in Polymer Science,* **70**, 121 (1985).

12. J. S. Higgins in *Polymer Blends and Mixtures,* NATO ASI Series, Martinus Nijhoff Publishers, 1985.

13. E. P. Cizek. US Patent 3 383 435 to General Electric Co. (1968).

14. T. Nishi and T. Wang. *Macromolecules,* **8**, 909 (1975).

15. V. B. Singh and D. J. Walsh. *Macromol. Sci.-Phys.*, **B25**, 65 (1986).

16. D. R. Paul, J. W. Barlow and H. Keskkula. *Encyclopedia of Polymer Science,* Wiley, NY, 12, 399 (1998).

17. F.N. Kelly and F. Bueche, *J. Polym. Sci.* **50**, 549 (1961).

18. P. R. Couchman and F. E. Karasz, *Macromolecules* **11**, 117 (1978).

19. M. Gordon and J. S. Taylor, *J. Appl. Chem.* **2**, 493 (1952).

20. T. G. Fox, *Bull. Am. Phys. Soc.* **2**, 123 (1956).

21. D. J. Wals, S. Rostami and V. B. Singh. *Makromol. Chem.*, **186**, 145 (1985).

22. H. D. Keith and F. J. Padden. *Journal of Applied Physics,* **35**, 1270 (1964).

23. H. D. Keith and F. J. Padden. *Journal of Applied Physics,* **34**, 2409 (1963).

24. H. D. Keith and F. J. Padden. *Journal of Applied Physics,* **35**, 1286 (1964).

25. B. S. Hsiao and B. B. Sauer. *J. Polym. Sci. Polym. Phys. Ed.,* **31**, 901 (1993).

26. J. E. Harris and L. M. Robeson in *Contemporary Topics in Polymer Science Vol. 6*, Plenum Press, New York (1989).

27. J. F. Bristow and D. S. Kalika. *Macromolecules*, **27**, 1808 (1994).

28. K. M. Kit and J. M. Schultz. *J. Polym. Sci.,* **36**, 873 (1998).

29. S. D. Hudson, D. D. Davis and A.J. Lovinger. *Macromol.,* **25**, 1759 (1992).

30. Runt et *al.* Macromol., **25**, 3902 (1995).

31. R. J. Krishnaswamy and D. S. Kalika. *Polym. Engg. Sci.,* **36**, 786 (1996).

32. S. Kunz, P. W. R. Beaumont and M. F. Ashby, *J. Mater. Sci.,* **16**, 3141 (1981).

33. A. F. Yee, *Polym. Eng. Sci.,* **17**, 213 (1977).

34. A. G. Evans, S. Williams and P. W. R. Beaumont. *J. Mater. Sci.,* **20**, 3668 (1985).

35. Sigl et *al. Acta Metall.* **36**, 945 (1988).

36. Alla Margolina and S. Wu. *Polymer,* **29**, 2170 (1988).

37. X. Wang, H. Saito and T. Inone, *Jpn. J. Polym. Sci. Tech.,* **49**, 555 (1992).

38. J. E. Harris and L. M. Robeson, *J. Appl. Polym. Sci.,* **35**, 1877 (1988).

39. D. Brinklow, *Polym. News,* **21**, 316 (1996).

40. N. Ishihara, M. Kuramoto and M. Uoi. *Macromol.,* **21**, 3356 (1988).

41. G. Guerra, V. M. Vitagliano, C. D. Rosa, V. Petraccone and P. Corradini. *Macromol.,* **21**,1539 (1990).

42. A. M. Evans, E.J.C. Keller, J. Knowles, C. Galiotis, C. J. Carriere and E. H. Andrews. *Polym. Eng. Sci.,* **37**, 153 (1997).

43. R. Napolitano and B. Pirozzi. *Macromol.,* **26**, 7225 (1993).

44. R. D. Wesson. *Polym. Eng. Sci.,* **34**, 1157 (1994).

45. S. Cimmino, E. D. Pace, E. Martuscelli and C. Silvestre. *Polymer,* **32**, 1080 (1991).

46. E. M.Woo and F. S. Wu. *Macromol. Chem. Phys.,* **199**, 2041 (1998).

47. S. Cimmino, E. D. Pace, E. Martuscelli and C. Silvestre. *Polymer Commun.,* **32**, 251 (1991).

48. G. Guerra, V. M. Vitagliano, C. D. Rosa, V. Petraccone, P. Corradini and F. Karasz. *Polym. Commun.* **32**, 30, (1991).

49. F. S. Wu, *Master's Thesis, National Cheng Kung Univ., Taiwan,* 1997.

50. S. Cimmino, E. D. Pace, E. Martuscelli and C. Silvestre. *Polymer,* **34**, 214, (1993).

51. G. Guerra, V. M. Vitagliano, C. D. Rosa, V. Petraccone and P. Corradini. J. *Polym. Sci.*, **29**, 265, (1991).

52. S. Cimmino, E. D. Pace, E. Martuscelli and C. Silvestre. *Polymer,* **34**, 2799, (1993).

53. J. Heijboer, *J. Polym. Sci., Part C.* **16**, 3755 (1968).

54. J. Stoneling, F. F. Karasz, and W. J. Macknight, *Polym. Eng. Sci.* **10**, 133 (1970).

55. G. D. Wignall, H.R. Child, and F. Li-Araveno, *Polymer* **21**, 131 (1980).

56. W. Wenig and T. Schoeller, *Angew. Makromol. Chem.* **130**, 155 (1985).

57. S. Ziaee and D. R. Paul, *Polymeric Materials Science* **75**, 14 (1996).

58. A. F. Yee and M. A. Maxwell, *J. Macromol. Sci.-Phys.* **B 17(3)**, 543 (1980).

59. A. M. Serrano, G. E. Welsch, and R. Gibala, *Polym. Eng. Sci.*, **22**, 946 (1982).

60. Byoungchul Chun, *Ph.D dissertation*, University of Michigan, 1988.

61. W. M. Prest and R. S. Porter. *J. Polym. Sci.: A-2,* **10**, 1639 (1972).

62. C. B. Bucknall, D. Clayton and W. E. Keast, *J. Mater. Sci.* **7**, 1443 (1972).

63. S. Wu. *Polym. Engg. Sci.,* **30**, 753 (1990).

64. Jia-ni Chu and J. M. Schultz. *J. Mater. Sci.,* **25**, 3746 (1990).

65. S. C. Kim and H. R. Brown. *J. Mater. Sci.*, **22**, 2589 (1987).

VITA

Gyanendra Dutt was born on 09 February 1976 in Delhi, India. He received his Bachelor of Technology degree in Chemical Engineering from Harcourt Butler Technological Institute, Kanpur, India in June 1997. He joined the Polymer Engineering program in Department of Materials Science and Engineering at University of Tennessee, Knoxville in August 1997 and received the degree of Master of Science in December 1999.